2007

Wood liquefaction in the presence of phenol with a weak acid catalyst and its potential for novolac type wood adhesives

Hui Pan
Louisiana State University and Agricultural and Mechanical College

WOOD LIQUEFACTION IN THE PRESENCE OF PHENOL WITH A WEAK ACID CATALYST AND ITS POTENTIAL FOR NOVOLAC TYPE WOOD ADHESIVES

A Dissertation

Submitted to the Graduate Faculty of the
Louisiana State University and
Agricultural and Mechanical College
in partial fulfillment of the
requirements for the degree of
Doctor of Philosophy

in

The School of Renewable Natural Resources

by
Hui Pan
B.S., Northeast Forestry University, China, 1993
M.S., Northeast Forestry University, China, 2002
December 2007

ACKNOWLEDGEMENTS

There are many people I would like to thank for their support and effort. First, I am grateful to my major professor, Dr. Todd Shupe. He has always provided me a "spacious" environment to do my research, offered me every chance he could have to meet people in our area, and most importantly, encouraged me for every small progress I have made. I would like to express my special thanks to Dr. Chung-Yun Hse. He has been an excellent guide for me to be a real researcher. Beside the science, his positive thinking and wealth of experiences has always been an inspiration to me. His guidance, patience, and time were invaluable in the completion of this work. I would also like to thank my other committee members, Dr. Richard Vlosky, Dr. Paul Russo, and Dr. Steven Hall. I am grateful for their time and effort spent in reviewing this research. I also appreciate all their suggestions and guidance.

I would like to express my thanks to Dr. Tom Eberhardt for his valuable discussion and suggestion during the course of this work. I want to thank Dr. Tom Elder for generously lending me his reference books and offered me information and resources when I am looking for a postdoc position. I also appreciate Dr. Les Groom for teaching me to use the AFM and all the help during my stay at SRS, Pineville. I want thank Dr. Chi So for helping me to solve all my computer problems. I also sincerely appreciate Mr. Dale Huntsberry, Ms. Donna Edwards, Ms. Karen Reed, and Ms. Janie Gurgainers for their help on my experiments and my stay at SRS, Pineville.

Additionally, I would like to thank Dr. Ge Wang, Dr. Yan Yu, and Dr. Daochun Qing at INBAR, Beijing, for their help during my experiments there. I also want thank Dr. Rafael Cueto in the LSU Chemistry Department for his valuable help on my HPLC

and GPC experiments. I want express my sincere thanks to Dr. Yong Lei for his valuable help, Dr. Qinglin Wu at LSU School of Renewable Natural Resources, Dr. Kun Lian in CAMD, LSU for kindly providing their DSC equipment.

I wish to thank Ms Haiqing Chen and Ms Grace Lee for giving me the feeling like home when I lived with them. I want to thank Dr. Jun Ai for having given me an ear and encouraging words along the way of this work.

Finally, I want to express my deepest gratitude to my husband, my parents, and my brother. My husband gave me his best understanding upon my going back to school and pursuing an academic career. Without his support, I would never have been able to go this far. I wish to particularly thank my parents, who have never stopped supporting me and never lost faith in me through all the challenges.

TABLE OF CONTENTS

LIST OF TABLES

LIST OF FIGURES

ABSTRACT

Wood liquefaction was conducted using phenol as a reagent solvent with oxalic acid as a catalyst. A series of studies were done on liquefied wood, liquefied wood residues, novolac-type liquefied wood resins, and bio-composites fabricated from liquefied wood resin. The results of the liquefied wood residue characterization revealed that the liquefaction reactions conducted in different reaction vessels underwent different liquefaction mechanisms. The crystallinity indexes of the liquefied wood residues were higher than that of the original wood, indicating that the amorphous lignin was the most susceptible component in wood to the liquefaction reaction. Fe^{2+} and Fe^{3+} ions were found to have catalytic effects during liquefaction reaction. The cure kinetic study of two typical liquefied wood resins (LWR) showed that the activation energies of liquefied wood resin were higher than conventional phenolic resins and close to that of a lignin-phenol-formaldehyde resin from another study. It was found that LWR followed an autocatalytic cure mechanism. Two kinetic models were proposed for LWR based on the isothermal differential scanning calorimetry (DSC) methods. The flexural strengths of the composites were comparable to that of similar products reported by other researchers, indicating that the liquefied wood resin and liquefied wood residue from a weak-acid-catalyzed liquefaction could be successfully applied to molded bio-composite products as a substitute for conventional novolac resin.

CHAPTER 1

INTRODUCTION

1.1 Biomass Conversion Technologies for Fuels and Chemicals

"Biomass" is a generic term for all animate organic matter, including crops, forestry, marine products, and some organic waste, such as municipal solid waste and agricultural waste.[1,2] It is a traditional source of energy and is still responsible for around 40-50% of the energy supply in many developing countries that rely on low-tech and inefficient cooking and heating methods.[2,3] With the diminishing supply of crude oil, and environmental concerns, biomass provides a renewable source for fuels and chemicals as a substitute for petroleum. Biomass can be converted to liquid and gaseous products that can then be used directly in internal-combustion engines or for organic synthesis.[4] The two main routes for biomass conversion are biochemical and thermochemical processes.[5]

1.1.1 Biochemical conversion of biomass

Biochemical conversion of biomass is completed through alcoholic fermentation to produce liquid fuels and anaerobic digestion or fermentation to produce bio-gas.[6] Much of the effort in biochemical conversion research is aligned with the sugar platform technologies that make use of crops or lignocellulosic materials as feedstocks for ethanol production via saccarification and fermentation processes.[7] However, the current costs of bio-ethanol are much higher than the costs of gasoline from fossil sources.[3] The price of the feedstocks contributes more than 55% of the bio-ethanol cost. The most commonly used biomass feedstocks, such as corn and sugar cane, have to compete directly with the

food sector.[8] Lignocellulosic biomass, such as agricultural residues and forestry residues, are, in principle, suitable for used as inexpensive feedstocks, but the technology for this process differs from that of the starch-to-ethanol because of the complex chemical structures of lignocellulosic materials.[3,8] Recent research has been conducted on the pre-treatment of lignocellulosic biomass before the fermentation process or growing biomass to be used for bio-ethanol on agriculturally degraded land to give better economic prospects of bio-ethanol production.[8,9]

1.1.2 Thermochemical conversion of biomass

The three main thermochemical conversion processes of biomass are pyrolysis, direct liquefaction, and gasfication. Pyrolysis is the thermal degradation of biomass by heat in the absence of oxygen, which results in the production of charcoal (solid), bio-oil (liquid), and fuel gas products.[2] Direct liquefaction corresponds to a thermal and catalyzed reaction of biomass.[10] The differences between pyrolysis and direct liquefaction are that (1) pyrolysis is conducted in the temperature range of 650 to 800 K while the temperature range of direct liquefaction is around 525 to 600 K and (2) direct liquefaction is normally conducted under pressure of about 5 to 10 MPa.[1] Gasification is a form of pyrolysis which is performed at high temperature (up to 1273 K) in order to optimize gas production.[5,10] The resulting gas is a mixture of carbon monoxide, hydrogen, and methane, together with carbon dioxide and nitrogen.[5]

Pyrolysis produces fuels with high fuel-to-feed ratios, which makes it the most competitive bio-fuel to fossil fuels.[5] Reported yields on crude oil vary from 20 to 70% depending on the pyrolysis methods.[5,11] Generally, biomass derived pyrolysis oil, which

is highly oxygenated and has poor thermal stability, requires further upgrading by lowering the oxygen content via hydrogenation.[5, 12] Similar to the production of bio-ethanol, pyrolysis fuel production does not appear to be a viable route at current petroleum prices.[12] There are several issues that the pyrolysis process must address in the future: (1) large- scale demonstration of the thermochemical conversion and upgrading process; (2) completion of the refinery cycle to produce marketable liquid fuels from biomass; (3) demonstration of chemical separation technologies; (4) determination of the compatibility of biomass liquefaction products with existing petroleum refinery systems.[13]

1.2 Biomass Liquefaction via Solvolysis

Solvolysis liquefaction of biomass dissolves biomass in an organic solvent at moderate temperature (120 to 250 °C).[14] Partial solvolysis of biomass provides valuable chemicals, mainly pure cellulose and phenolic compounds, and complete solvolysis provides fuels.[15] Different organic solvents have been used in liquefaction, such as polyhydric alcohols,[16] phenol,[17] ethylene carbonate,[18,19] dioxane,[20] ethanol,[21] acetone,[20] supercritical phenol,[22] and supercritical alcohols.[23] Different processing methods have also been studied, such as using microwaves as the heat source in the liquefaction reaction.[24]

1.2.1 Biomass liquefaction with polyhydric alcohols

Aliphatic alcohols (from C1 to C7) or polyols have been known for a long time to selectively dissolve the basic components of wood.[15] Yao et al. [25] investigated various

polyols or their combination with other polar solvents as reagent solvents in biomass liquefaction, such as polyethylene glycol (PEG), polycaprolactone (PCL303), PEG/glycerin, PEG/1,1,1-tris (hydroxymethl) propane (TMP), and ε-caprolactone (CPL)/glycerin. The results showed that the liquefaction reaction using PEG/glycerin achieved the lowest residue content among all other tested solvents. Krzan et al.[26] studied different combinations of polyols with organic acids or mineral acids and reported that a combination of propylene glycol (PG) as the reagent solvent and maleic anhydride as the acid catalyst showed the best liquefaction results. The effects of ozone pre-treatment on wood, liquefaction time, temperature, and wood species on wood liquefaction with polyhydric alcohols have also been investigated.[27-29]

Various products have been made from liquefied biomass with polyhydric alcohols. Epoxy resins were synthesized from PEG/glycerol liquefied wood as were epoxy compounds such as diglycidyl ether of biphenol A (DGEBA) and diglycidyl ether of ethylene glycol oligomers (DGEEG).[30,31] The viscoelastic and mechanical properties of the liquefied wood-based epoxy resins suggested that they would be well suited for matrix resins for natural fiber reinforced composites.[32,33] Starch, wood/starch mixtures, corn bran, bark/starch mixture have been liquefied and used to prepare polyurethane foams.[34-37] Compared to conventional polyurethane foam, liquefied biomass based foams have an advantage of potential bio- and photodegradability.[37, 38] Efforts has also been made to recover the polyols from bio-based foams after their glycolysis degradation.[39] Polyurethane films, resins, and isocyanate adhesives have also been synthesized from PEG/glycerol liquefied wood.[40-44]

Research has been conducted on fundamental aspects of biomass liquefaction with polyhydric alcohols. The liquefaction mechanism of polysaccharides with alcohol has been studied using glucose and cellobiose as model compounds.[45] Condensation reactions of degraded lignocellulose and the formation of wood residue during wood liquefaction have also been investigated.[16, 46, 47] The liquefied products of cellulose have been fractionated and analyzed.[48] A new method to determine the hydroxyl value of the liquefied products has been developed based on the consumption of the NCO group.[49]

1.2.2 Biomass liquefaction with phenol

Phenol is one of the most common reagent solvents used in biomass liquefaction. It can be applied in the liquefaction reaction with or without a catalyst. Pu et al.[50-52] have studied the liquefaction of wood in the presence of phenol without a catalyst. They have reported that wood can be converted to dioxane soluble products at 250 ºC with phenol (wood to phenol ratio larger than 1/1). In general, lignin was liquefied in the initial stage of the liquefaction (about 10 min. at 250 ºC), and the cellulosic component was mostly resistant to liquefaction. Although phenolysis of wood without a catalyst could be a prospective technique for preparing liquefied wood, relatively high reaction temperatures are needed to compensate the absence of catalyst.

With neutral solvents, the liquefaction process is controlled by pyrolysis and is achieved at higher "severities" or longer reaction times. The best liquefaction is achieved via catalysis by acids and bases.[15] A few studies have been done on biomass liquefaction with a base catalyst. Alma et al [53, 54] investigated the catalytic effects of a variety of alkalis and metallic salts (acidic or basic) on biomass liquefaction with phenol. They

reported that most alkalis and metallic salts were effective catalysts giving low biomass residue content, however, they were not effective catalysts to achieve a high amount of combined phenol. NaOH was found to be the most efficient alkaline catalyst in the dissolution of biomass in phenol at an elevated temperature of 250 ˚C.

Both strong acids, such as sulfuric acid [55] and hydrochloric acid, [56] and weak acid, such as oxalic acid, [57] can be used as catalysts in biomass liquefaction. The resulting liquefied wood using a strong acid catalyst can achieve a higher combined phenol and lower wood residue content than those using a weak acid catalyst. The addition of a small amount of sulfuric acid greatly enhanced the dissolution of wood, which favored hydrolytic cleavages along the cellulosic chain.[15]

Liquefied wood resin can be obtained by removal of the wood residue and free phenol (un-reacted phenol) after the liquefaction reaction. The flow temperature and viscosity of the liquefied wood resin were found to be higher than the commercial novolac resin and increased as the amount of combined phenol increased.[58,59] The flexural properties of molded products from liquefied wood were enhanced with an increase of the amount of combined phenol and became comparable to the commercial novolac moldings when the combined phenol reached 75% and above.[60, 61] It was also reported that liquefied wood resins have a much better hydrophilic compatibility with wood fillers than conventional novolac resins.[60]

Liquefied wood can further react with formaldehyde to form novolac [57, 61-64] or resol [54, 65] type phenolic resins under acidic or alkaline conditions. It was reported that almost all of the free phenol remaining from the liquefaction reaction can be converted to resin by a condensation reaction with formaldehyde. The thermofluidity of the co-

condensed resin was improved greatly and thus has a much lower flow temperature and viscosity than liquefied wood resin.[57, 61] The mechanical properties of the molding products from the co-condensed resin were also much better than those from the liquefied wood resins.[57, 61, 63]

Efforts have also been made to liquefy other types of biomass with phenol, such as corn bran, [66, 67] bark, [62] and grapevine cane waste [68] to be used as the raw materials for phenolic resins. In addition to the traditional phenolic resins, new types of materials with liquefied wood, such as wood ceramics [69] and wood-plastic composites [70] have been studied as well. A new method using liquefaction technique to recycle preservative treated wood has been proposed by Lin and Hse.[71] CCA-treated wood was first liquefied and then the preservative metals were removed by precipitation. The resulting preservative-free liquefied wood can be further used in phenolic resins.[72]

Despite these many advances in liquefaction technology, the mechanism of wood liquefaction is not clearly understood due to the complicated structure and chemical composition of wood. Lignin and cellulose model compounds were liquefied with phenol individually and the liquefied products were analyzed to reveal the possible reaction pathways of lignin and cellulose during the liquefaction reactions with phenol.[73-75] Liquefied products of cellulose in the presence of phenol were characterized by FT-IR and NMR to identify the reaction intermediates and the substitution pattern of phenol with liquefied cellulose.[76,77] A kinetic study has also been conducted on wood liquefaction reaction with phenol.[78]

1.3 Objectives

Although many studies have been done on wood liquefaction and some progress has been made in the past decades, numerous technical and fundamental challenges remain. For example, most previous studies on wood liquefaction have focused on completely converting wood into a liquid via a strong acid catalyst or high reagent solvent to wood ratios, which has resulted in a liquefaction process that is not economically feasible because special production equipment is required due to the high corrosiveness of the strong acids. In my research on wood liquefaction for novalac type resin applications, I have focused on a process with a weak acid catalyst system. Although the significant difference of a weak-acid-catalyzed system to a strong acid system is the high wood residue content, which might not be desirable for most applications, the less corrosive of weak acid together with potential application of wood residue as filler in molding products provides a unique opportunity to enhance the economic feasibility of the new system. Furthermore, since lignin is very susceptible to phenol liquefaction, [50] it can also partially substitute for phenol in the phenolic resin synthesis. Therefore, my goal is to determine the optimum degree of wood liquefaction to liquefy lignin *in situ* and leave maximum amount of crystalline cellulose that can be used as a filler in molded products.

Thus, the objectives of this study were (1) to characterize liquefied wood and liquefied wood residue from a weak acid catalyzed system, (2) examine the properties of a novolac resin formulated from liquefied wood, and (3) evaluate the physical and mechanical properties of compression molded products fabricated with the novolac type liquefied wood resin.

1.4 References

1. Demirbas, A. 2000. Mechanisms of liquefaction and pyrolysis reactions of biomass. Energy Convers. Mgmt. 41: 633-646.

2. Demirbas, A. and Arin, G. 2002. An overview of biomass pyrolysis. Energy Sources 24: 471-482.

3. Hamelinck, C. N., and Faaij A. P. C. 2006. Outlook for advanced biofuels. Energy Policy 34: 3268-3283.

4. Rustamov, V. R., Abdullayev, K. M., and Samedov, E. A. 1998. Biomass conversion to liquid fuel by two-stage thermochemical cycle. Energy Convers. Mgmt. 39(9): 869-875.

5. Demirbas, A. 2001. Biomass resource facilities and biomass conversion processing for fuels and chemicals. Energy Convers. Mgmt. 42: 1357-1378.

6. Demirbas, M. F., and Balat, M. 2006. Recent advances on the production and utilization trends of bio-fuels: A global perspective. Energy Convers. Mgmt. 47: 2371-2381.

7. Boateng, A. A., Hicks, K. B., Flores, R. A., and Gutsol, A. 2007. Pyrolysis of hull-enriched byproducts from the scarification of hulled barley. J. Anal. Appl. Pyrolysis 78: 95-103.

8. Campo, I. D., Alegria, I., Zazpe, M., Echeverria, M., and Echeverria, I. 2006. Diluted acid hydrolysis pretreatment of agri-food wastes for bio-ethanol production. Ind. Crops Prod. 24: 214-221.

9. Tilman, D., Hill, J., and Lehman, C. 2006. Carbon-negative biofuels from low-input high-diversity grassland biomass. Science 314: 1598-1600.

10. Lede, J. 1999. Solar thermochemical conversion of biomass. Sol. Energy 65(1): 3-13.

11. Meier, D., Larimer, D. M., and Faix, O. 1986. Direct liquefaction of different lignocellulosics and their constituents. 1. Fractionation, elemental composition. Fuel 65(7): 910-915.

12. Amen-Chen, C., Pakdel, H., and Roy, C. 2001. Production of monomeric phenols by thermochemical conversion of biomass: a review. Bioresour. Technol. 79: 277-299.

13. Elliott, D. C., Beckman, D., Bridgwater, A. V., Diebold, J. P., Gevert, S. B., and Solantausta, Y. 1991. Developments in direct thermochemical liquefaction of biomass: 1983-1990. Energy Fuels 5:399-410.

14. Rezzoug, S. A., and Capart, R. 2002. Liquefaction of wood in two successive steps: solvolysis in ethylene-glycol and catalytic hydrotreatment. Appl. Energy 72: 631-644.

15. Rezzoug, S. A., and Capart, R. 1996. Solvolysis and hydrotreatment of wood to provide fuel. Biomass Bioenergy 11(4): 343-352.

16. Yao, Y., Yoshioka, M., and Shiraishi, N. 1993. Combined liquefaction of wood and starch in a polyethylene glycol/glycerin blended solvent. Mokuzai Gakkaishi 39(8):930-938.

17. Lin, L., Yao, Y., Yoshioka, M., and Shiraishi, N. 1997. Molecular weights and molecular weight distributions of liquefied wood obtained by acid catalyzed phenolysis. J. Appl. Polym. Sci. 64(7): 351-357.

18. Yamada, T., and Ono, H. 1999. Rapid liquefaction of lignocellulosic waste by using ethylene carbonate. Bioresour. Technol. 70: 61-67.

19. Xie, T., and Chen F. 2005. Fast liquefaction of bagasse in ethylene carbonate and preparation of epoxy resin from the liquefied product. J. Appl. Polym. Sci. 98: 1961-1968.

20. Mun, S. P., Hassan, E. M., and Hassan, M. 2004. Liquefaction of lignocellulosic biomass with dioxane/polar solvent mixtures in the presence of an acid catalyst. J. Ind. Eng. Chem. 10(3): 473-477.

21. Mun, S. P., Hassan, E. M., and Hassan, M. 2004. Liquefaction of lignocellulosic biomass with mixtures of ethanol and small amout of phenol in the presence of methanesulfonic acid catalyst. J. Ind. Eng. Chem. 10(5): 722-727.

22. Lee, S. H., and Ohkita, T. 2003. Rapid wood liquefaction by supercritical phenol. Wood Sci. Technol. 37(1): 29-38.

23. Yamazaki, J., Minami, E., and Saka, S. 2006. Liquefaction of beech wood in various supercritical alcohols. J. Wood Sci. 52: 527-532.

24. Krzan, A. and Kunaver, M. 2006. Microwave heating in wood liquefaction. J. Appl. Polym. Sci. 101: 1051-1056.

25. Yao, Y., Yoshioka, M., and Shiraishi, N. 1994. Soluble properties of liquefied biomass prepared in organic solvents. I. The soluble behavior of liquefied biomass in various diluents. Mokuzai Gakkaishi 40(2): 176-184.

26. Krzan, A., Kunaver, M., and Tisler, V. 2005. Wood liquefaction using dibasic organic acids and glycols. Acta. Chim. Slov. 52: 253-258.

27. Kobayashi, M., Asano, T., Kajiyama, M., and Tomita, B. 2005. Effect of ozone treatment of wood on its liquefaction. J. Wood Sci. 51: 348-356.

28. Rezzoug, S. A., and Capart, R. 2003. Assessment of wood liquefaction in acidified ethylene glycol using experimental design methodology. Energy Convers. Mgmt. 44: 781-792.

29. Kurimoto, Y., Doi, S., and Tamura, Y. 1999. Species effects on wood liquefaction in polyhydric alcohols. Holzforschung 53: 617-622.

30. Kobayashi, M., Enjyouji, I., Tomita, B., and Hatono Y. Liquefied wood /epoxy resin adhesives. In: Wood Adhesive 2000, Forest Products Society, Madison, USA. 267-272 pp.

31. Kobayashi, M., Tukamoto, K., and Tomita, B. 2000. Application of liquefied wood to a new resin system synthesis and properties of liqufed wood/epoxy resins. Holzforschung 54(1): 93-97.

32. Kobayashi, M., Hatano, Y., and Tomita, B. 2001. Viscoelastic properties of liquefied wood/epoxy resin and its bond strength. Holzforschung 55(6): 667-671.

33. Kishi, H., Fujita, A., Miyazaki, H., Matsuda, S. and Murakami, A. 2006. Synthesis of wood-based epoxy resins and their mechanical and adhesive properties. J. Appl. Polym. Sci. 102: 2285-2292.

34. Yao, Y., Yoshioka, M., and Shiraishi, N. 1996. Water-absorbing polyurethane foams from liquefied starch. J. Appl. Polym. Sci. 60: 1939-1949.

35. Yao, Y., Yoshioka, M., and Shiraishi, N. 1995. Rigid polyurethane foams from combined liquefaction mixtures of wood and starch. Mokuzai Gakkaishi 41(7):659-668.

36. Lee, S. H., Yoshioka, M., and Shiraishi, N. 2000. Liquefaction of corn bran in the presence of alcohols and preparation of polyurethane foam from its liquefied polyol. J. Appl. Polym. Sci. 78: 319-325.

37. Ge, J., Zhong, W., Guo, Z., Li, W., and Sakai, K. 2000. Biodegradable polyurethane materials from bark and starch. I. Highly resilient foams. J. Appl. Polym. Sci. 77: 2575-2580.

38. Lee, S. H., Teramoto, Y., and Shiraishi, N. 2002. Biodegradable polyurethane foam from liquefied waste paper and its thermal stability, biodegradability, and genotoxicity. J. Appl. Polym. Sci. 83: 1482-1489.

39. Lee, S. H., Ohkita, T., and Teramoto, Y. 2005. Polyol recovery from biomass-basded polyurethane foam by glycolysis. J. Appl. Polym. Sci. 95: 975-980.

40. Kurimoto, Y., Takeda, M., Doi, S., Tamura, Y., and Ono, H. 2001. Network structures and thermal properties of polyurethane films prepared from liquefied wood. Bioresour. Technol. 77: 33-40.

41. Kurimoto, Y., Takeda, M., Koizumi, A., Yamauchi, S., Doi, S., and Tamura, Y. 2000. Mechanical properties of polyurethane films prepared from liquefied wood with polymeric MDI. Bioresour. Technol. 74: 151-157.

42. Kurumoto, Y., Doi, S., Tamura, Y., and Ono, H. 2001. Wood species effects on the characteristics of liquefied wood and the properties of polyurethane films prepared from the liquefied wood. Biomass Bioenergy 21: 381-390.

43. Wei, Y., Cheng, F., Li, H., and Yu, J. 2004. Synthesis and properties of polyurethane resins based on liquefied wood. J. Appl. Polym. Sci. 92: 351-356.

44. Tohmura, S. I., Li, G. Y., and Qin, T. F. 2005. Preparation and characterization of wood polyalcohol based isocyanate adhesives. J. Appl. Polym. Sci. 98: 791-795.

45. Yao, Y. G. 1996. Liquefaction of wood and other biomass in the presence of alcohols and its application. Ph.D Dissertation, Kotyo University, Japan

46. Yamada, T., Hu, Y. H., and Ono, H. 2001. Condensation reaction of degraded lignocellulose during wood liquefaction in the presence of polyhydric alcohols. J Adhes Soci Japan 37(2):471-478

47. Kobayashi M., Asano T., Kajiyama M., Tomita B. 2004. Analysis on residue formation during wood liquefaction with polyhydric alcohol. J. Wood. Sci. 50:407-414.

48. Yamada, T., and Ono, H. 2001. Characterization of the products resulting from ethylene glycol liquefaction of cellulose. J. Wood Sci. 47: 458-464.

49. Ueno, T., Ashitani, T., and Sakai, K. 2002. New method to determine the hydroxyl value in liquefied bark as polyurethane material. J. Wood Sci. 48: 348-351.

50. Pu,S., Shiraishi, N. 1993. Liquefaction of wood without a catalyst I. time course of wood liquefaction with phenols and effects of wood/phenol ratios. Mokuzai Gakkaishi 39(4): 446-452.

51. Pu,S., Shiraishi, N. 1993. Liquefaction of wood without a catalyst II. Weight loss by gasification during wood liquefaction, and effects of temperature and water. Mokuzai Gakkaishi 39(4): 453-458.

52. Pu,S., Shiraishi, N. 1994. Liquefaction of wood without a catalyst IV. Effect of additives, such as acid, salt, and neutral organic solvent. Mokuzai Gakkaishi 40(8): 824-829.

53. Alma, M. H., Maldas, D., and Shiraishi, N. 1998. Liquefaction of several biomass wastes into phenol in the presence of various alkalis and metallic salts as catalysts. J. Polym. Eng. 18(3): 161-177.

54. Alma, M. H., and Bastiirk, M. A. 2001. Co-condensation of NaOH catalyzed liquefied wood wastes, phenol, and formaldehyde for production of resol type adhesives. Ind. Eng. Chem. Res. 40: 5036-5039.

55. Alma, M. H., Yoshioka, M., Yao, Y., and Shiraishi, N. 1998. Preparation of sulfuric acid catalyzed phenolated wood resin. Wood Sci. Technol. 32: 297-308.

56. Alma, M. H., Yoshioka, M., Yao, Y., and Shiraishi, N. 1995. Preparation and characterization of phenolated wood using hydrochloric acid as a catalyst. Wood Sci. Technol. 29: 39-47.

57. Alma, M. H., Yoshioka, M., Yao, Y., and Shiraishi, N. 1995. Preparation of oxalic acid catalyzed resinified phenolated wood and its characterization. Mokuzai Gakkaishi 41(12): 1122-1131.

58. Alma, M. H., Yoshioka, M., Yao, Y., and Shiraishi, N. 1996. The preparation and flow properties of HCl catalyzed phenolated wood and its blends with commercial Novolak resin. Holzforschung 50: 85-90.

59. Lee, S. H., and Wang, S. Q. 2005. Effect of water on wood liquefaction and the properties of phenolated wood. Holzforschung 59: 628-634.

60. Lin, L., Yoshioka, M., Yao, Y., and Shiraishi, N. 1995. Physical properties of moldings from liquefied wood resins. J. App. Polymer Sci. 55: 1563-1571.

61. Alma, M. H., Yoshioka, M., Yao, Y., and Shiraishi, N. 1995. Some characterizations of hydrochloric acid catalyzed phenolated wood-based materials. Mokuzai Gakkaishi 41(8): 741-748.

62. Alma, M. H., Kelley, S. S. 2000. Thermal stability of novolac type thermosettings made by the condensation of bark and phenol. Polym. Degrad. Stab. 68: 413-418.

63. Lee, S. H., Teramoto, Y., and Shiraishi, N. 2002. Acid catalyzed liquefaction of waste paper in the presence of phenol and its application to novolac type phenolic resin. J. Appl. Polym. Sci. 83: 1473-1481.

64. Li. G. Y., Q, T. F., Tohmura, S., and Atsushi, I. 2004. Preparation of phenol formaldehyde resin from phenolated wood. J Fore. Res. 15(3): 211-214.

65. Lee, S. H.; Teramoto, Y.; Shiraishi, N. 2002. Resol type phenolic resin from liquefied phenolated wood and its application to phenolic foam. J Appl Polym Sci 84: 468472.

66. Lee, S. H.; Yoshioka, M.; Shiraishi, N. 2000. Preparation and properties of phenolated corn bran/phenol/formaldehyde co-condensed resin. J Appl Polym Sci. 77:2901-2907.

67. Lee, S. H., Yoshioka, M. and Shiraishi, N. 2000. Liquefaction and product identification of corn bran (CB) in phenol. J. Appl. Polym. Sci. 78: 311-318.

68. Alma, M. H., and Basturk, M. A. 2006. Liquefaction of grapevine cane waste and its application to phenol-formaldehyde type adhesive. Ind. Crop. Prod. 24: 171-176.

69. Zhao, B. Y., Hirose, T., Okaba, T., Zhang, D. Fan, T. X., and Hu, K. A. 2002. Wood ceramics prepared from wood powder/phenolated wood composite. J Porous Mater. 9:195-201.

70. Doh, G. H., Kang, I. A., Lee, S. Y., Kong, Y. T., Jeong, C.S. and Lim, B. S. 2005. Mechanical properties and creep behavior of liquefied wood polymer composites. Compo. Struc. 68: 225-233.

71. , Lin, L.; Hse, C. Y. 2005. Liquefaction of CCA-treated wood and elimination of metals from the solvent by precipitation. Holzforschung 59: 285-288.

72. Shiraishi, N., and Hse, C. Y. 2000. Liquefaction of the used creosote-treated wood in the presence of phenol and its application to phenolic resin. In. Wood Adhesive 2000, Forest Products Society, Madison, USA. 259-266 pp.

73. Lin, L., Yao, Y., Yoshioka, M., and Shiraishi, N. 2001. Liquefaction mechanism of β-O-4 lignin model compound in the presence of phenol under acid catalysis. I. Structural characterization of the reaction products. Holzforschung 55: 617-624.

74. Lin, L., Yao, Y., Yoshioka, M., and Shiraishi, N. 2001. Liquefaction mechanism of β-O-4 lignin model compound in the presence of phenol under acid catalysis. Part 2. Reaction behavior and pathway. Holzforschung 55: 625-630.

75. Lin, L., Yao, Y., Yoshioka, M., and Shiraishi, N. 2004. Liquefaction mechanism of cellulose in the presence of phenol under acid catalysis. Carbohy. Polym. 57: 123-129.

76. Yamada, T., Ono, H., Ohara, S., and Yamaguchi, A. 1996. Characterization of the products resulting from direct liquefaction of cellulose I. Identification of intermediates and the relevant mechanism in direct phenol liquefaction of cellulose in the presence of water. Mokuzai Gakkaishi 42(11): 1098-1104.

77. Zhang Y., Ikeda A., Hori N., Takemura A., Ono H., and Yamada T. 2006. Characterization of liquefied product from cellulose with phenol in the presence of sulfuric acid. Bioresour. Technol. 97:313-321.

78. Alma, M. H., Acemioglu, B. 2004. A kinetic study of sulfuric acid catalyzed liquefaction of wood into phenol. Chem. Eng. Commun. 191(7): 968-980.

CHAPTER 2

CHARACTERIZATION OF LIQUEFIED WOOD AND LIQUEFIED WOOD RESIDUES FROM DIFFERENT LIQUEFACTION CONDITIONS

2.1 Introduction

Wood liquefaction using phenol as the reagent solvent and an acid catalyst has long been studied as a novel technique to utilize biomass as an alternative to petroleum-based products. A variety of general studies has been conducted on wood liquefaction with phenol. The effects of water, catalyst type, catalyst concentration, liquefaction temperature and time, and phenol to wood ratio have been investigated.[1-3] The molecular weight and flow properties of the liquefied wood have also been characterized.[4,5] A model compound of lignin has been used to demonstrate the reaction mechanism of lignin during wood liquefaction.[6,7] However, a comprehensive understanding of the mechanism of wood liquefaction in the presence of phenol has not yet been clearly established. Cellulose, hemicellulose, and lignin are the three main components of wood. The strong network of cellulose, hemicellulose, and lignin and the crystalline structure of some regions of cellulose make wood extremely resistant to liquefaction, even under severe reaction conditions. Therefore, wood residue always occurs as part of a liquefied wood mixture, especially when a weak acid is used as a catalyst. The residue content (i.e., the amount of wood residue remaining after liquefaction) is a typical measure of the extent of a liquefaction reaction. A comprehensive study on liquefied wood residue is still lacking. It is important to study the characteristics of the wood components after liquefaction. Research on liquefied wood residues provides a new approach to better

understand some fundamental aspects of wood liquefaction. Therefore, the objectives of this chapter were to characterize the liquefied wood and liquefied wood residue from different liquefaction conditions by high performance liquid chromatography (HPLC), gel permeation chromatography (GPC), Fourier transform infrared spectroscopy (FT-IR), X-ray diffraction (XRD) and scanning electronic microscopy (SEM).

2.2 Experimental

2.2.1 Materials

Chinese tallow (*Triadica sebifera* syn. *Sapium sebiferum)* tree wood was sawn on a laboratory table saw and the sawdust was collected. The particles were oven dried at 70-80 ºC to a moisture content of 3 - 5% and then reduced in a Wiley mill to fine powder of 20 - 200 mesh. Liquid industrial grade phenol (90% concentration) was used as the liquefaction reagent. All other chemicals were reagent grade.

2.2.2 Preparation of liquefied wood and liquefied wood residues

Wood powder, phenol, and oxalic acid were mixed in a container until a uniform mixture was obtained. The mixture was then transferred to a 1L three-neck glass reactor equipped with a condenser and a stirring system. The liquefaction procedure was also conducted in a 1L Parr reactor. The experimental variables and their levels are listed in Table 2.1. Oxalic acid was used as a catalyst at was 5% based on the amount of phenol. The liquefied mixture was diluted with methanol and filtered with Whatman medium flow filter paper. The insoluble residues were oven dried at 105 °C overnight and stored in a desiccator. The residue content of the liquefied wood was calculated by equation (1):

$$RC(\%) = \frac{W_r}{W_o} \times 100 \qquad (1)$$

RC is the residue content, W_r is the oven-dried weight of the solid wood residue after the filtration, and W_o is the weight of the original wood powder.

Table 2.1. Liquefaction variables and their levels.

	Cooking Method	Liquefaction Temperature	Phenol to Wood Ratio
1	Atmospheric	150 °C	1/1
2	Sealed	180 °C	2/1
3			3/1

2.2.3 Characterization of liquefied wood

2.2.3.1 Measurement of free phenol by high performance liquid chromatography (HPLC)

The amount of free phenol (i.e., unreacted phenol) in the liquefied wood mixture was measured on a Perkin Elmer series 200 HPLC with an Alltima HP C18 ODS column (250 × 4.6 mm). Methanol/water (1/2, v/v) mixture was used as the mobile phase with a flow rate of 1.0 ml/min. The wavelength of the UV-Vis detector in the HPLC series was set at 272 nm. A series of phenol solutions of known concentration (0.06, 0.1, 0.15, 0.3, 0.5, and 0.7%) were used as the standard to calculate the amount of free phenol. The calibration curve is shown in Figure 2.1.

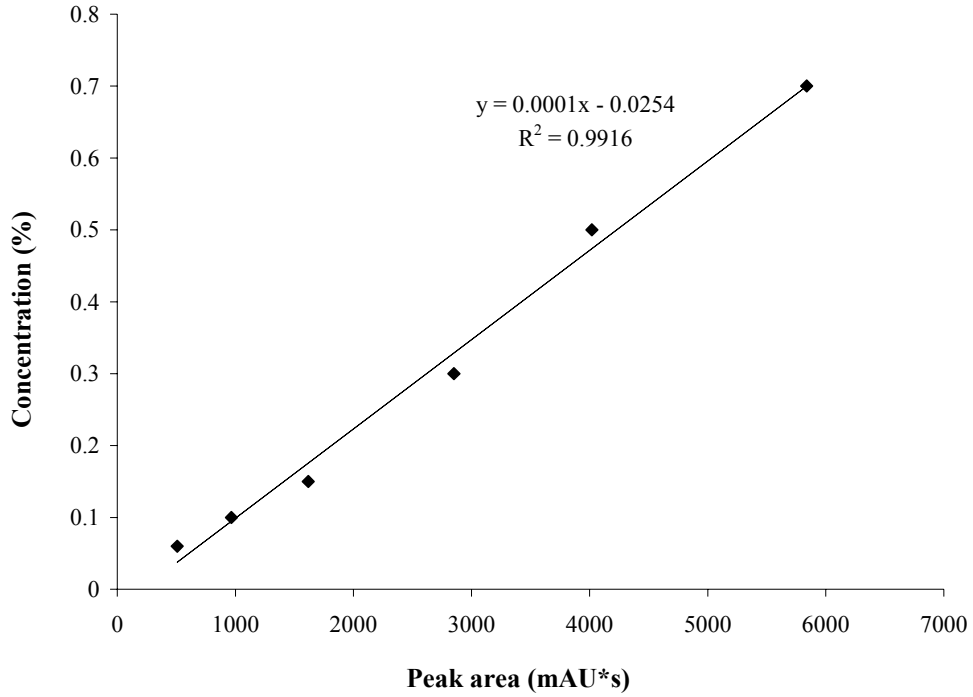

Figure 2.1. Calibration curve of free phenol calculation.

The percent of phenol conversion in the liquefaction reaction was determined by equation 2 as following:

$$Phenol\,Conversion(\%) = \frac{W_t - W_f}{W_t} \times 100 \qquad (2)$$

Where W_t is the total amount of phenol used in the liquefaction, and W_f is the amount of free phenol remained in the liquefied wood mixture.

2.2.3.2 Measurement of molecular weight by gel permeation chromatography (GPC)

The GPC measurements were performed on a Waters-Wyatt GPC system equipped with multi-angle laser light scattering and differential refraction index detectors. Two Jordi Flash Gel Mixed Bed columns (250 × 10 mm) were used in series. Tests were conducted

at ambient temperature using tetrahydrofuran (THF)/methanol (90/10) mixture as the mobile phase at a flow rate of 1.0 ml/min. Liquefied wood samples were dissolved in the same solvent as the mobile phase at a concentration of 5 mg/ml in solution. The amount of each sample injection was 100 µl.

Polystyrene standards with a concentration of 1mg/ml were used for calibration (molecular weight as follows: 393.4k, 223.2k, 111.4k, 44.1k, 31.6k, 13.2k, 3.68k, 2.33k, and 820). The calibration curve was plotted with the logarithm of average molecular weight as a function of elution volume as shown in Figure 2.2.

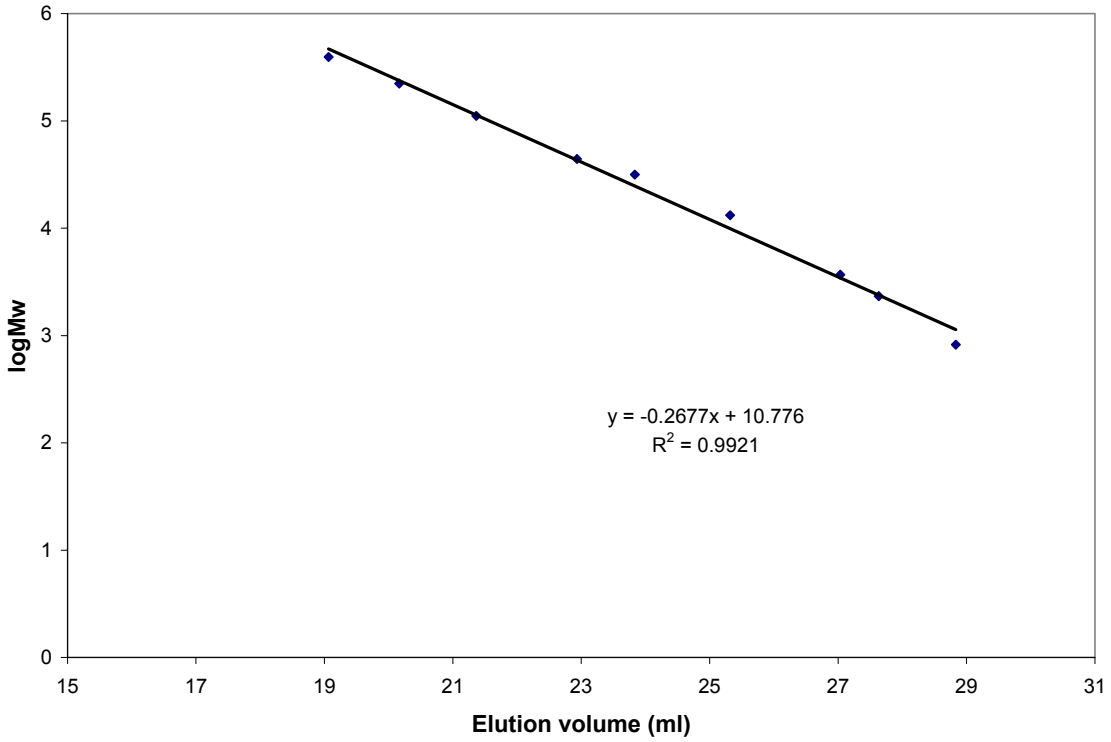

Figure 2.2. Calibration curve of polystyrene standards.

2.2.4 Characterization of liquefied wood residue

2.2.4.1 Chemical analyses

The liquefied wood residues were first extracted in a Soxhlet apparatus to yield extractive-free materials in accordance with ASTM (1996a)[8], Klason lignin (ASTM 1996b)[9], holocellulose (ASTM 1971a)[10], and α-cellulose (ASTM 1971b)[11] were determined based on the extractive-free residues.

2.2.4.2 FT-IR spectroscopy

The FT-IR analysis of the liquefied wood residues was performed by a Nicolet Nexus 670 spectrometer equipped with a Thermo Nicolet Golden Gate MKII Single Reflection ATR accessory. A small amount of residue was applied directly on the diamond crystal.

2.2.4.3 X-ray diffraction analysis

The degree of crystallinity of the residues was measured by X-ray diffraction. The liquefied wood residues from different liquefaction conditions were pressed into disks and analyzed with a PANalytical X´PERTPROSuper X-ray diffractometer. The X-ray diffractograms were recorded from 0 to 40º at a scanning speed of 1º/s and sampling rate of 2 data/s. The crystallinity index (CrI) of the liquefied wood residue was calculated using the Segal method[12] per the following equation:

$$CrI(\%) = \frac{I_{002} - I_{am}}{I_{002}} \times 100 \qquad (3)$$

where I_{002} is the intensity of the diffraction from the (002) plane at 2θ=22.6º, and I_{am} is the intensity of the background scatter measured at 2θ=18.5º.

2.2.4.4 Scanning electron microscopy

A SEI Qanta 200HV scanning electron microscope (SEM) was used to observe the structure and the surface morphology of the liquefied wood residues from different liquefaction conditions. The samples were coated with gold using a vacuum sputter coater before the SEM observations.

2.3 Results and Discussion

2.3.1 Characterization of liquefied wood

2.3.1.1 Residue content and free phenol

The average residue content of liquefied wood from different liquefaction conditions is shown in Figure 2.3. The residue content consistently decreased as the phenol to wood ratio (P/W) increased from 1/1 to 3/1. The liquefied wood reacted in the sealed system had a substantially lower residue content than from the atmospheric system. The reason for this phenomenon can be attributed to the more thorough penetration of phenol into the wood powder in the sealed liquefaction system than in the atmospheric system. Therefore, more reaction sites in the wood powder can be reached by phenol in the former situation. It can also be seen in Figure 2.3 that liquefaction temperature has a significant effect on residue content of the liquefied wood. Liquefied wood reacted at 180 ºC had a lower residue content than that from 150 ºC.

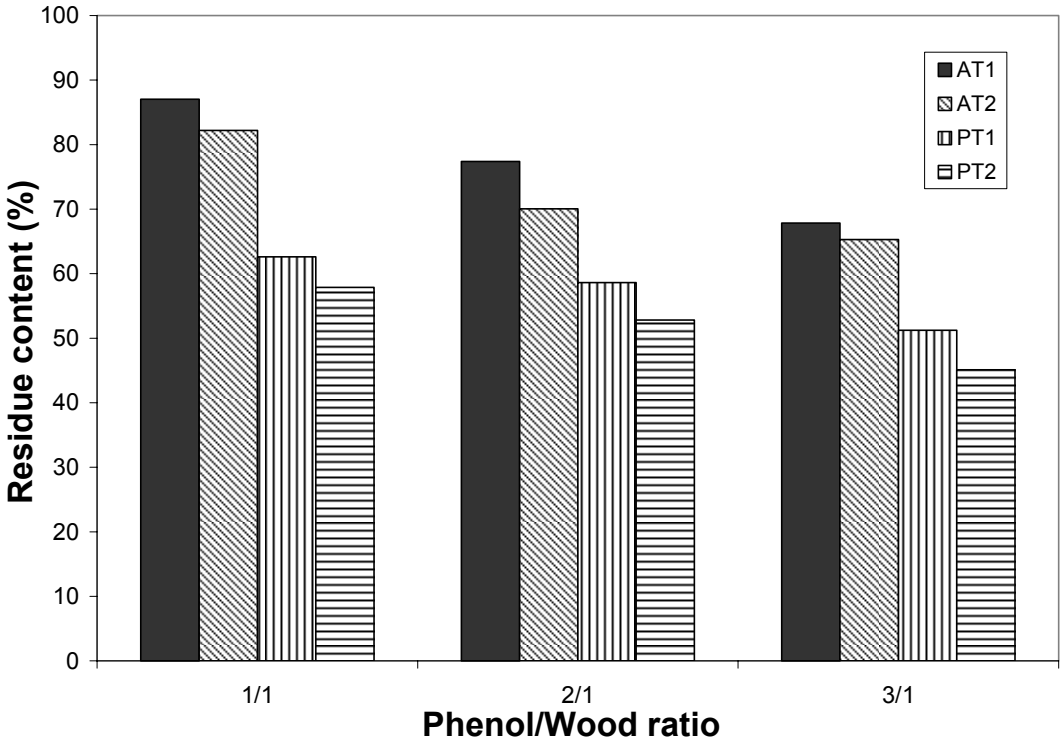

Figure 2.3. Average residue content of liquefied wood residues.(Note AT1 = 150 °C, atmospheric system; AT2 = 180 °C, atmospheric system; PT1 = 150 °C, sealed system; PT2 = 180 °C, sealed system.)

The percentage of free phenol in the liquefied wood mixture and phenol conversion of the liquefaction reaction under different conditions are listed in Table 2.2. The three-way ANOVA results are summarized in Table 2.3. It can be seen that only phenol to wood ratio (P/W) has a significant effect on the percentage of free phenol and phenol conversion. The average amount of free phenol increased and the phenol conversion decreased as the P/W ratio increased. This result was expected since the amount of phenol used in the liquefaction increased. It is not precise simply to use the percent of free phenol and phenol conversion alone as the measurement of the extent of liquefaction. However, the amount of free phenol will affect the polymerization reaction

of liquefied wood mixture and formaldehyde. The details will be discussed in the next chapter.

Table 2.2. Average percentage of free phenol (%) and phenol conversion (%) of the liquefaction reaction.

		150 ˚C			180 ˚C		
		1/1	2/1	3/1	1/1	2/1	3/1
A[a]	Free phenol (%)	56.21	63.02	69.47	55.50	54.73	70.12
	Phenol conversion (%)	33.49	23.05	12.01	22.50	29.10	12.72
P[b]	Free phenol (%)	54.79	51.12	62.80	50.94	64.61	68.28
	Phenol conversion (%)	29.41	35.59	11.40	23.12	13.72	11.71

[a]Liquefaction in the atmospheric three neck flask.
[b]Liquefaction in the sealed Parr reactor.

Table 2.3. ANOVA results on the free phenol and phenol conversion of the liquefaction by GLM procedure.

Source	df	Type III SS	Mean Square	F Value	Pr > F
1. dependent variable: percentage of free phenol					
M[a]	1	0.1708	0.1708	0.00	0.9529
T[b]	1	12.6785	12.6785	0.27	0.6124
P[c]	2	1292.7744	646.3872	13.79	0.0008
M*P	2	44.2110	22.1055	0.47	0.6350
T*P	2	55.1522	27.5761	0.59	0.5704
2. dependent variable: percentage of phenol conversion					
M[a]	1	10.4804	10.4804	0.15	0.7062
T[b]	1	171.4900	171.4900	2.44	0.1444
P[c]	2	1101.4389	550.7194	7.83	0.0067
M*P	2	0.8692	0.4346	0.01	0.9938
T*P	2	103.4169	51.7084	0.74	0.4998

[a]Reactor type.
[b]Liquefaction temperature.
[c]Phenol to wood ratio.

2.3.1.2 Molecular weight and molecular weight distribution of the liquefied wood

The number average molecular weight (Mn), weight average molecular weight (Mw), and the polydispersities (Mn/Mw) of the liquefied wood are summarized in Table

2.4. For the liquefaction conducted in the atmospheric three neck flask, the liquefied wood had slightly higher Mn, Mw, and Mw/Mn at 180 ˚C than at 150 ˚C. It is known that lignin is very susceptible to the liquefaction reaction, and decomposed lignin has a tendency to undergo a re-condensation reaction.[13, 14] It is possible that a re-condensation reaction would be favored under higher liquefaction temperatures and result in higher average molecular weight. In the sealed Parr reactor, the average molecular weight of the liquefied wood decreased as the P/W ratio increased. It might be expected that the sealed Parr reactor provided a more severe reaction condition than the atmospheric three neck flask under the same liquefaction temperature. Therefore, the re-condensation reaction could occur at lower temperatures in the Parr reactor. However, an excessive amount of phenol could effectively retard the re-condensation of the decomposed wood components and prevent the increase in the molecular weight of the resulting liquefied wood.[4]

Table 2.4. Average molecular weight and polydispersity (Mw/Mn) of the liquefied wood.

		Three neck flask[a]			Parr reactor[a]		
	P/W[b]	Mn	Mw	Mw/Mn	Mn	Mw	Mw/Mn
150 ˚C[c]	1/1	939.8	1386.0	1.47	1041.2	1570.6	1.51
	2/1	952.2	1681.0	1.77	1023.4	1566.1	1.53
	3/1	957.2	1477.8	1.54	960.9	1489.0	1.55
180 ˚C[c]	1/1	1071.6	1683.3	1.57	1038.5	2024.2	1.95
	2/1	1076.6	1694.6	1.57	1011.9	1560.3	1.54
	3/1	1057.9	1666.4	1.58	967.6	1384.7	1.43

[a]Two types of reactors used in wood liquefaction reaction.
[b]Phenol to wood ratio in wood liquefaction reaction.
[c]Temperature of wood liquefaction reaction.

2.3.2 Characterization of liquefied wood residue

2.3.2.1 Chemical analyses

Table 2.5 presents the mean values of Klason lignin, holocellulose, and α-cellulose contents of the liquefied wood residues from different liquefaction conditions. In general, the Klason lignin contents of the liquefied wood residue consistently decreased as P/W ratio increased and were lower than that of the original Chinese tallow tree wood (20.3%)[15] except for the residue from P/W ratio 1/1 in the sealed system. The liquefied wood residue yielded a lower Klason lignin content at the higher temperature in the atmospheric system. These results were consistent with the residue content of the liquefied wood (Figure 2.3) because the high temperature and P/W ratio were expected to promote the extent of the wood liquefaction reaction,[16] and lignin is the most reactive wood component in the liquefaction reaction.[13] However, the liquefied wood residue in the sealed system yielded extremely high Klason lignin contents at P/W ratio 1/1. A possible explanation to this phenomenon might be the recondensation reaction of the decomposed lignin units. Several studies reported that the monomeric units of lignin have a tendency to undergo secondary condensation reactions.[14,17] Pu[13] found that the Klason lignin content of the residue gradually increased at lower P/W ratios with an increase in reaction time. Furthermore, Lin[16] reported that guaiacol, an intermediate of the liquefaction reaction of the lignin model compound guaiacylglycerol-β-guaiacyl ether (GG), mostly remained intact in the reaction because of the existence of an excess amount of phenol which competed with it in the nucleophilic reaction. Therefore, with an increase in P/W ratio, the excess amount of phenol can also retard the tendency of the lignin re-condensation reaction. However, in the process of solvolysis during wood

liquefaction, it is also possible that the phenol reacted with the dissolved lignin to form an intermediate insoluble new substance that was retained in the residue which in turn effected the Klason lignin determination.

Table 2.5. Mean chemical composition value of liquefied wood residues (The numbers in the parentheses are standard deviations).

P/W	Klason Lignin (%)		Holocellulose (%)		α -cellulose (%)	
	150 °C	180 °C	150 °C	180 °C	150 °C	180 °C
Atmospheric cooking						
1/1	17.65(0.57)	15.44(0.29)	69.78(0.41)	71.65(0.43)	42.80(1.09)	47.06(0.25)
2/1	13.25(0.91)	9.16(0.20)	73.68(0.89)	81.25(0.13)	49.38(0.05)	54.09(0.12)
3/1	10.04(0.34)	7.41(0.36)	79.68(0.36)	82.05(0.19)	52.46(0.17)	51.48(0.49)
Sealed cooking						
1/1	26.67(0.45)	40.35(0.59)	63.93(0.16)	53.76(1.57)	39.42(0.32)	30.09(0.15)
2/1	10.63(0.16)	18.98(0.60)	83.56(0.41)	75.86(0.33)	54.63(2.41)	48.33(0.78)
3/1	2.92(0.21)	1.42(0.49)	92.85(0.17)	92.17(0.48)	60.39(0.73)	53.74(0.11)

Holocellulose consists of hemicellulose and cellulose. As listed in Table 2.5, the average holocellulose content in the residue increased as the P/W ratio increased. The residues from the higher liquefaction temperature (e.g., 180 ºC) had a higher mean holocellulose content than from the lower temperature (e.g., 150 ºC) in the atmospheric liquefaction system. The result is the opposite in the sealed liquefaction system. As mentioned above, lignin is the most susceptible component in wood that reacts with phenol during liquefaction.[13] The higher the reaction temperature, the more lignin was removed from the wood and dissolved into the solvent, and therefore the relatively higher amount of residual holocellulose. Several studies have reported that the thermal degradation of wood occurs at around 200 ºC.[18, 19] However, the effect of temperature on thermal degradation of wood differs between wood species, and the characteristics of

thermal degradation of the three wood components are different from each other. In general, the thermal degradation of lignin, hemicellulose, and cellulose occurs at around 100, 200, and 300 ºC, respectively.[18] However, with the additional factor of pressure associated with temperature in the reaction, thermal degradation in wood can be observed as low as 100 ºC.[19] The research of Stamm[20] showed that heating in a sealed system causes more rapid degradation than heating in an open system. Therefore, the severe thermal degradation of holocellulose at 180 ºC in a sealed reaction system could be the reason for the lower holocellulose content compared to that of the atmospheric system.

The α-cellulose content of the residue showed a very similar trend as the holocellulose content. The influence of P/W ratio, liquefaction temperature, and cooking method on α-cellulose content of the residue are also similar with those of holocellulose and were discussed in the previous paragraph. The only difference between these two contents is that the residues from the higher liquefaction temperature (e.g., 180 ºC) consistently had a lower α-cellulose content than those at a liquefaction temperature of 150 ºC, which could also be due to the degradation of cellulose at higher temperature.

2.3.2.2 FT-IR spectroscopy

FT-IR spectra of woody materials are complex due to the various functional groups that exist in wood components and the complicated chemical environment of the wood components. Many peaks in wood IR spectra are broad and often overlap with neighboring peaks. However, the FT-IR spectra of the residues from atmospheric and sealed cooking systems did show some differences between each other and to that of the original wood (Figure 2.4). A broad peak at around 3328 cm^{-1} is due to the –OH groups

either from carbohydrates or lignin.[21, 22] The peak at 2900 cm^{-1} represents the C-H stretch in methyl and methylene groups.[23] These two peaks were exhibited in every individual spectrum of the residue from the different liquefaction conditions.

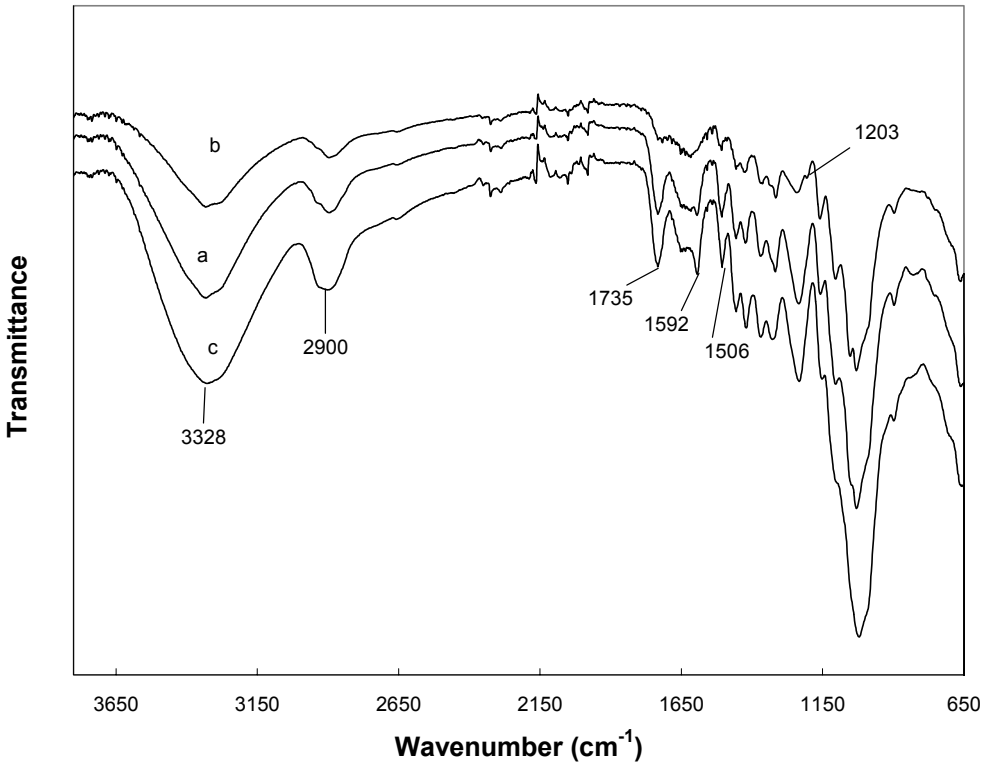

Figure 2.4. FT-IR spectra of residues from atmospheric (spectrum a), sealed cooking (spectrum b), and untreated wood (spectrum c). The P/W ratio was 1/1 and liquefaction temperature was 150 °C.

An intense absorbance at 1735 cm^{-1} occurred in both the spectra of the original wood and the residues from the atmospheric liquefaction systems, while it became a small shoulder or even disappeared (spectra not shown) in the spectra of residues from the sealed liquefaction systems. This indicates different liquefaction reactions under a pressurized metal reactor versus an atmospheric glass reactor. It is known that the absorption bands from 1710 to 1740 cm^{-1} mainly arise from the carbonyl (C=O) stretch in unconjugated ketone, ester, or carboxylic groups in carbohydrates and not from

lignin.[21, 24] It is also known that carbonyl groups occur abundantly with the methyl and acetyl ester groups in pectin, the acetyl ester groups in xylan, and in the oxidative products of cellulose.[25-27] However, the wood species used in this experiment, Chinese tallow tree (*Triadica sebifera* syn. *Sapium sebiferum),* is not rich in pectin,[15] and the most profound effects of cellulose oxidation occur at 250 °C,[26] which is far beyond the temperature used in this experiment. Consequently, the absorbance band at 1735 cm^{-1} in the spectra in this experiment is most likely attributed to the ester carbonyl group in xylan. The phenomenon of the absence of the 1735 cm^{-1} band in the spectra of the residue from the sealed liquefaction system is very similar to that of the wood or other natural cellulosic fiber treated with sodium hydroxide (NaOH).[28,29] This phenomenon of alkali treated natural fibers has been interpreted as the hydrolysis of the ester linkages in the xylan.[30] Xylans are closely associated with other plant cell wall constituents, such as lignin and pectic polysaccharides, by ferulic acid or uronic acid through ester linkages.[31, 32] In the presence of alkalis, the hydroxyl ions cause the saponification of these ester linkages and peel off the hemicellulose from their neighboring lignin or cellulose into solution.[33, 34]

Compared to the reaction conditions of the atmospheric liquefaction in the three neck flask, the disappearance of peak 1735 cm^{-1} in the sealed Parr reactor system could be due to the pressurized effect or the catalytic effect of the elements associated with the internal lining of the Parr reactor during the liquefaction process. To explore these two possible effects, a reaction of wood liquefaction was conducted in a sealed glass tube under the same conditions used in the liquefaction in a Parr reactor. Figure 2.5 shows the

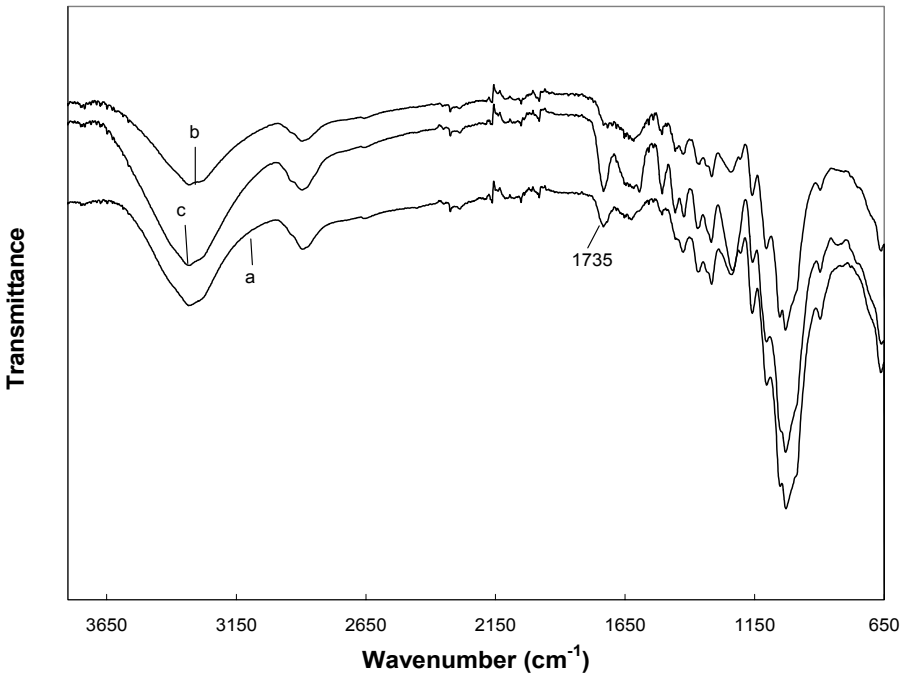

Figure 2.5. FT-IR spectra of residues from sealed glass tubing reactor (spectrum a), Parr reactor (spectrum b), and three neck flask (spectrum c).

spectrum of the LWR from three different reactors (i.e., a sealed glass tube, a Parr reactor, and a three neck flask reactor). By comparison of spectrum a (sealed glass tube) and spectrum c (three neck flask reactor), the similarity of a strong absorbance at 1735 cm^{-1} in both spectra indicates that the effect of pressure was not the cause of the breaking of the carbonyl bonds in the hemicellulose. Therefore, the catalytic effects of some metal elements associated with the Parr reactor is likely the main reason that caused the breaking of the ester carbonyl bonds in the hemicellulose during the liquefaction process.

The Parr reactor used in this experiment was made from stainless steel T316, composed of iron (65%), nickel (12%), chromium (17%), molybdenum (2.5%), manganese (2%), and silicon (1%).[35] It is well known that iron can be easily oxidized to Fe^{2+} or Fe^{3+} ions under acidic conditions, corresponding to the conditions used in this

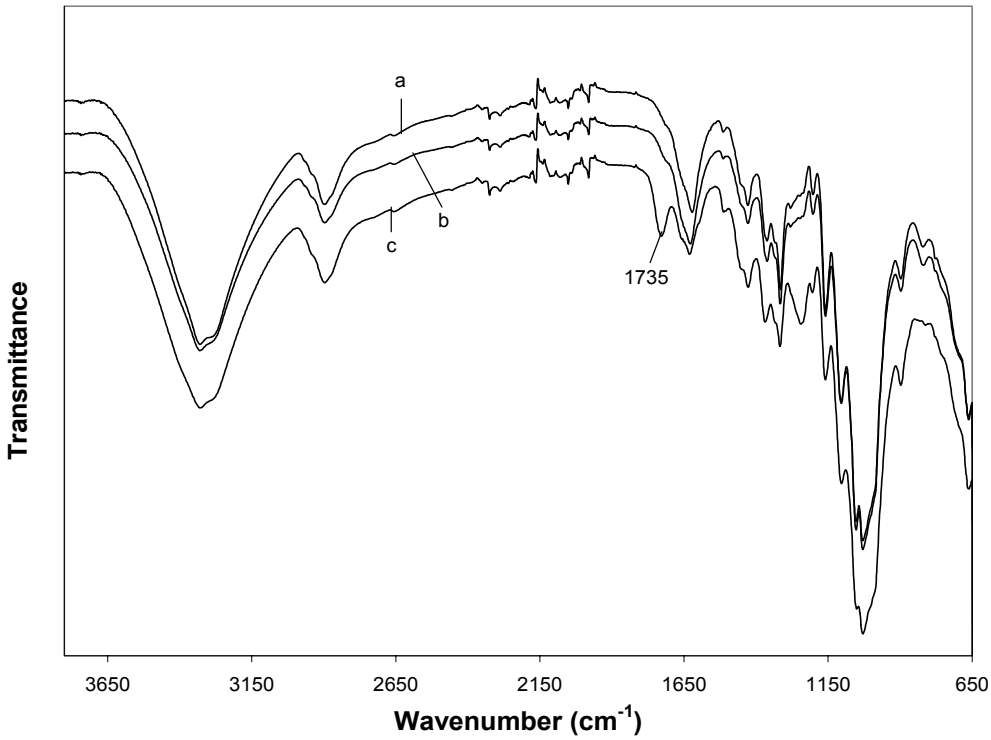

Figure 2.6. FT-IR spectra of the liquefied wood residues from sealed glass tubing reactor with the addition of $FeCl_2$ (spectrum a), $FeCl_3$ (spectrum b) and untreated tallow wood particles (spectrum c). P/W ratio was 1/1 and liquefaction temperature was 150 °C.

experiment. In addition, iron is more active than most other metal elements present in the Parr reactor, and it constitutes the major element in T316 stainless steel. Therefore, it is postulated that Fe^{2+} and/or Fe^{3+} ions were the possible catalysts that helped to break the ester bond in xylan. Thus, a further experiment of wood liquefaction was conducted with the addition of a small amount of $FeCl_2$ or $FeCl_3$ in a sealed glass tube. Figure 2.7 shows the FT-IR spectra of the LWR with the addition of iron additives and untreated tallow wood particles. It can be seen that the 1735 cm^{-1} peak disappeared in the spectra of LWR with $FeCl_2$ and $FeCl_3$. Based on the above results, it is very likely that Fe^{2+} and/or Fe^{3+} ions released from the internal walls of the Parr reactor helped to break down the ester carbonyl bond in the xylan during the acidic wood liquefaction reaction and caused the differences in the FT-IR spectra between the liquefied wood residue from the Parr reactor

and the three neck flask. Some researchers have reported that some transition metals, especially iron species, can be used as redox catalysts in the pyrolysis of brown coal and the oxidation of phenol.[36,37] However, no research on the catalytic effect of iron ions on wood liquefaction has been reported yet. Further study is needed to study this possibility.

The absorbance at 1592 and 1506 cm^{-1} correspond to aromatic skeletal (lignin) vibrations.[21] In general, the intensities of these peaks diminished in the spectra of the liquefied wood residue from the atmospheric conditions and almost disappeared in that of the sealed condition, suggesting that the lignin might react to a greater extent under the sealed liquefaction conditions than the atmospheric condition.

The spectra of the liquefied wood residue from different P/W ratios are shown in Figure 2.7. It can be seen that the spectra were very similar except that the intensities at peak 1203 cm^{-1} increased as the P/W ratio increased. Meanwhile, this peak was absent in the spectra of the original wood and the residue from the atmospheric system (Figure 2.4). The absorbance at 1203 cm^{-1} is due to the –OH plane deformation,[21] indicating that this peak might be related to the phenol-lignin complex retained at the residue.

It is interesting to note that the FT-IR analysis of the lignin component of the residue has led to some indications that the spectral changes in the regions 1592, 1506, and 1203 cm^{-1} were related to the mechanism and characteristics of wood liquefaction. As discussed earlier, however, the determination of lignin content of the liquefied wood residue was related to the amount of the lignin dissolved into the liquefied wood, the extent of the recondensation reaction among the decomposed lignin, and the formation of the insoluble intermediate compounds from the reaction of the phenol and the dissolved

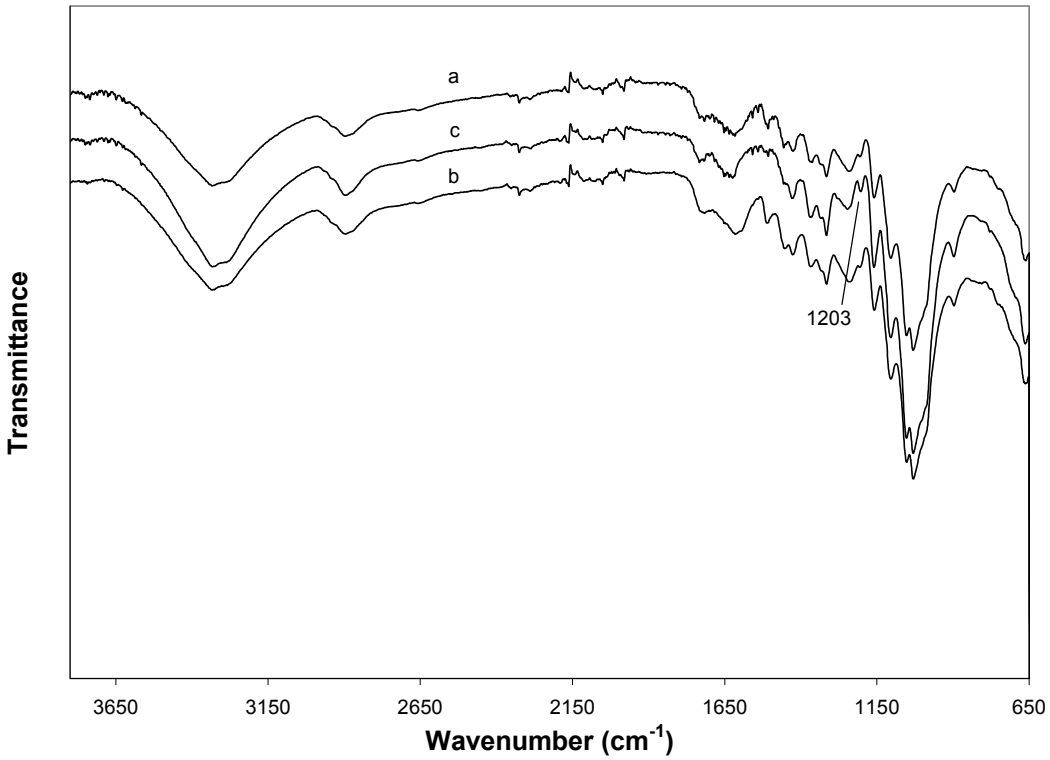

Figure 2.7. FT-IR spectra of residues from P/W ratio of 1/1 (spectrum a), 2/1 (spectrum b), and 3/1 (spectrum c) in a sealed liquefaction system at temperature of 150 °C.

lignin. Therefore, the extent of the effects of these reactions on the FT-IR spectra are rather complex and difficult to thoroughly understand. In order to clarify and characterize the possible formation of phenol-lignin compounds and/or recondensation of the decomposed lignin, it is necessary to apply qualitative and quantitative analysis by classical chemical methods together with HPLC and GC-MS. Such experimentation is under consideration.

No significant differences in the spectra of the residues from different temperature were observed (spectra not shown).

2.3.2.3 X-ray diffraction

The liquefied wood residue displayed a typical X-ray diffractogram pattern as that of cellulose I (Figure 2.6). In particular, the major diffraction planes of cellulose, namely 101,10$\bar{1}$, 002, and 040 are present at diffraction angles 2θ around 14.9, 16.3, 22.5, and 34.6 °, respectively.[38] However, unlike a pure cellulose sample, the peaks of 101 and 10$\bar{1}$ diffraction planes in the X-ray diffractograms of liquefied wood residue overlapped with each other and formed one broad peak. This phenomenon was also reported by other researchers[39, 40] and is likely caused by the existence of a small amount of hemicellulose and lignin in the liquefied wood residue.

Table 2.6. The X-ray crystallinity index (CrI, %) of the LWR from different liquefaction conditions. (The number in the parentheses are the standard deviation of the CrI value.)

Liquefaction temperature	150 °C			180 °C			Original wood particle
Phenol/wood ratio (w/w)	1/1	2/1	3/1	1/1	2/1	3/1	
Atmospheric system	55.11 (1.37)	60.18 (0.67)	59.59 (1.58)	58.14 (1.77)	62.60 (2.01)	61.09 (0.21)	45.85 (1.73)
Sealed system	54.86 (0.89)	62.43 (0.71)	63.72 (0.90)	48.44 (1.01)	60.98 (1.24)	65.87 (1.04)	

The X-ray crystallinity index (CrI) of the liquefied wood residues from different liquefaction conditions are listed in Table 2.8. In general, the CrI of the liquefied wood residue is higher than that of the original wood powder and increased as the P/W ratio

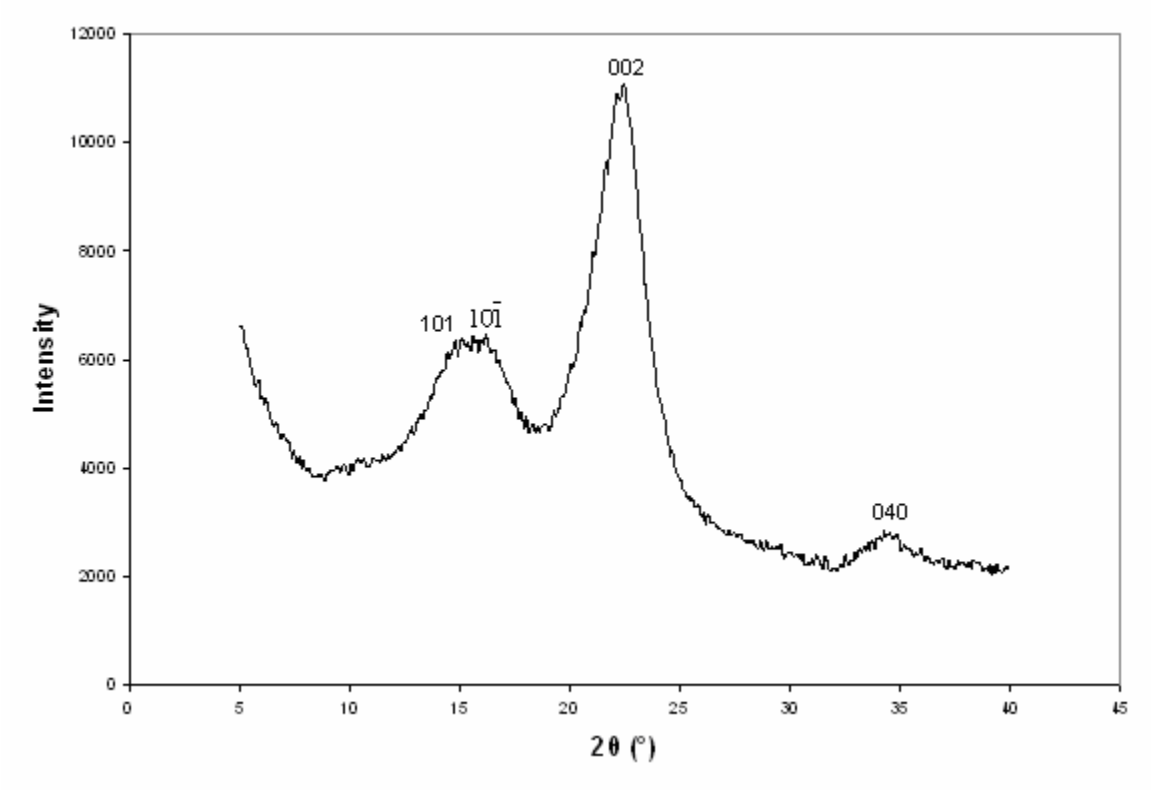

Figure 2.8. Typical XRD diffractogram of the liquefied wood residue.

increased from 1/1 to 3/1 except for the CrI values of the residue at P/W ratio 2/1 and 3/1 were very close in the atmospheric system. This result was expected because of the increasing amount of lignin that was removed from the amorphous region of the liquefied wood residue as the P/W ratio increased during the liquefaction process (Table 2.5). It is important to note that the CrI is used to indicate the relative, rather than the absolute, amount of the crystalline region in cellulose.[39] Therefore, when the lignin in the amorphous region decreased, the relative portion of the crystalline region of cellulose increased. A similar result was also found by other researchers.[41] It is also noted that the residue from the Parr reactor with a P/W ratio of 1/1 had the lowest crystallinity index (CrI) and the highest lignin content. The recondensed lignin should still be a highly branched amorphous polymer. Therefore, the low CrI of the residues from the Parr

reactor at P/W ratio 1/1 might be due to the high amount of recondensed lignin left in the residue, indicating a more severe lignin recondensation reaction in the Parr reactor than the three neck flask. The CrI result of the liquefied wood residue is very consistent with the α-cellulose content of the liquefied wood residue (Table 2.5). The higher the α-cellulose content in the liquefied wood residue, the higher the CrI value of the liquefied wood residue. In addition, the XRD result of the liquefied wood residue also gives a piece of supporting evidence for an explanation to the result in our previous study.[42] Namely, the liquefaction rate of the three wood components is in a decreasing order of hemicellulose, lignin, amorphous cellulose, and crystalline cellulose. There is no obvious evidence in this experiment of the liquefaction rate of hemicellulose. However, the lignin did undergo a faster liquefaction rate than the cellulose, thus leaving the crystalline cellulose almost intact in the liquefied wood residue since the crystalline structure in cellulose greatly limits the access to β-1,4-glycosidic bonds by reactants and catalysts.[43] In fact, water is almost completely excluded from the crystalline region in cellulose.[43] Conversely, the amorphous part of cellulose is more readily accessible by water and other reactants.[44]

2.3.2.4 Scanning electron microscopy

The SEM images of the original wood powder and the liquefied wood residues from P/W ratio 1/1 to 3/1 are shown in Figure 2.7a-d. The surface of the original wood powder is rough and many small fragments of cell wall components are present due to the mechanical processing procedures (Figure 2.7a). As seen from Figure 2.7b, most small fragments attached on the surface of the wood powder have been removed at the P/W

ratio 1/1, but the liquefied wood residue mostly remained in its original fiber bundles. As the P/W ratio increased to 2/1 and 3/1, the fiber bundles started to break down from the two ends to reduce the size of the fiber bundles mainly because the chemical penetration in the longitudinal direction is known to be several times greater than that across the grain of the fiber bundles. As the P/W ratio increased, eventually the bundles were broken down to individual fibers because the lignin, which works as the binding and supporting material in the middle lamella in wood tissue, had been gradually removed, starting from the outer layer and progressing to inside of the fiber bundles (Figure 2.9c-d). These results also correspond well with that of the chemical analyses and X-ray diffraction.

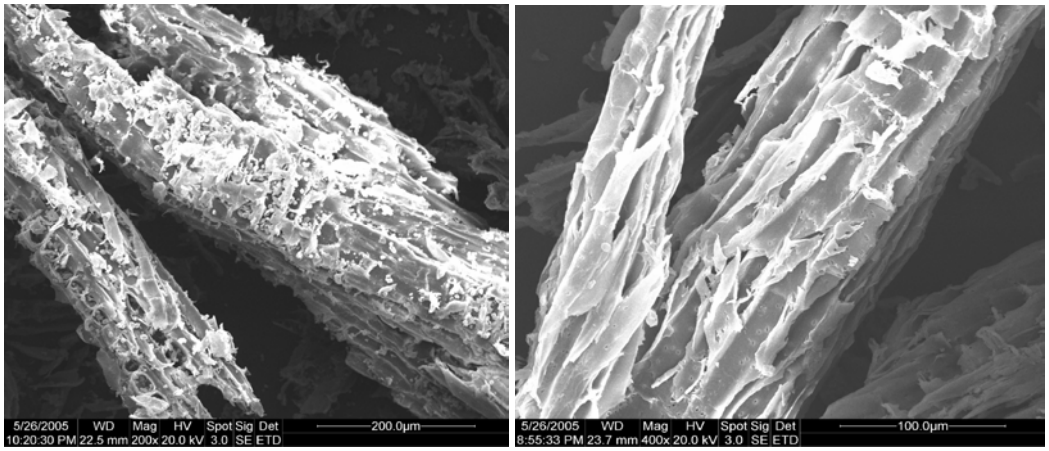

(a) (b)

Figure 2.9. SEM micrographs of the original Chinese tallow tree wood (a), the liquefied wood residue at P/W ratio 1/1 (b), 2/1 (c), and 3/1 (d). (figure continued)

2.4 Conclusions

The percentage free phenol in the liquefied wood mixture increased while the phenol conversion decreased with the increase of the P/W ratio. The liquefied woods

(c)

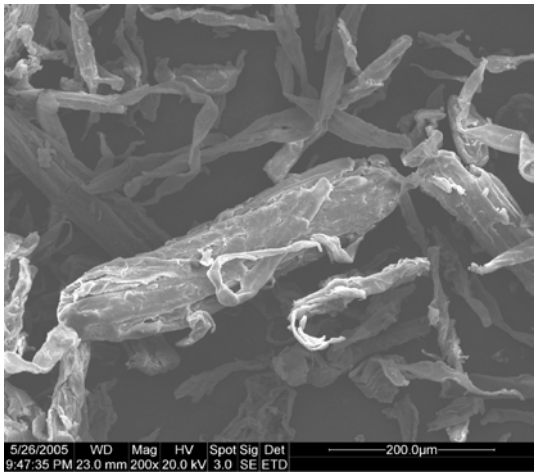

(d)

made in the atmospheric three neck flask have higher average molecular weight under higher liquefaction temperature. The average molecular weight of the liquefied wood conducted in the sealed Parr reactor decreased as the P/W ratio increased.

All three experimental variables (e.g., P/W ratio, liquefaction temperature, and cooking method) had significant effects on the characteristics of the liquefied wood residues. Higher P/W ratio and temperature resulted in lower residue content in the sealed liquefaction system. Lignin is the most susceptible wood component to the liquefaction reaction among the three main wood components and can be mostly removed from wood at a P/W ratio of 3/1 in a sealed reaction system. However, lignin also undergoes a recondensation reaction when there is insufficient reagent solvent (i.e., phenol) in the sealed reaction system. The holocellulose and α-cellulose contents of the residues increased with the increase of P/W ratio, which is consistent with the decrease of Klason lignin content. The difference in the FT-IR spectra of the residues from atmospheric and sealed cooking also confirms the significant effects of these two cooking methods on wood liquefaction and the characteristics of the residues. The CrI of

liquefied wood residue is higher than original wood powder and slightly increased as the P/W ratio increased, indicating that lignin undergoes a faster liquefaction rate than crystalline cellulose.

2.5 References

1. Lee, S. H., and Wang, S. Q. 2005. Effect of water on wood liquefaction and the properties of phenolated wood. Holzforschung 59: 628-634.

2. Alma, M. H., Yoshioka, M., Yao, Y., and Shiraishi, N. 1995. Preparation and characterization of phenolated wood using hydrochloric acid as a catalyst. Wood Sci. Technol. 29: 39-47.

3. Alma, M. H., Yoshioka, M., Yao, Y., and Shiraishi, N. 1998. Preparation of sulfuric acid catalyzed phenolated wood resin. Wood Sci. Technol. 32: 297-308.

4. Lin, L., Yao, Y., Yoshioka, M., and Shiraishi, N. 1997. Molecular weights and molecular weight distributions of liquefied wood obtained by acid catalyzed phenolysis. J. Appl. Polym. Sci. 64(7): 351-357.

5. Alma, M. H., Yoshioka, M., Yao, Y., and Shiraishi, N. 1996. The preparation and flow properties of HCl catalyzed phenolated wood and its blends with commercial Novolak resin. Holzforschung 50: 85-90.

6. Lin, L., Yao, Y., Yoshioka, M., and Shiraishi, N. 2001. Liquefaction mechanism of β-O-4 lignin model compound in the presence of phenol under acid catalysis. I. Structural characterization of the reaction products. Holzforschung 55: 617-624.

7. Lin, L., Yao, Y., Yoshioka, M., and Shiraishi, N. 2001. Liquefaction mechanism of β-O-4 lignin model compound in the presence of phenol under acid catalysis. Part 2. Reaction behavior and pathway. Holzforschung 55: 625-630.

8. American Society for Testing and Materials (ASTM). 1996. Standard test method for preparation of extractive-free wood. ASTM D 1105-96.

9. American Society for Testing and Materials (ASTM). 1996. Standard test method for acid-insoluble lignin in wood. ASTM D 1106-96.

10. American Society for Testing and Materials (ASTM). 1971a. Standard method of test for holocellulose in wood. ASTM D 1104-56.

11. American Society for Testing and Materials (ASTM). 1971b. Standard method of test for α-cellulose in wood. ASTM D 1103-60.

12. Segal, L., Creely, J.J., Martin, A.E., and Conrad, C.M. 1959. An empirical method for estimating the degree of crystallinity of native cellulose using the X-ray diffractometer. Textile Res J. 29: 786-794.

13. Eberhardt, T.L., Li, X., Shupe, T.F., and Hse, C.Y. 2007. Chinese tallow tree utilization: characterization of extractives and cell wall chemistry. Wood Fiber Sci. in press.

14. Lin, L.Z. 1996. Characterization of phenolated wood and study on the liquefaction mechanism of lignin. Ph.D dissertation, Kyoto University.

15. Pu, S., and Shiraishi, N. 1993. Liquefaction of wood without a catalyst I. time course of wood liquefaction with phenols and effects of wood/phenol ratios. Mokuzai Gakkaishi 39(4): 446-452.

16. Sarkanen, K.V. 1963. In Wood Chemistry, Browning, B. L., Ed.; Interscience publisher: New York, Chap. 5.

17. Kobayashi, M., Asano, T., Kajiyama, M., and Tomita, B. 2004. Analysis on residue formation during wood liquefaction with polyhydric alcohol. J. Wood Sci. 50: 407-414.

18. Elder, T. 1990. In Wood and Cellulosic Chemistry, Hon, D.; Shiraishi, N., Ed.; Marcel Dekker: New York.

19. Fengel, D.; Wegener, G. 1984. Wood Chemistry, Ultrastructure, Reactions; Walter de Gruyter: Berlin and New York, 319p.

20. Stamm, A. J. 1964. Wood and Cellulose Science; The Ronald press company: New York, 305p.

21. Schwanninger, M., Rodrigues, J.C., Pereira, H., and Hinterstoisser, B. 2004. Effects of short-time vibratory ball milling on the shape of FT-IR spectra of wood and cellulose. Vib Spectrosc. 36: 23-40.

22. Faix, O. 1991. Classification of lignin from different botanical origins by FT-IR spectroscopy. Holzforschung 45(Suppl.): 21-27.

23. Vázquez, G.; Antorrena, G.; Freire, S. 1997. FTIR, 1H and 13C NMR characterization of acetosolv-solubilized pine and eucalyptus lignins. Holzforschung 51:158-166.

24. Hoareau, W., Trindade, W.G., Siegmund, B., Castellan, A., and Frolini, E. 2004. Sugar cane bagasse and curaua lignins oxidatized by chlorine dioxide and reacted with furfuryl alcohol: characterization and stability. Polym. Degrad. Stab. 86: 567-576.

25. Sun, R.C., Fang, J.M., Goodwin, A., Lawther, J.M., and Bolton, A.J. 1998. Factionation and characterization of polysaccharides from abaca fiber. Carbohydr. Polym. 37: 351-359.

26. Bjarnestad, S., and Dahlman, O. 2002. Chemical compositions of hardwood and softwood pulps employing photoacoustic Fourier transform infrared spectroscopy in combination with partial least-squares analysis. Anal. Chem. 74: 5851-5858.

27. Lojewska, J., Miskowiec, P., Lojewski, P., and Proniewicz, L.M. 2005. Cellulose oxidative and hydrolytic degradation: In situ FTIR approach. Polym. Degrad. Stab. 88: 512-520.

28. Sun, J.X., Mao, F.C., Sun, X.F., and Sun, R.C. 2004. Comparative study of hemicelluloses isolated with alkaline peroxide from lignocellulosic materials. J. Wood Chem. Technol. 24: 239-262.

29. Mwaikambo, L.Y., and Ansell, M.P. 2002. Chemical modification of hemp, sisal, jute, and kapok fibers by alkalization. J. Appl. Polym. Sci. 84:2222-2234.

30. Cyran, M., Courtin, C.M., and Delcour, J.A. 2004. Heterogeneity in the fine structure of alkali-extractable arabinoxylans isolated from two rye flours with high and low breadmaking quality and their coexistence with other cell wall components. J. Agric. Food. Chem. 52: 2671-2680.

31. Kacurakova, M., Wellner, N., Ebringerova, A., Hromadkova, Z., Wilson, R.H., and Belton, P.S. 1999. Characterization of xylan-type polysaccharides and associated cell wall components by FT-IR and FT-Raman spectroscopies. Food Hydrocolloids 13: 35-41.

32. Sun, R.C., Fang, J.M., Rowlands, P., and Bolton, J. 1998. Physicochemical and thermal characterization of wheat straw hemicelluloses and cellulose. J. Agric. Food Chem. 46: 2804-2809.

33. Sun, R.C., and Hughes, S. 1999. Fractional isolation and physic-chemical characterization of alkali-soluble polysaccharides from sugar beet pulp. Carbohydr .Polym. 38: 273-281.

34. Xu, F., Sun, J.X., Liu, C.F., and Sun, R.C. 2006. Comparative study of alkali- and acidic organic solvent-soluble hemicellulosic polysaccharides from sugarcane bagasse. Carbohydr. Res. 341: 253-261.

35. Parr Instrument Co. 2006. http://www.parrinst.com/default.cfm?page_id=107

36. Domazetis, M., Raoarun, M., and James, B.D. 2006. Low-temperature pyrolysis of brown coal containing iron hydroxyl complexes. Energy Fuels 20:1997-2007.

37. Calleja, G., Melero, J.A., Martinez, F., and Molina, R. 2005. Activity and resistance of iron-containing amorphous, zeolitic and mesostructured materials for wet peroxide oxidation of phenol. Water Res. 39:1741-1750.

38. Freire, C. S. R.; Silvestre, A. J. D.; Neto, C. P.; Belgacem, M. N.; Gandini, A. 2006. Controlled heterogeneous modification of cellulose fibers with fatty acids: effect of reaction conditions on the extent of esterification and fiber properties. J Appl Polym Sci. 100:1093-1102.

39. Ouajai, S., and Shanks, R.A. 2005. Composition, structure and thermal degradation of hemp cellulose after chemical treatments. Polym. Degrad. Stab. 89: 327-335.

40. Garvey, C. J.; Parker, I. H.; Simon, G. P. 2005. On the interpretation of X-ray diffraction powder patterns in terms of the nanostructure of cellulose I fibers. Macromol Chem Phys. 206:1568-1575.

41. Trindade, W.G., Hoareau, W., Megiatto, J.D., Razera, A.T., Castellan, A., and Frollini, E. 2005. Biomacromolecules 6: 2485-2496.

42. Pan, H.; Shupe, F. T.; Hse, C. Y. 2005. Preliminary investigation of bio-composites fabricated from liquefied wood, phenol, formaldehyde co-condensation resin. In Wood Adhesive 2005, San Diego, 257p.

43. Zhao, H., Kwak, J.H., Wang, Y., Franz, J A., White, J.M., and Holladay, J.E. 2006. Effects of crystallinity on dilute acid hydrolysis of cellulose by cellulose ball-milling study. Energy Fuels 20: 807-811.

44. Vittadini, E., Dickinson, L.C., and Chinachoti, P.C. 2001. ^{1}H and ^{2}H NMR mobility in cellulose. Carbohydr. Polym. 46: 49-57.

CHAPTER 3

SYNTHESIS, CHARACTERIZATION, AND CURE KINETICS OF NOVOLAC TYPE LIQUEFIED WOOD RESIN

3.1 Introduction

The technique of wood liquefaction in the presence of phenol with oxalic acid as a catalyst and the characterization of liquefied wood and liquefied wood residue have been discussed in the previous chapter. Liquefied wood can be applied as a precursor in preparing various products, such as phenolic resins and polyurethane foams, depending on the reagent solvent used in the liquefaction. Novolac type liquefied wood resin (LWR) can be prepared from the condensation reaction of formaldehyde and liquefied wood using phenol as the reagent solvent. Some studies have been done to investigate the effects of several variables, such as phenol to formaldehyde molar ratio, and catalyst concentration on the physical properties of LWR and mechanical properties of the molded products from LWR.[1-3] It has been reported that the further condensation reaction of liquefied wood and formaldehyde is an effective method to convert the unreacted phenol (i.e., free phenol) remaining from the liquefaction stage and therefore, greatly improve the thermal flow properties and the mechanical properties of the original liquefied wood.[2]

A comprehensive understanding of the cure kinetics of a resin is crucial for the optimization of bond strength of the resin and the mechanical properties of the products. An accurate cure kinetic model helps to predict the cure behavior of the resin for process design and control, and thus optimize the cure process. Differential scanning calorimetry (DSC) has been an universal tool to elucidate key cure process parameters such as the

extent and rate of chemical conversion of polymer cure reaction.[4] Many studies have investigated the cure kinetics of phenol-formaldehyde (PF) resins using dynamic and/or isothermal DSC. The Kissinger equation is primarily used in the dynamic DSC to calculate the activation energy of the cure reaction of PF resin.[5-7] The advantage of dynamic DSC is that it can provide extensive information of the cure reaction from only a single dynamic scan.[4] However, this method assumes a n*th* order mechanism of the cure reaction. For the majority of thermoset cure reactions, the dynamic DSC usually over estimates the kinetic parameters with respect to isothermal data.[8, 9] Lei et al.[10] summarized a detailed isothermal DSC method in his study of the cure kinetics of PF resins used for oriented strandboard. Wang et al.[11] compared the abilities of two model-free kinetic methods to model and predict cure kinetics of commercial PF resols. Since PF resin is the most commonly used adhesive in the wood composite industry, the effects of wood and wood-resin interactions on the cure kinetics of the PF resin have been studied.[12-14] Some other factors, such as additives and the NaOH to phenol ratio during the synthesis process, also affected the cure kinetics of the PF resins.[8,15,16] Lignin is the most susceptible wood component to liquefaction reaction.[17,18] Thus, the LWR should have some similarity with the lignin-phenol-formaldehyde (LPF) resins. The cure kinetics of the LPF resins showed that the LPF resin had a higher activation energy than a typical PF resin.[9, 19, 20]

Despite many advances in liquefied wood resin, some fundamental aspects of this new resin system are still lacking. The objectives of this chapter are to 1) synthesize liquefied wood resins, 2) characterize the resins by gel permeation chromatography

(GPC) and Fourier transform infrared (FT-IR), and 3) study the cure properties and build cure kinetic models for the resins based on DSC analysis.

3.2 Experimental

3.2.1 Materials

The raw materials for wood liquefaction are the same as in Chapter 2. Hexamethyleneteramine (HMTA) and calcium hydroxide were used as a hardener and an accelerator, respectively, in the cure reaction. All other chemicals were of reagent grade.

3.2.2 Synthesis of novolac type liquefied wood resin

The procedures for synthesis of the novolac type LWR are shown in Figure 3.1. The wood liquefaction parameters were the same as in Chapter 2. After the liquefaction reactions, the mixture was combined with formaldehyde (36%) at a phenol/formaldehyde molar ratio of 1/0.8 (phenol was based on the initially charged amount) and additional oxalic acid (7% of phenol, w%), and then refluxed under continuous stirring at 105 °C for 80 min. The co-condensed mixture was then diluted with acetone and vacuum filtered to separate the undissolved wood residue and the dissolved resin. Finally, the LWR was obtained by pressure-reduced removal of the acetone and stored in a refrigerator for further characterization.

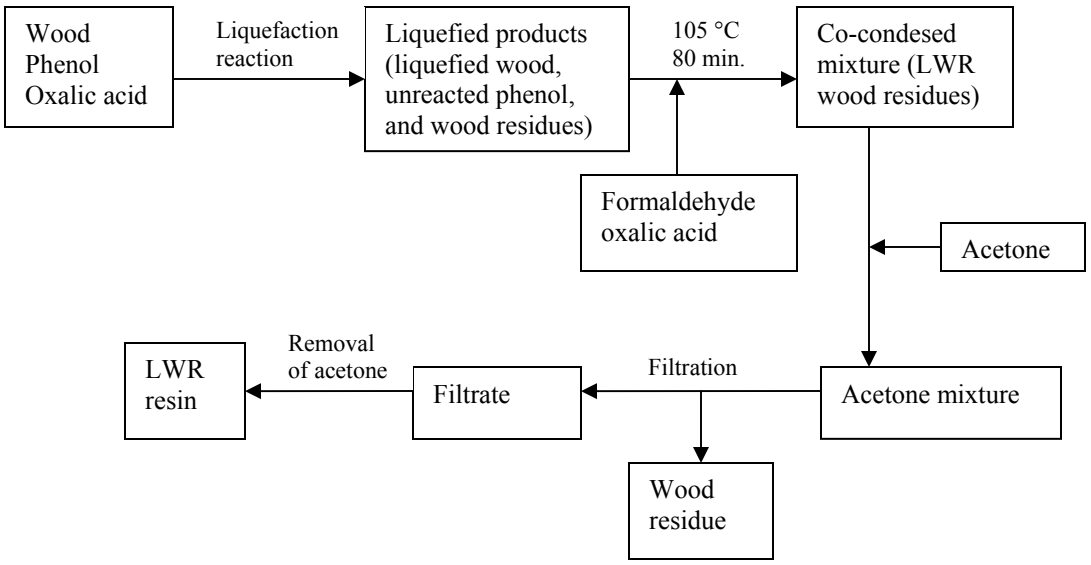

Figure 3.1 Flowchart of synthesis of LWR.

3.2.3 Gel permeation chromatography (GPC)

The GPC measurements were performed using a Waters-Wyatt GPC system equipped with multi-angle laser light scattering (did not use in this experiment) and differential refraction index detectors. Two Jordi Flash Gel Mixed Bed columns (250 × 10 mm) were used in series. Tests were conducted at ambient temperature using tetrahydrofuran (THF)/methanol (90/10) mixture as the mobile phase at a flow rate of 1.0 ml/min. Resin samples were dissolved in the same solvent as the mobile phase at a concentration of 5 mg/ml in solution. The amount of each sample injection was 100 µl.

The calibration curve was the same as in Chapter 2.

3.2.4 Fourier transform infrared spectroscopy (FT-IR)

The FT-IR analysis of the LWR was performed using a Nicolet Nexus 670 spectrometer equipped with a Thermo Nicolet Golden Gate MKII Single Reflection ATR accessory. A small amount of resin was applied directly on the diamond crystal.

3.2.5 Differential scanning calorimetry (DSC)

The DSC measurements on the cure reactions of the LWR were performed using a TA Instrument DSC-Q100 calorimeter. Two typical LWR were chosen in the cure kinetic study: LWR1, made from liquefied wood reacted in the atmospheric three neck flask with P/W ratio 2/1 and liquefaction temperature 180 ˚C; and LWR2, made from liquefied wood reacted in a sealed Parr reactor with the same P/W ratio and temperature as the LWR1. LWR, HMTA, and calcium hydroxide were homogeneously mixed in a weight ratio of 1/0.2/0.25. A small amount (10-15mg) of the sample was placed in a high volume DSC sample pan that can withstand vapor pressures up to 10 MPa.

Two empty sample pans were used at cure temperature to obtain a steady isothermal baseline. Four cure temperatures (120, 125, 130, and 135 °C) were employed in the isothermal heating experiments for each LWR. A continuous curve was obtained for each run showing the rate of heat generated by the sample per gram as a function of time. The reaction was considered complete when the rate curve leveled off to the baseline. For each sample, after the first isothermal run, the sample was rapidly cooled in the DSC cell to 25 °C, and the same isothermal run was started again. The curve used to calculate the heat of cure was obtained by subtracting the curve of the second isothermal run from the first run. The total area under the exothermal curve, based on the

extrapolated baseline at the end of the reaction, was considered the isothermal heat of cure at a given temperature. Dynamic scans were also conducted with four heating rates (5, 10, 15, and 20 °C/min.) in a scanning temperature range from 25 to 200 °C.

3.3 Results and Discussion

3.3.1 Gel permeation chromatography

The number average (Mn), weight average (Mw) molecular weight, and the polydispersity (Mw/Mn) of the LWR were calculated using the calibration curve and the results were given in Table 3.1.

Table 3.1. Average molecular weight and polydispersity (Mw/Mn) of the LWR synthesized from liquefied wood reacted in different conditions.

		Three neck flask[c]			Parr reactor[c]		
	P/W[b]	Mn	Mw	Mw/Mn	Mn	Mw	Mw/Mn
150 ˚C[a]	1/1	1207.5	2378.3	1.97	1336.7	3822.5	2.86
	2/1	1454.3	3476.6	2.39	1284.5	2692.9	2.09
	3/1	1589.7	3920.8	2.46	1224.6	2644.8	2.13
180 ˚C[a]	1/1	1277.6	2794.8	2.19	1246.2	3052.1	2.44
	2/1	1458.1	3720.8	2.55	1270.0	3679.9	2.89
	3/1	1489.9	3831.5	2.56	1118.9	2249.7	2.00

[a]Temperature of wood liquefaction reaction.
[b]phenol to wood ratio in wood liquefaction reaction.
[c]two types of reactors used in wood liquefaction reaction.

It can be seen that the LWR made from the liquefied wood using two types of reactors (i.e., atmospheric three neck flask and sealed Parr reactor) had the opposite trends for Mn and Mw as the P/W ratio changed from 1/1 to 3/1. The Mn and Mw of the LWR from the three neck flask increased while they slightly decreased with the liquefied wood from the Parr reactor as the P/W ratio increased. Figure 3.2 (three neck flask

system) and 3.3 (Parr reactor system) illustrated the changes in GPC chromatograms of the LWR with the P/W ratio. Figure 3.4 and 3.5 demonstrated the difference between the GPC chromatograms of the LWR made from the liquefied wood conducted in two different reactors at P/W ratio of 1/1 and 3/1, respectively. All of the GPC chromatograms of the LWR exhibit similar shapes of two broad peaks and are partially overlaid on each other. This lack of separation between different species is a typical behavior of phenolic resin in conventional GPC and results from the multiplicity of phenolic resin species having similar hydrodynamic volumes.[21]

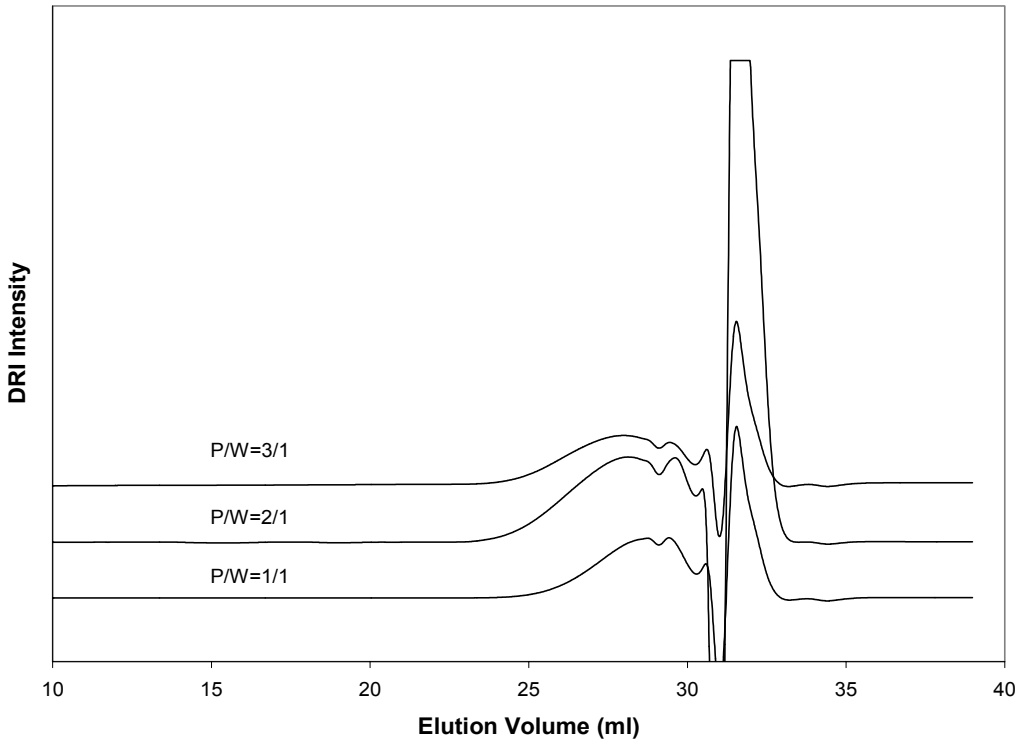

Figure 3.2. GPC chromatogram of the LWR made from the liquefied wood using atmospheric three neck flask at different P/W ratios.

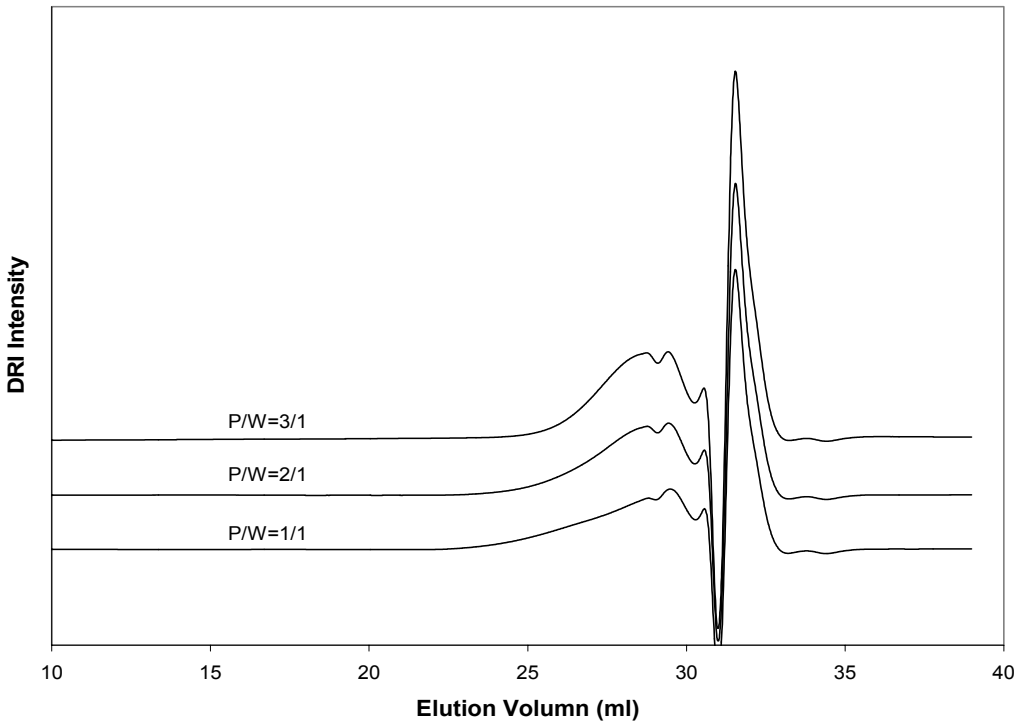

Figure 3.3. GPC chromatogram of the LWR made from liquefied wood using a sealed Parr reactor at different P/W ratios.

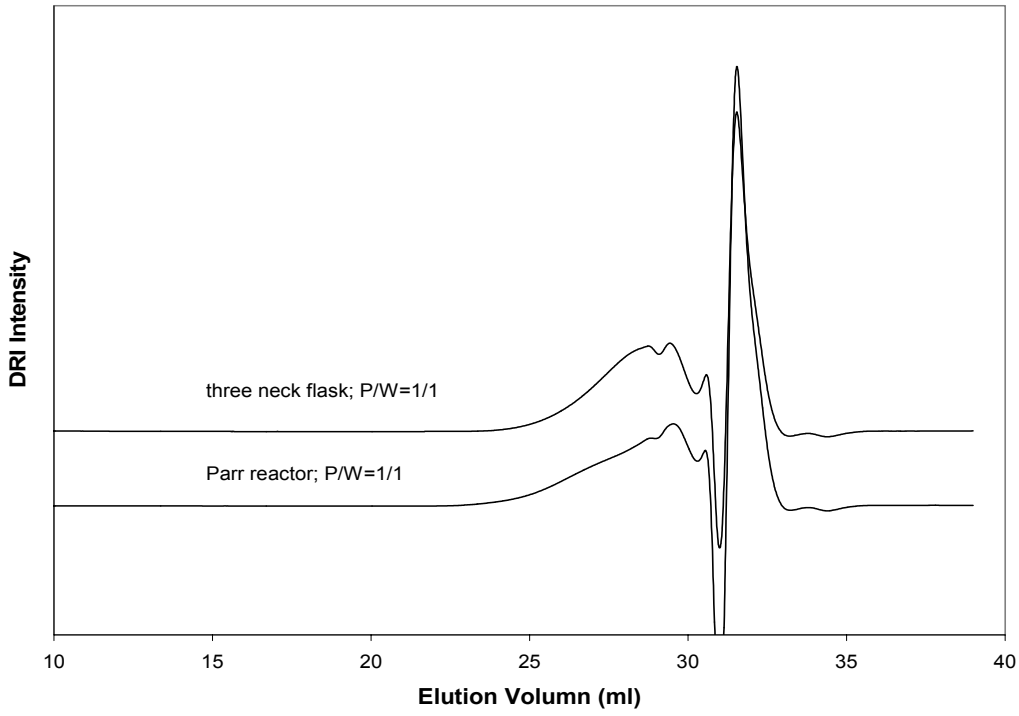

Figure 3.4. GPC chromatograms of LWR using two type of reactors at a P/W ratio of 1/1.

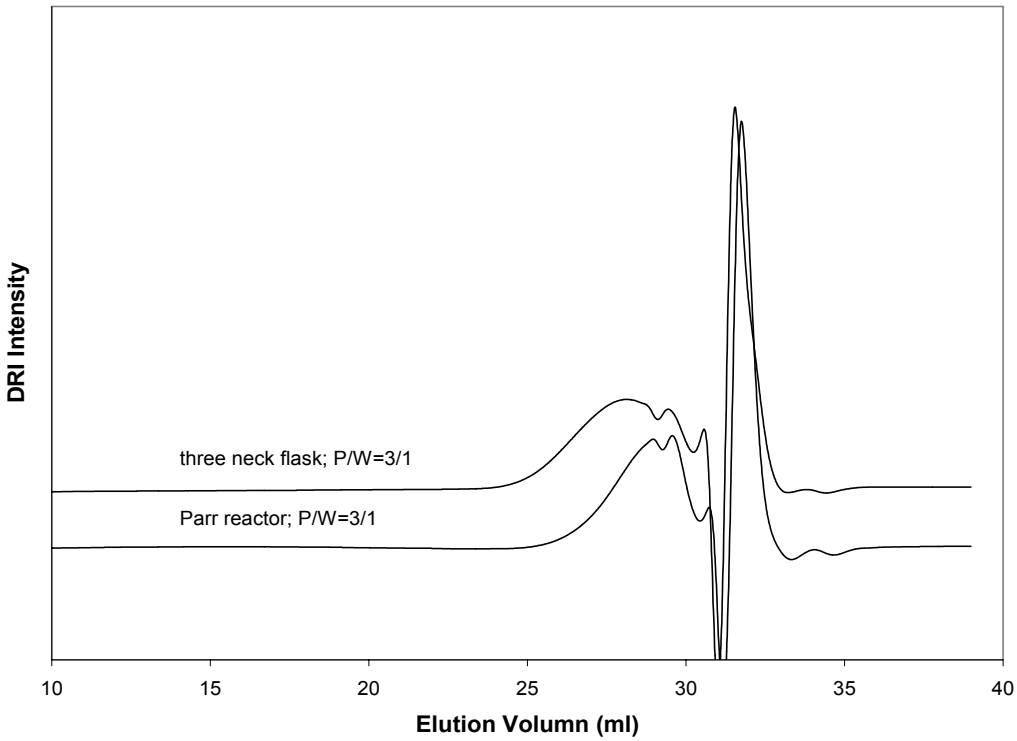

Figure 3.5. GPC chromatograms of the LWR using two type of reactors at P/W ratio of 3/1.

It can be speculated that there were two different effective compositions in the liquefied wood mixture that can react with formaldehyde during the polymerization process: free phenol remaining from the liquefaction stage and the decomposed wood components (i.e., liquefied wood). Moreover, most liquefied wood consists of decomposed lignin fragments with the C2 and/or C6 position blocked by methoxyl groups. Therefore, liquefied wood should be less active than phenol in the polymerization reaction because of fewer reaction sites and steric hindrance. Based on the results from Chapter 2, wood liquefaction conducted in the Parr reactor has a greater extent of liquefaction, in other words, more wood components have been decomposed into liquid, than that in the three neck flask system. As a result, it is very likely that the polymerization reaction between free phenol and formaldehyde dominated the resin synthesis process of the LWR made from the liquefied wood using the three neck flask,

and therefore, the average molecular weight increased with the increased amount of free phenol (i.e., increasing of the P/W ratio, see Chapter 2). Compared with the three neck flask, the condensation reaction in the resin synthesis system with the liquefied wood from the Parr reactor was less effective because of the existence of large amounts of decomposed wood components. Consequently, it has lower average molecular weight than the LWR made from the liquefied wood using the atmospheric three neck flask.

3.3.2 FT-IR spectroscopy

Figure 3.6 to 3.8 show the FT-IR characteristics of the novolac-type liquefied wood resins. The assignment of the main bands showed in the spectra is summarized in Table 3.2 according to the literature.

In general, novolac-type LWR showed a similar FT-IR absorbance to that of a conventional novolac resin. However, with the incorporation of wood components, the FT-IR spectra of the LWR contained some different bands compared with that of the conventional novolac resin. Figure 3.6 and 3.7 show the FT-IR spectra of two typical LWR compared with a conventional novolac resin. The major difference in the spectra between the LWR and the conventional novolac is the absorbance in the carbonyl region. Moreover, changes in the liquefaction conditions result in LWR with different absorbance pattern in this region. As shown in Figure 3.6, the LWR made from the liquefied wood reacted in the atmospheric three neck flask has 3 peaks at 1735, 1697, and 1654 cm^{-1} due to the ester carbonyl stretch, aryl ketone or aldehyde carbonyl stretch, and the di-substituted alkene $C=CH_2$, respectively. The LWR made from the liquefied wood

reacted in the sealed Parr reactor showed one broad peak centered at 1708 cm^{-1} mainly due to the aryl aldehyde C=O stretch (Figure 3.7).

Table 3.2. FT-IR assignment of the LWR.

Wavenumber (cm^{-1})	Assignment	References
3350	phenolic and methylol –OH stretch	22
3017	Aryl–H stretch	23
2916	Aliphatic $–CH_2$ asymmetric stretch	23,24,25
2838	Aliphatic $–CH_2$ symmetric stretch	23,24,25
1735	Ester C=O stretch	26
1708	Aryl aldehyde C=O stretch	26
1697	Aryl aldehyde, ketone C=O stretch	26
1654	di-substituted C=C (*gem*) stretch	26
1610	Aromatic C=C strctch	22,24,25,27
1510	Semicircle aromatic C=C stretch	22,24,25,27
1475	Tetra substituted ring	24
1456	Semicircle ring stretch	24
1436	Aliphatic $–CH_2$ scissor bending	24,25
1350	Phenolic OH in plane deformation	22,24,25,26
1328	CH_3 attached to the aromatic ring	24
1215	Phenolic OH bending, C-O stretch	26
1168	Alkyl-phenol C-O stretch	25
1099	Aromatic CH in plane deformation	22,24,25
1040	Single bond C-O stretch, $-CH_2OH$ vibrations	27
1013	Aliphatic ethers C-O-C stretch	26
940	$-CH=CH_2$	26
908	Aliphatic CH_2 wag	24,25
885	Tetra substituted ring	22,24,27
811	Adjacent 2H, para-substituted	22,28
753	Adjacent 4H, ortho-substituted	22,28
691	Adjacent 5H, phenol	22,24,27

However, the conventional novolac resin showed no absorbance in this region as expected. The spectra of the LWR also showed 2 weak bands at 1475 and 885 cm^{-1} caused by the tetra substituted (1, 2, 4, and 6) ring which did not occur in the spectra of the novolac resin. A possible explanation for this result could be the existence of some lignin fragments, most of which are tetra substituted aromatic rings, in the LWR. A sharp peak at 691 cm^{-1} in the spectra of the LWR represents the mono substituted aromatic ring

(i.e., phenol). This peak diminished in the spectra of the novolac resin, indicating that the LWR synthesized in this study contained a higher amount of free phenol than the conventional novolac resin. Based on the above discussion, the absorbance at 1735, 1708, 1697, 1654, 1475, and 885 cm^{-1} are very likely associated with the wood components that reacted with phenol during the liquefaction reaction.

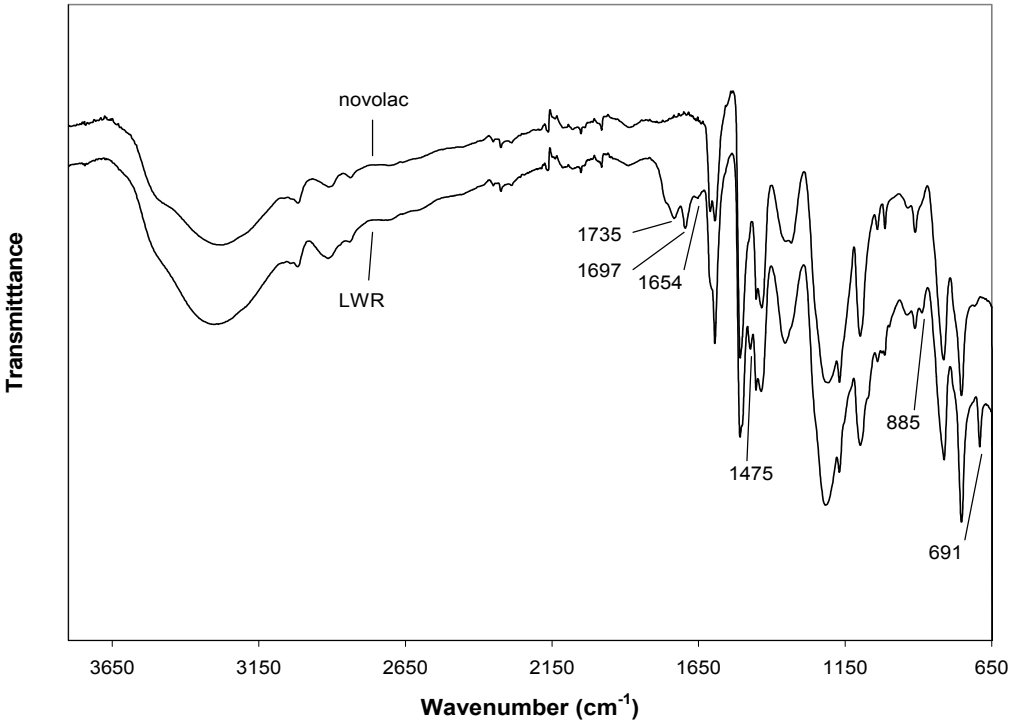

Figure 3.6. FT-IR spectra of LWR (three neck flask; P/W=2/1; 150 °C) and conventional novolac resin.

Figures 3.8-3.11 show the spectra of the LWR made from liquefied wood reacted at different phenol to wood (P/W) ratios during the liquefaction. As shown in Figure 3.8 (atmospheric, liquefaction temperature 150 °C), the peak at 2838 and 1436 cm^{-1}, which are associated with CH_2 stretch and bending, have a higher intensity at P/W ratio 2/1 and 3/1 than P/W ratio 1/1. A sharp peak at 1697 cm^{-1} occurred in the spectra of the LWR from P/W ratio 2/1, and the intensity of this peak increased dramatically when the P/W

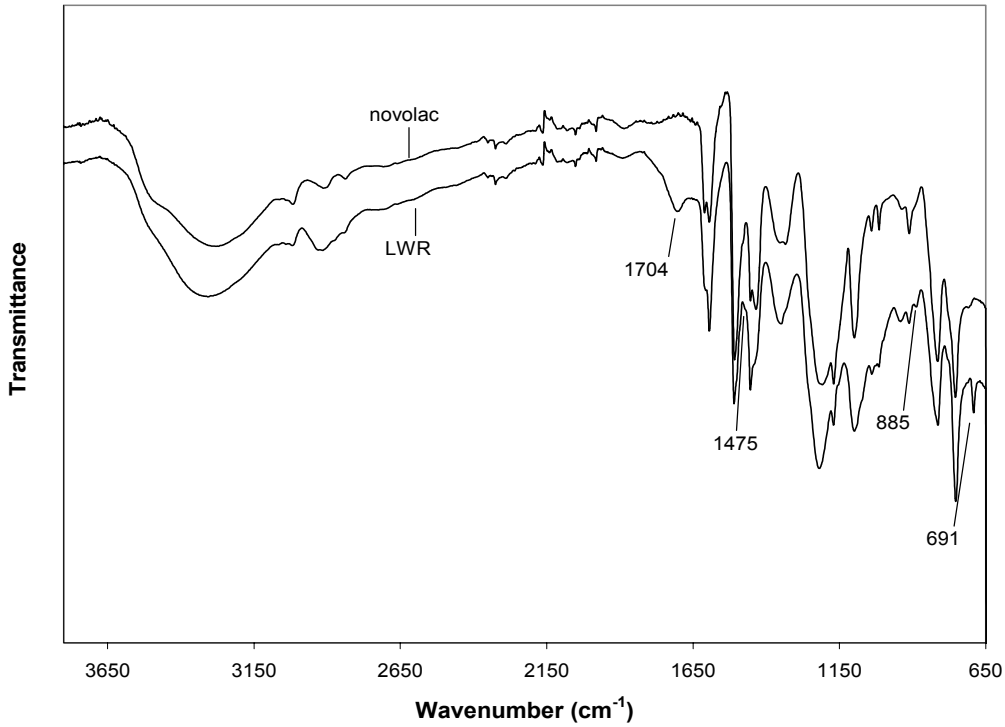

Figure 3.7. FT-IR spectra of the LWR (Parr reactor; P/W=2/1; 180 °C) and the conventional novolac resin.

ratio increased to 3/1. Meanwhile, the peak at 1654 cm^{-1} diminished from P/W ratio 1/1 to 2/1 and almost disappeared in the spectra of LWR from P/W ratio 3/1. The two other peaks that increased in intensity with an increase of P/W ratio are 1475 and 1013 cm^{-1}, which were caused by tetra substituted ring and ether C-O-C stretch, respectively. On the contrary, peaks at 1654 and 940 cm^{-1} were due to the di-substituted alkene and $–CH=CH_2$ alkene, respectively, decreased in intensity as the P/W ratio increased. The FT-IR spectra of the LWR made from liquefied wood with liquefaction temperature of 180 °C (Figure 3.9) showed very similar features as that of temperature of 150 °C (Figure 3.8).

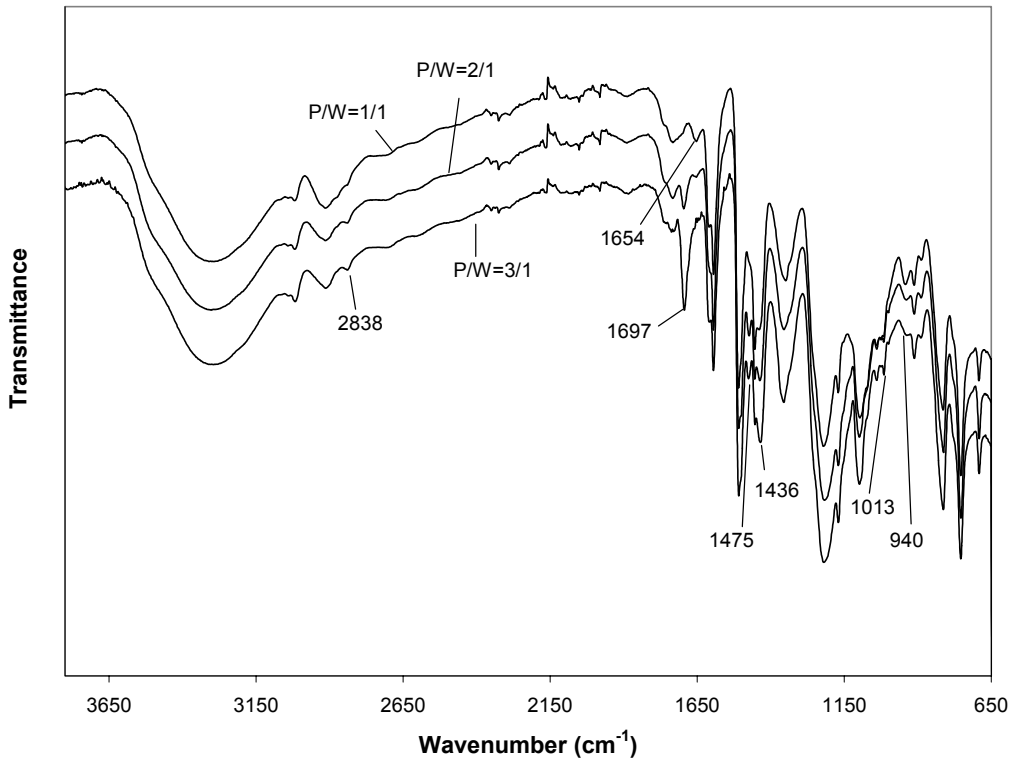

Figure 3.8. FT-IR spectra of the LWR at 3 P/W ratios (three neck flask, 150 °C)

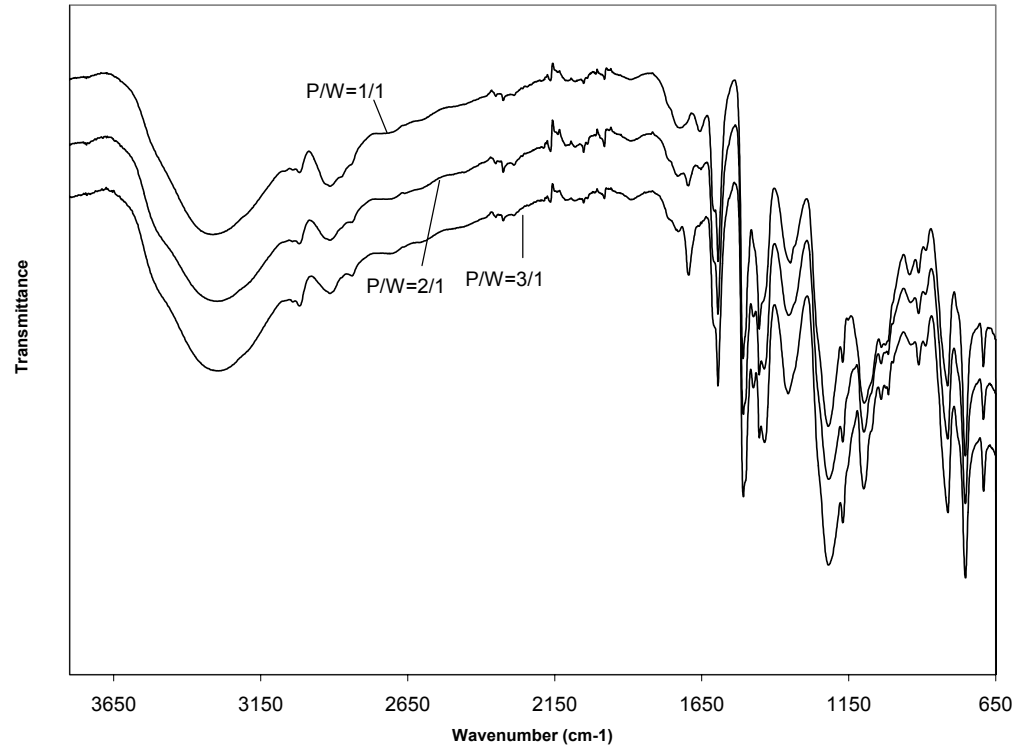

Figure 3.9. FT-IR spectra of the LWR at 3 P/W ratios (three neck flask, 180 °C).

The LWR from the sealed Parr reactor did not exhibit significant differences in the FT-IR spectra among the three P/W ratios (Figure 3.10, 3.11). Similar to the LWR from the atmospheric system, the absorbance at 2838, 1475, 1436, and 1013 cm^{-1} showed a weak increasing trend as the P/W ratio increased. Unlike the spectra of the LWR from the atmospheric system, a weak band at 1328 cm^{-1} occurred in the spectrum of the LWR from the sealed Parr reactor at P/W ratio 1/1 while it disappeared in the spectra of that from P/W ratios 2/1 and 3/1. On the other hand, the absorbance at 908 cm^{-1} due to the aliphatic CH_2 wag occurred as an intense peak in the spectra of the LWR from P/W ratio 2/1 and 3/1, but decreased in intensity as the P/W ratio decreased to 1/1.

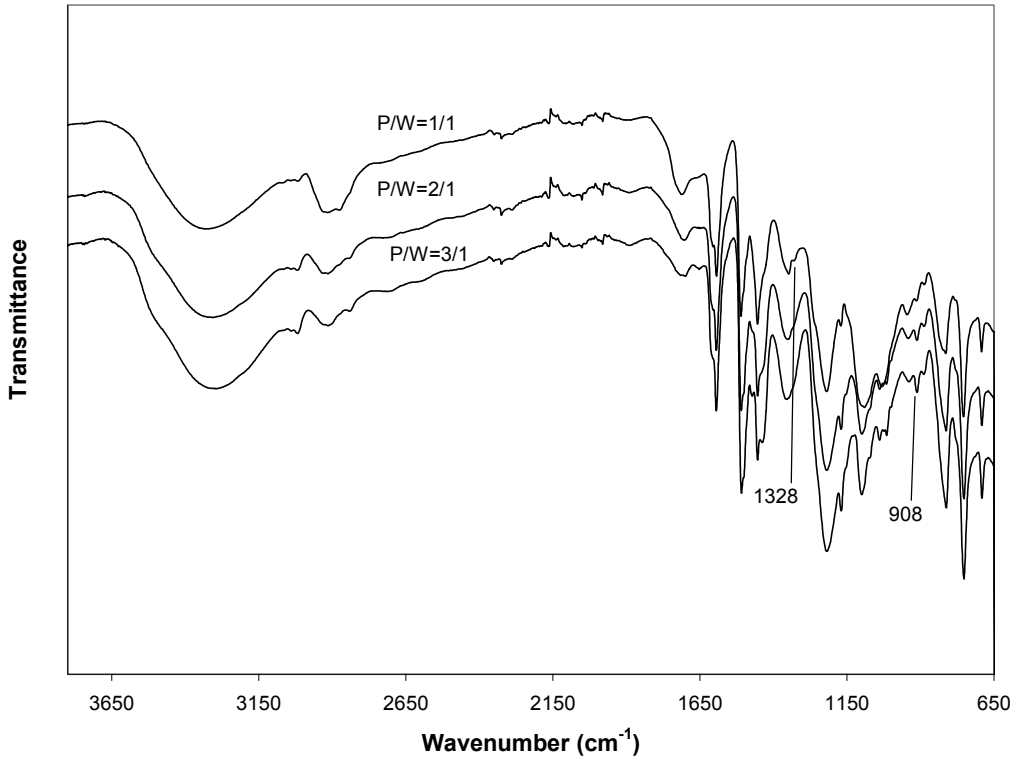

Figure 3.10. FT-IR spectra of the LWR at 3 P/W ratios (Parr reactor, 150 °C).

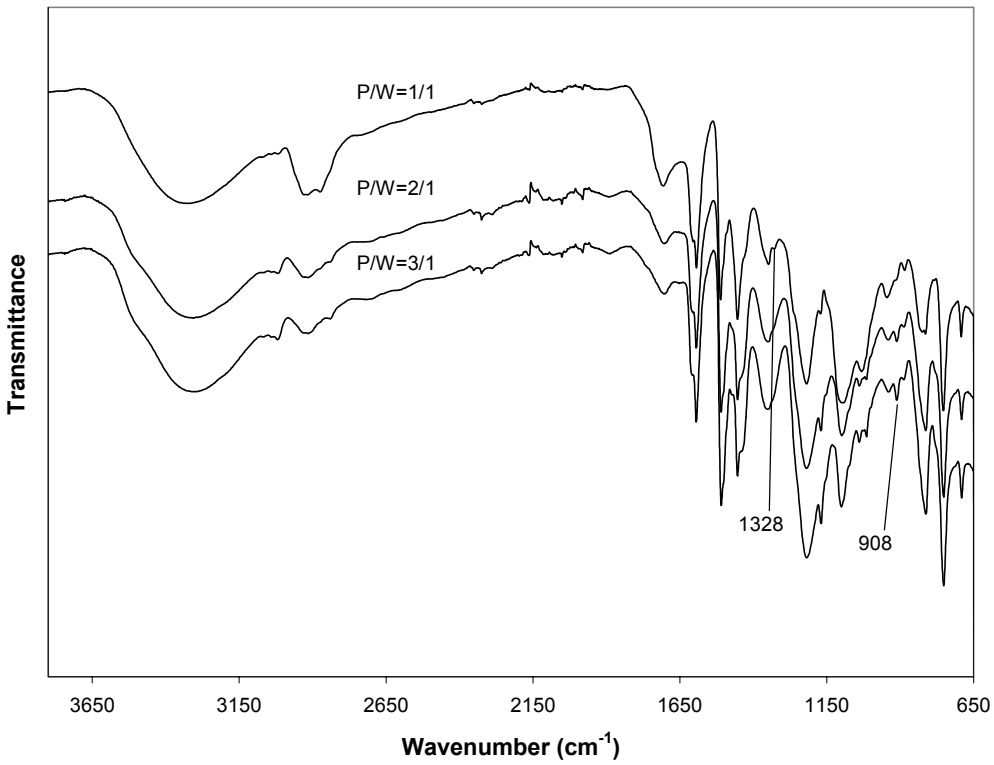

Figure 3.11 FT-IR spectra of the LWR at 3 P/W ratios (Parr reactor, 180 °C).

As described in Chapter 2, liquefaction reaction conducted in the atmospheric three neck flask and the sealed Parr reactor underwent different liquefaction mechanisms. The FT-IR spectra of the LWR made from the liquefied wood reacted in these two systems also implied different reactions in the liquefaction stage of two systems (Figure 3.12-14). The spectra of the LWR from the three neck flask shows an absorbance at 1735 cm^{-1} due to the ester carbonyl groups in the carbohydrate components in wood, which does not occur in the spectra of the LWR from the Parr reactor. This result is consistent with the FT-IR result of the liquefied wood residues (Chapter 2), indicating that the ester carbonyl groups have been broken down during the liquefaction reaction when using the Parr reactor. It is also noted that the LWR from the three neck flask displayed 3 bands (i.e., 1735, 1697, and 1654 cm^{-1}) in the 1800-1600 cm^{-1} region while the LWR from the

Parr reactor only showed one peak at 1708 cm^{-1} in the same region, which might due to the different liquefaction extent of the carbohydrate components of wood. Namely, the hemicellulose compounds might still exist in the liquefied wood conducted in the atmospheric three neck flask system, but they might be oxidized or decomposed in the system using the sealed Parr reactor.

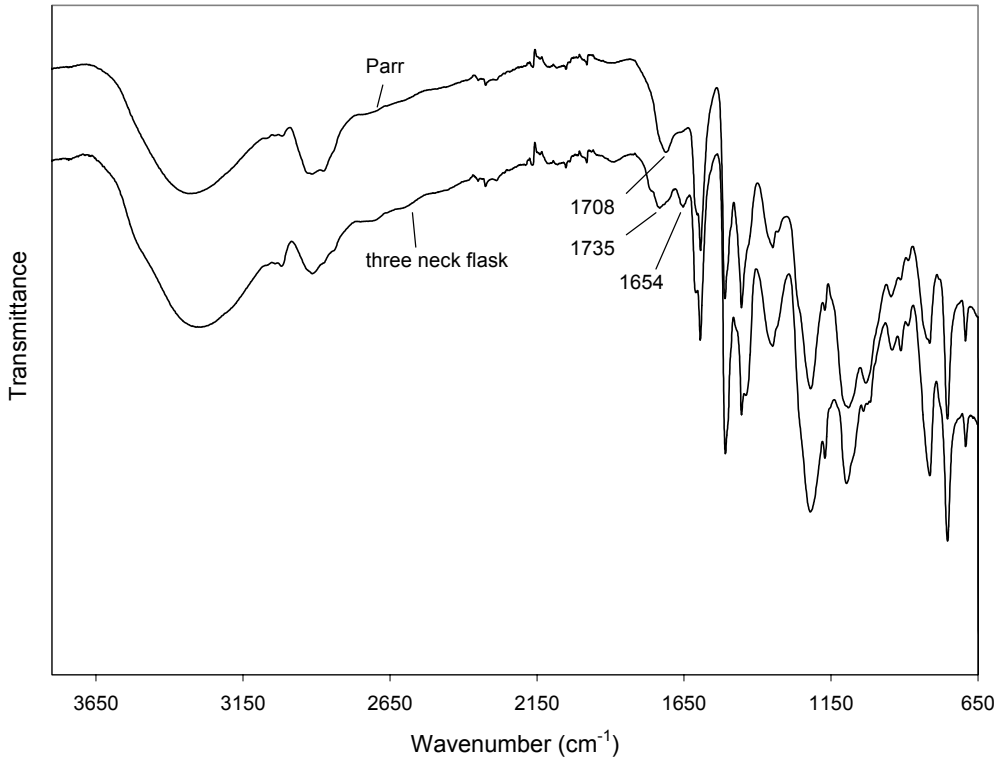

Figure 3.12 FT-IR spectra of the LWR from two types of reactors (P/W=1/1; 150 °C)

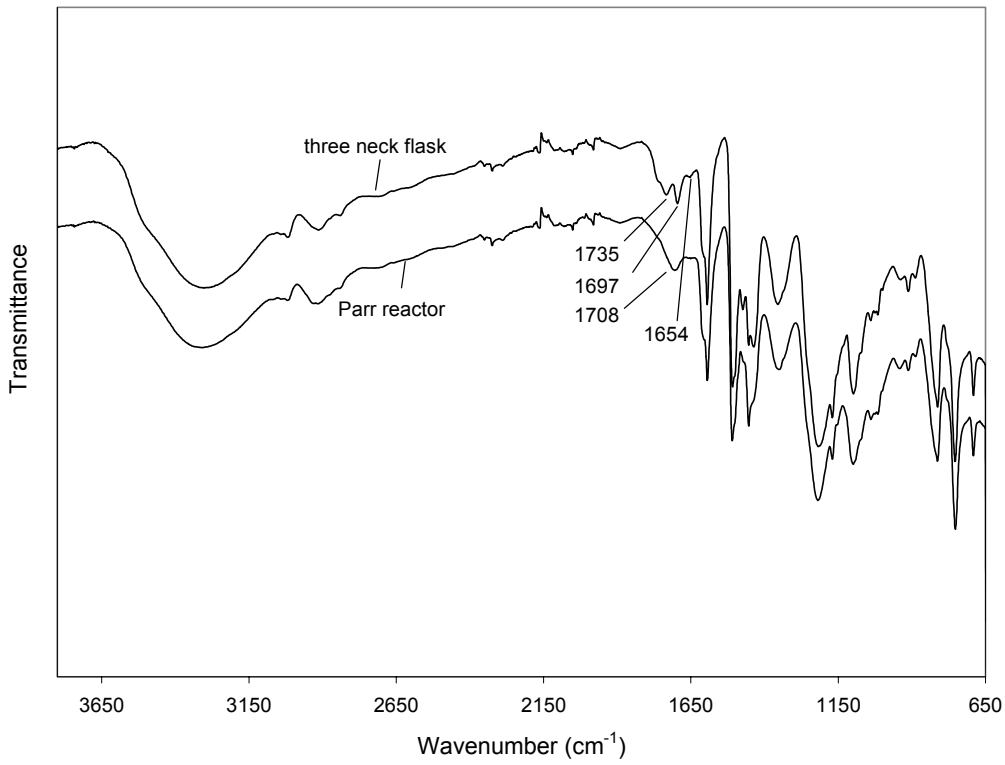

Figure 3.13 FT-IR spectra of the LWR from two types of reactors (P/W=2/1; 150 °C)

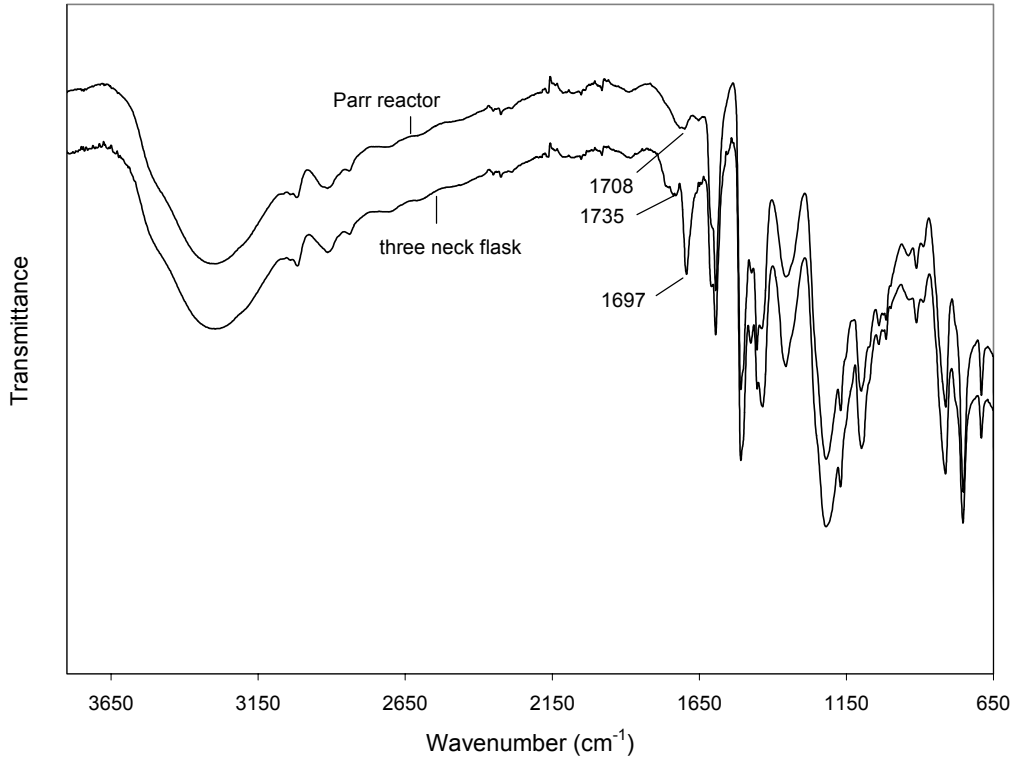

Figure 3.14 FT-IR spectra of the LWR from two types of reactors (P/W=3/1; 150 °C)

3.3.3 Cure properties of the liquefied wood resin

Table 3.3. ANOVA results on cure properties of the LWR by the GLM procedure.

Source	df	Type III SS	Mean Square	F Value	Pr > F
1. dependent variable: onset temperature (To)					
M[a]	1	6.1509	6.1509	5.45	0.0378
T[b]	1	7.7634	7.7634	6.88	0.0223
P[c]	2	28.8582	14.4291	12.78	0.0011
M*P	2	56.3178	28.1589	24.95	<0.0001
T*P	2	20.9256	10.4630	9.27	0.0037
2. dependent variable: peak temperature (Tp)					
M[a]	1	75.9704	75.9704	169.96	<0.0001
T[b]	1	7.2600	7.2600	16.24	0.0017
P[c]	2	102.5526	51.2763	114.71	<0.0001
M*P	2	133.9599	66.9799	149.85	<0.0001
T*P	2	12.7891	6.3945	14.31	0.0007

[a]reactor type
[b]liquefaction temperature
[c]phenol to wood ratio

The effects of three variables in the liquefaction stage (i.e., reactor type, liquefaction temperature, and phenol to wood ratio) on the cure onset temperature (To) and peak temperature (Tp) of the LWR were analyzed by ANOVA and the results are listed in Table 3.3. All of the three variables had significant effects on the cure properties of the LWR. On average, the LWR made from the liquefied wood using the three neck flask and under lower liquefaction temperature (150 °C) had lower To and Tp than those using the Parr reactor and under higher temperature (180 °C). And the To and Tp of the LWR decreased as the phenol to wood (P/W) ratio increased.

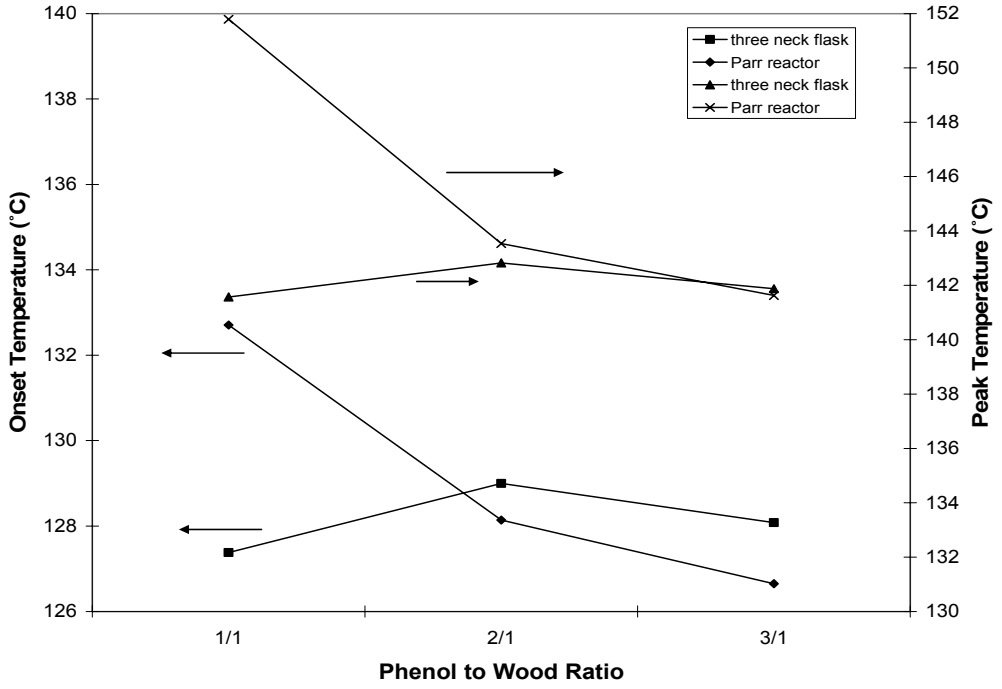

Figure 3.15. Interaction plot of liquefaction temperature and P/W ratio.

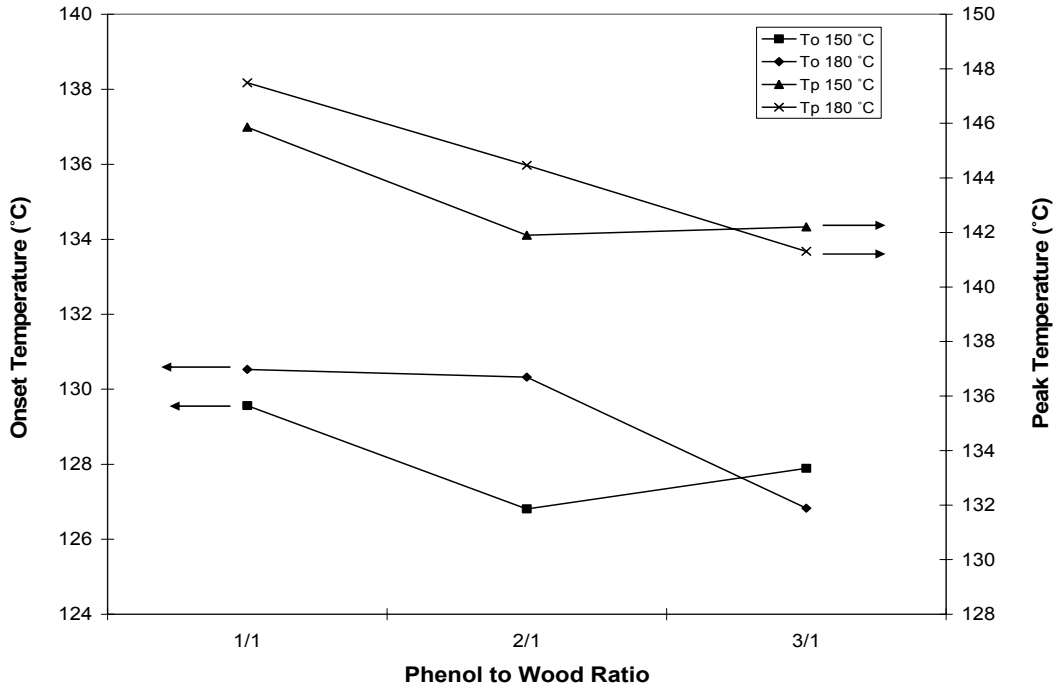

Figure 3.16. Interaction plot of reactor type and P/W ratio.

The P/W ratio variable had significant interactions with both reactor type and liquefaction temperature as shown in Figure 3.15 and 3.16. With the liquefied wood

from the sealed Parr reactor, both the To and Tp of the LWR decreased as the P/W ratio increased. However, they increased from P/W ratio of 1/1 to 2/1 then decreased slightly as the P/W ratio increased to 3/1 with the liquefied wood from the atmospheric three neck flask system (Figure 3.15). The effects of the P/W ratio on the To and Tp of the LWR also showed a similar interaction trend with the variable of liquefaction temperature. It can be seen from Figure 3.16 that the To and Tp of the LWR made from the liquefied wood obtained at higher temperature dropped from 130.5 °C and 147.5 °C to 126.8 °C and 141.3 °C, respectively. But with the lower liquefaction temperature, the To and Tp decreased from P/W ratio 1/1 to 2/1 then increased as the P/W ratio increased to 3/1.

3.3.4 Cure kinetics of the liquefied wood resin

3.3.4.1 Dynamic DSC analysis

Table 3.4. Cure temperatures of two liquefied wood resins at different heating rate.

Heating rate, Φ (°C/min)	Onset temperature (°C)		Peak temperature (°C)	
	LWR1	LWR2	LWR1	LWR2
0[a]	115.8	113.3	128.7	129.9
5	121.0	118.6	134.2	135.2
10	127.1	125.6	142.5	143.8
15	133.5	131.2	148.8	150.0
20	137.6	136.4	153.5	154.4

[a]Extrapolated values from the intercepts of the onset temperatures and peak temperatures versus heating rate plots, respectively.

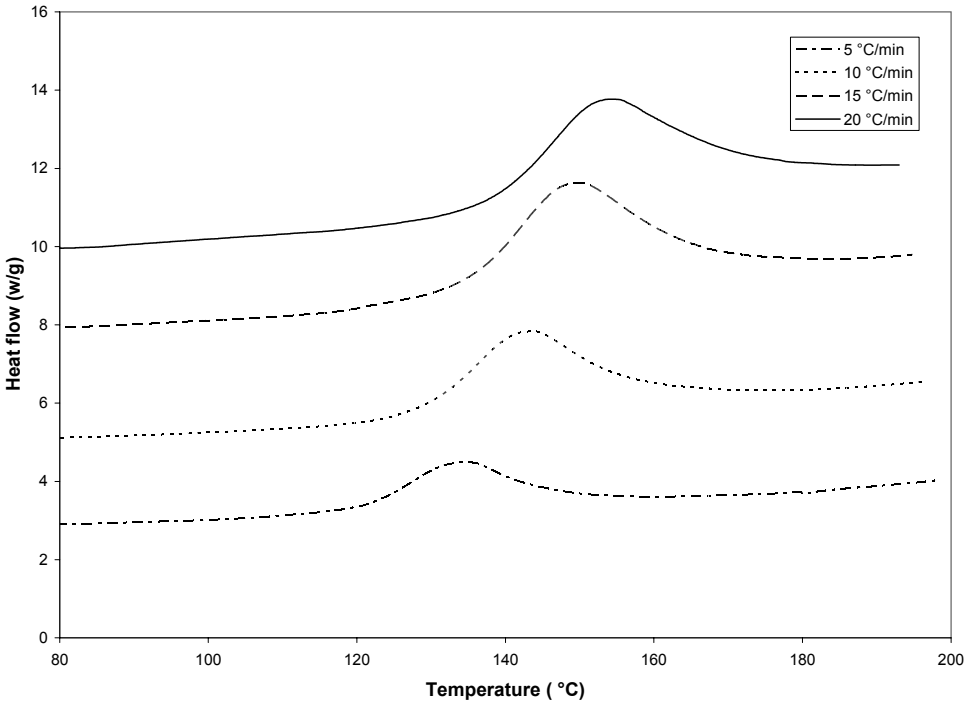

(a)

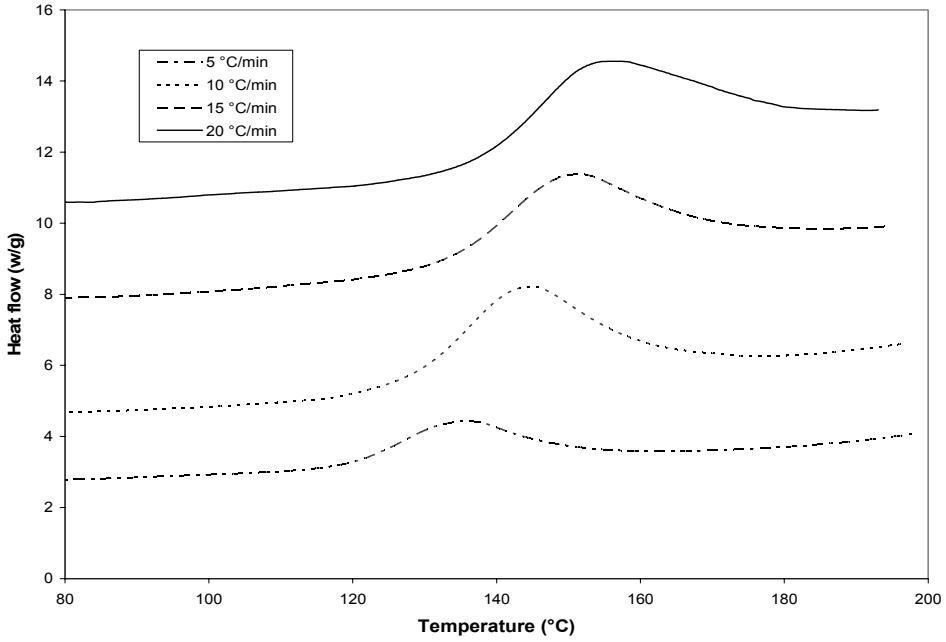

(b)

Figure 3.17. Dynamic DSC curves of LWR1 (a) and LWR2 (b).

The dynamic DSC curves of the two LWR at different heating rates are shown in Figure 3.17 and the results are listed in Table 3.4. The onset (To) and peak (Tp) temperatures of both resins shifted to higher temperatures with increased heating rate. The actual cure temperatures are independent of heating rate. In other words, they are the temperatures at a heating rate of zero.[10] As listed in Table 3.4, the cure reaction of LWR1 resin starts at about 116 °C and reached the highest cure rate at around 129 °C. Compared to LWR1, the liquefied wood resin LWR2 had a lower onset temperature of 113 °C and a slightly higher peak temperature of 130 °C. The result shows that the two liquefied resins synthesized under atmospheric and sealed conditions have similar cure activities at the higher temperature of 130 °C while the resin from the sealed condition (LWR2) was more active at lower temperature than that from the atmospheric condition (LWR1).

Most other studies on the cure kinetics of LPF resin have used the dynamic DSC method. To compare with the LPF resin, the dynamic method developed by Kissinger[29] was also used in this experiment. The Kissinger equation is:

$$\ln\left(\frac{\phi}{T_p^2}\right) = -\frac{E}{R}\cdot\frac{1}{T_p} + \ln\left(\frac{RA}{E}\right) \qquad (1)$$

where Φ is the heating rate (K/s), T_p the peak temperature (K) at the given heating rate, and R is the gas constant. The activation energy (E) can be obtained by linear regression of Equation 1. Based on this method, the activation energies of the LWR1 and LWR2 were 96.55 and 97.54 KJ/mol, respectively. These values were higher than typical PF resin reported by other researchers.[9,10] However, they were similar to that of a LPF

resin.[19] This result may be due to the lower reactivity of the lignin fragments that are incorporated into the resin compared with the phenol.[9,19]

3.3.4.2 Isothermal cure kinetics

In general, two kinetic models are used in the cure of thermosetting materials in terms of the mechanisms of their cure reaction: n^{th}-order and autocatalytic. For thermosets that follow the n^{th}-order kinetics, the conversion rate (dα/dt) is proportional to the concentration of unreacted materials and can be expressed as Equation (2):

$$\frac{d\alpha}{dt} = k(1-\alpha)^n \tag{2}$$

where α is the conversion of the reactant at time t, n the reaction order, and k is the temperature dependent rate constant given by the Arrhenius Equation (3):

$$k = A\exp(-E/RT) \tag{3}$$

where E is the activation energy, R is the gas constant, T is the absolute temperature, and A is the pre-exponential factor. Autocatalytic thermoset cure reactions are the type where one of the reaction products is also a catalyst for further reactions.[8] Thus, the reactions are characterized by an accelerating isothermal conversion rate and reach the maximum rate between 20 to 40% of conversion, typically.[8] The reaction rate is defined as Equation (4):

$$\frac{d\alpha}{dt} = k'\alpha^m(1-\alpha)^n \tag{4}$$

where m and n are the reaction orders and k' the rate constant also given by the Arrhenius Equation (3). To take into account the autocatalytic reactions that the initial reaction rate is not zero, a generalized expression was proposed by Kamal[30] as follows:

$$\frac{d\alpha}{dt} = (k_1 + k_2\alpha^m)(1-\alpha)^n \tag{5}$$

where k_1 and k_2 are the rate constants, and k_1 can be determined as the reaction rate at t=0:

$$k_1 = \left(\frac{d\alpha}{dt}\right)_{t=0} \tag{6}$$

The basic assumption of the application of DSC for the thermoset curing is that the measured heat flow (dH/dt) is proportional to the conversion rate (dα/dt), and this has proven to be a reasonably good assumption[4]. The rate of change in the conversion can therefore be defined as follows:

$$\frac{d\alpha}{dt} = \frac{dH/dt}{\Delta H_0} \tag{7}$$

where ΔH_o is the total reaction heat associated with the cure process.

A series of isothermal DSC curves of the reaction rate as a function of time for the two liquefied wood resins are shown in Figure 3.18. It can be seen that with an increase of the cure temperature, the peak values of the reaction rate increased and shifted to shorter reaction times. The maximum conversion rate (dα/dt) occurring at t≠0 suggests an autocatalytic cure kinetic mechanism of these two resins. By partial integration of the areas under the curves in Figure 3.18, the fractional conversion as a function of time was obtained and plotted in Figure 3.19. Both of the liquefied wood resins reached about 70% conversion within 20 minutes at the testing temperatures. Generally, the higher the isothermal cure temperature, the sooner the reaction reaches the same level of conversion.

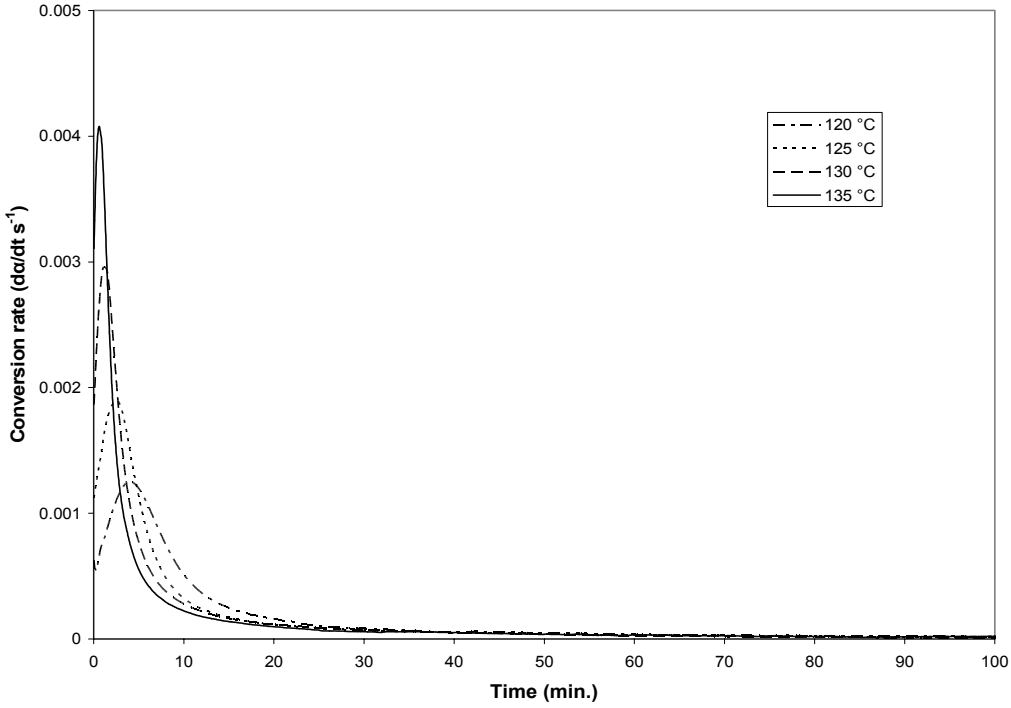

(a)

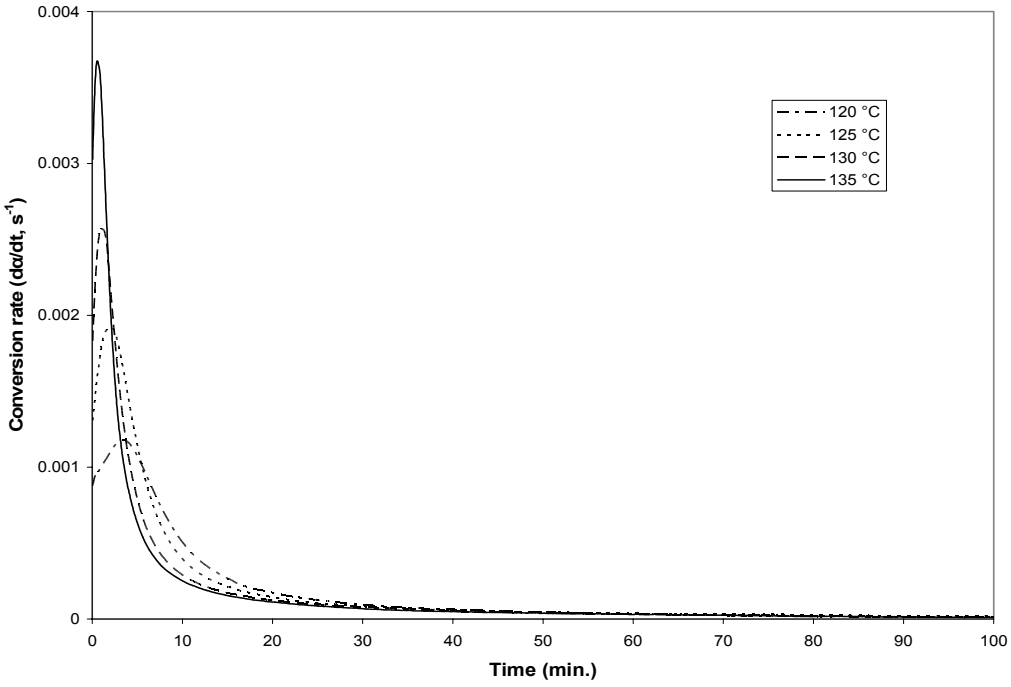

(b)

Figure 3.18. Conversion rate as a function of time at different isothermal temperatures of LWR1 (a) and LWR2 (b).

But the cure time was prolonged after the conversion reached 80% at the higher cure temperature of 135 °C compared with that at 125 and 130 °C. This phenomenon is possibly due to the onset of vitrification at higher cure temperatures. The mobility of the reaction groups could have been hindered, and the rate of conversion would then be controlled by diffusion rather than chemical factors.[31, 32]

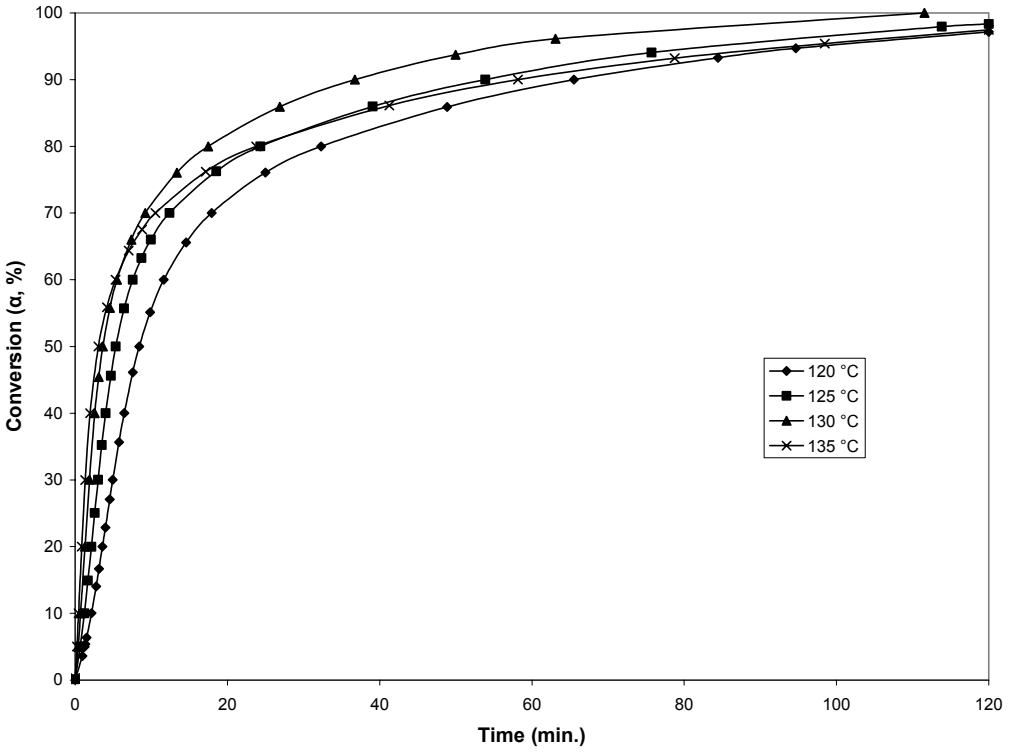

(a)

Figure 3.19. Conversion as a function of time at different isothermal temperatures of LWR1 (a) and LWR2 (b). (figure continued)

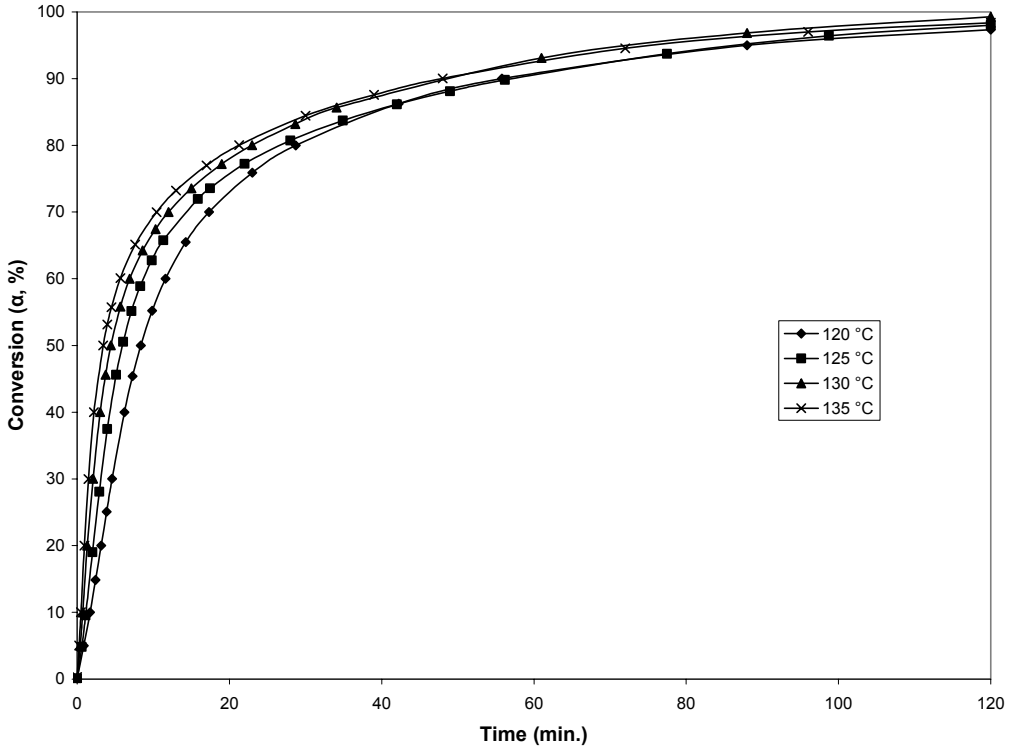

(b)

Figure 3.20 shows the curves of the conversion rate as a function of conversion. It is clearly shown that the cure reaction of both liquefied wood resins follows an autocatalytic kinetics mechanism with the maximum conversion rate in the 10 to 30% conversion region.

Table 3.5: Isothermal cure kinetic parameters of two liquefied wood resins.

Temp. (°C)	LWR1				LWR2			
	k_1 (10^{-4}, s^{-1})	k_2 (10^{-2}, s^{-1})	n	m	k_1 (10^{-4}, s^{-1})	k_2 (10^{-2}, s^{-1})	n	m
120	6.62	1.15	3.03	1.20	8.54	0.59	2.53	1.01
125	10.93	1.71	3.19	1.14	12.69	0.86	2.42	0.90
130	17.99	1.78	3.09	0.95	17.81	0.87	2.87	0.74
135	29.84	1.81	3.49	0.81	29.36	1.13	3.04	0.74

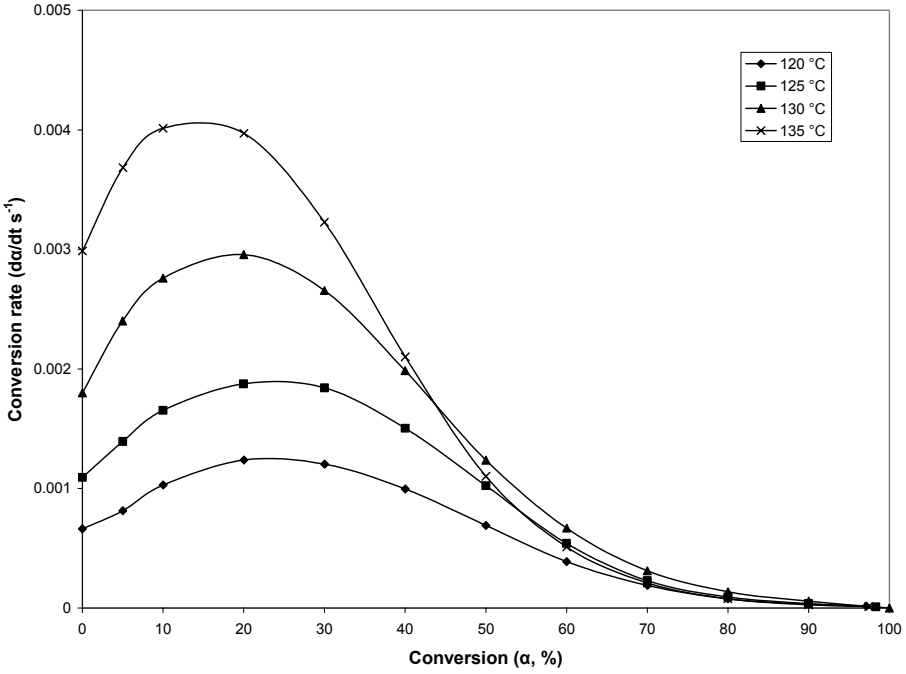

(a)

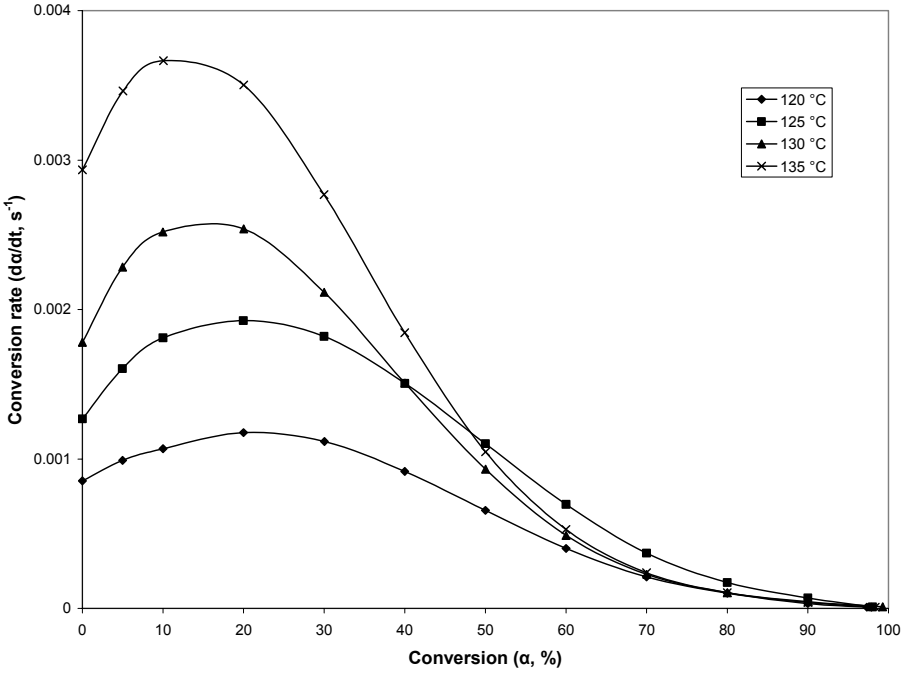

(b)

Figure 3.20. Conversion rate versus conversion plots of LWR1 (a) and LWR2 (b).

Table 3.6. Activation energies and pre-exponential factors of two liquefied wood resin.

Resin	E_1 (kJ/mol)	$\ln A_1$	E_2 (kJ/mol)	$\ln A_2$
LWR1	133.76	33.61	37.61	7.15
LWR2	107.70	25.87	52.82	11.08

According to Eq. 5 and using nonlinear regression, [10, 32] the kinetic parameters of the two liquefied wood resins were calculated and summarized in Table 3.5. The average overall order (m+n) of the cure reactions of LWR1 and LWR2 were 4.22 and 3.57, respectively. Both rate constants k_1 and k_2 obey the Arrhenius form (Eq. 3). From linear regression, the associated activation energies (E1 and E2) and the pre-exponential factors were calculated and are listed in Table 3.6. The LWR1 resin has a higher activation energy for k_1 and a lower activation energy for k_2. As shown in Eq. 5, the term $k_2\alpha^m$ represents the influence of the reaction products on the conversion rate and k_1 governs the early stage autocatalytic reaction.[4,32,33] As shown in Table 3.1, LWR1 was believed to have higher average molecular weight than LWR2. Due to the molecular mobility, the reactions between functional groups on the molecules with low-molecular-weight occur more readily than those of high-molecular-weight molecules. As a consequence, LWR1 had a higher initial activation energy than LWR2 (Table 3.6), but the LWR1 resin had a lower activation energy for the subsequent reaction than LWR2. This might be due to a higher wood residue percentage in LWR2 in which the incorporated lignin fragments retarded further polymerization (or condensation) of the LWR2.

Thus, the kinetic equation for the liquefied wood resin LWR1 is as follows:

$$\frac{d\alpha}{dt} = \left[3.94 \times 10^{14} \exp(-\frac{16087}{T}) + 1278 \exp(-\frac{4523}{T}) \alpha^{1.02} \right] (1-\alpha)^{3.20} \qquad (8)$$

And the kinetic equation for the LWR2 is

$$\frac{d\alpha}{dt} = \left[1.73\times10^{11}\exp(-\frac{12953}{T}) + 65190\exp(-\frac{6352}{T})\alpha^{0.85}\right](1-\alpha)^{2.72} \qquad (9)$$

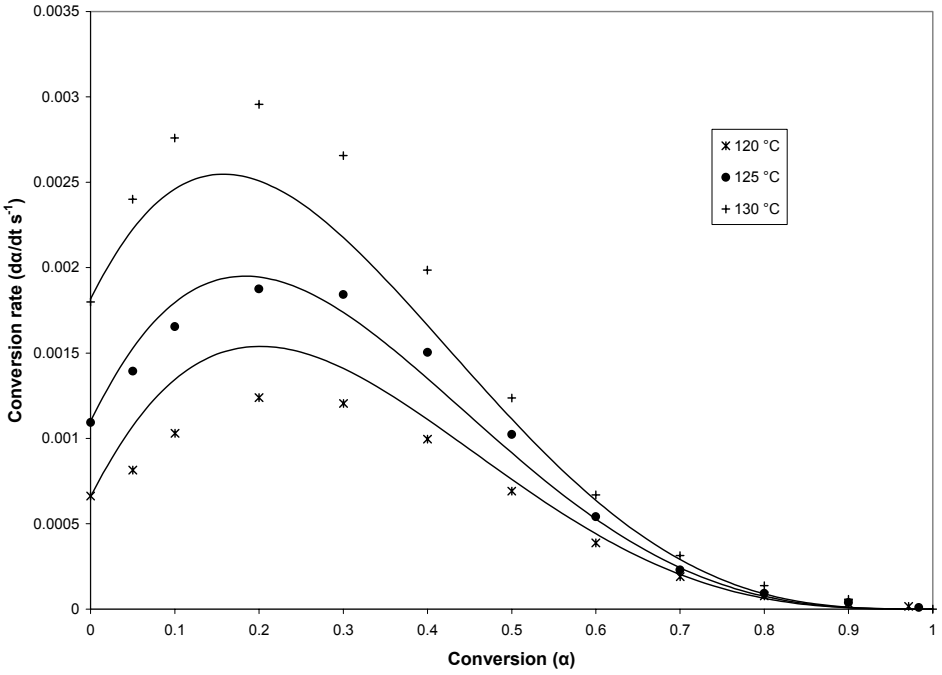

(a)

Figure 3.21. Comparison of the theoretical (lines) and experimental (symbols) conversion rate versus conversion of LWR1 (a) and LWR2 (b). (figure continued)

Figure 3.21 shows the comparison between the experimental data with the conversion rates obtained from the kinetic models (Eq. 8 and Eq. 9). It is clear that most predicted values agree with the experimental data.

3.4 Conclusions

Different liquefaction conditions have significant effects on the properties of the LWR. The average molecular weight of the LWR made from the liquefied wood reacted

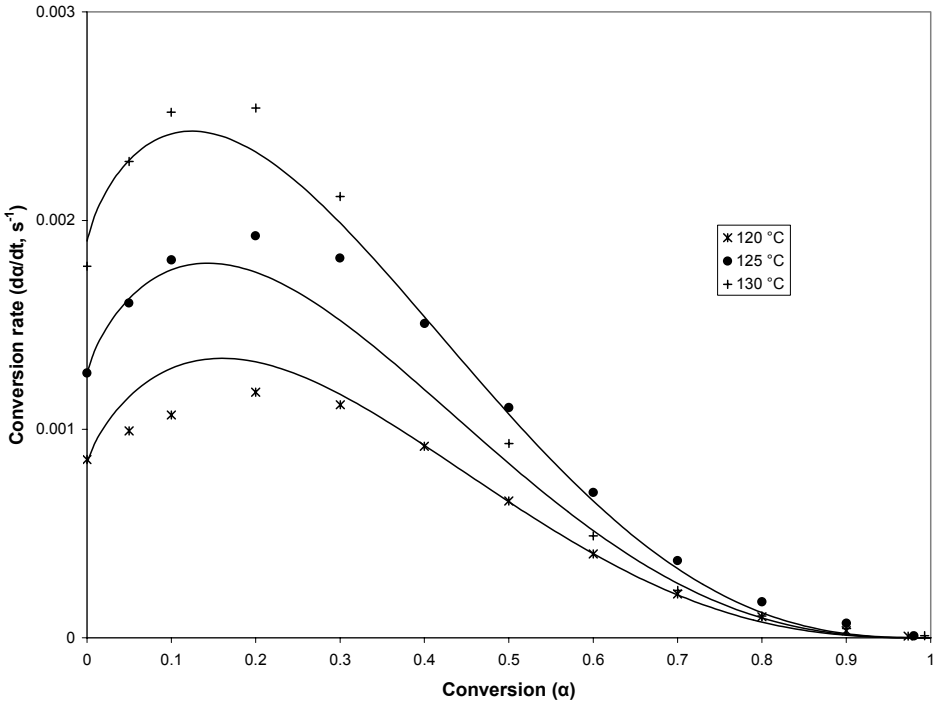

(b)

in the atmospheric three neck flask increased with the increasing P/W ratio. However, it decreased with the increasing P/W ratio using the sealed Parr reactor. On average, the LWR made from the liquefied wood reacted in the sealed reactor had lower molecular weight that those from the atmospheric three neck flask.

The FT-IR spectra of the LWR are similar to that of the conventional novolac resin but also displayed a major difference in the 1800-1600 cm^{-1} region. The LWR from the two different reactors gave different FT-IR absorbance, indicating different liquefaction species occurring in the different reactor systems.

On average, the LWR made from the liquefied wood using the three neck flask and under lower liquefaction temperature (150 °C) had lower To and Tp than those using the Parr reactor and under higher temperature (180 °C). And the To and Tp of the LWR

decreased as the phenol to wood (P/W) ratio increased. The cure kinetic results of two typical LWR showed the activation energies of the LWR were similar to that of the LPF resin but higher than typical phenolic resins. The isothermal DSC results revealed that both LWR from the atmospheric three neck flask and the sealed Parr reactor followed an autocatalytic cure mechanism. However, the LWR from the atmospheric system had a higher E1 but lower E2 than that from the sealed system.

3.5 References

1. Alma, M. H., Yoshioka, M., Yao, Y., and Shiraishi, N. 1995. Preparation of oxalic acid catalyzed resinified phenolated wood and its characterization. Mokuzai Gakkaishi 41(12): 1122-1131.

2. Lin, L., Yoshioka, M., Yao, Y., and Shiraishi, N. 1995. Preparation and properties of phenolated wood/phenol/formaldehyde cocondensed resin. J. App. Polymer Sci. 58: 1297-1304.

3. Lee, S. H.; Yoshioka, M.; Shiraishi, N. 2000. Preparation and properties of phenolated corn bran/phenol/formaldehyde co-condensed resin. J Appl Polym Sci. 77:2901-2907.

4. Boey, F.Y.C. and Qiang, W. 1999. Experimental modeling of the cure kinetics of an epoxy-hexaanhydro-4-methylphthalicanhydride (MHHPA) system. Polym. 41:2081-2094.

5. Tsoul, C.T., Yin, H.W., and Shiah, T.C. 2004. Reaction kinetics behavior of phenol formaldehyde wood adhesives by differential thermal analysis and its application. Taiwan Forestry Sci. 19:297-310.

6. He, G. and Yan, N. 2005. Influence of the synthesis conditions on the curing behavior of phenol-urea-formaldehyde resol resins. J Appl Polym Sci. 95:13681375.

7. Sarbajna, R. and Ray, B.C. 2004. Curing studies of novolac resins using differential scanning calormetry. J Polym Mater 21:71-80.

8. Park, B.D., Riedl, B., Hsu, E.W., and Shields, J. 1999. differential scanning calorimetry of phenol-formaldehyde resins cure accelerated by carbonates. Polym 40:1689-1699.

9. Alonso, M.V., Oliet, M., Perez, J.M., Rodriguez, F., and Echevrria, J. 2004. Determination of curing kinetic parameters of lignin-phenol-formaldehyde resol resins by several dynamic differential scanning calorimetry methods. 2004. Thermochim Acta 419:161-167.

10. Lei, Y., Wu, Q., and Lian, K. 2006. Curing kinetics of aqueous phenol-formaldehyde resins used for oriented strandboard manufacturing: Analytical technique. J Appl Polym Sci 100:1642-1650.

11. Wang, J., Laborie, M.P., and Wolcott, M.P. 2005. Comparison of model-free kinetic methods for modeling the cure kinetics of commercial phenol-formaldehyde resins. Thermochim Acta 439:68-73.

12. Pizzi, A., Mtsweni, B., and Parsons, W. 1994. Wood-induced catalytic activation of PF adhesives autopolymerization vs. PF/wood cobalent bonding. J Appl Polym Sci 52:1847-1856.

13. He, G. and Riedl, B. 2004. Curing kinetics of phenol formaldehyde resin and wood-resin interactions in the presence wood substrates. Wood Sci Technol 38: 69-81.

14. Lei, Y. and Wu, Q. 2006. Cure kinetics of aqueous phenol-formaldehyde resins used for oriented strandboard manufacturing: Effect of wood flour. J Appl Polym Sci 102:3774-3781.

15. Park, B.D., Riedl, B., Kim, Y.S., and So, W.T. 2002. Effect of synthesis parameters on thermal behavior of phenol-formaldehyde resol resin. J Appl Polym Sci 83:1415-1424

16. Lei, Y. and Wu, Q. 2006. Cure kinetics of aqueous phenol-formaldehyde resins used for oriented strandboard manufacturing: effect of zinc borate. J Appl Polym Sci 101:3886-3894.

17. Pu,S., Shiraishi, N. 1993. Liquefaction of wood without a catalyst I. time course of wood liquefaction with phenols and effects of wood/phenol ratios. Mokuzai Gakkaishi 39(4): 446-452.

18. Pan, H., Shupe, F.T., and Hse, C.Y. 2007. Characterization of liquefied wood residues from different liquefaction conditions. J Appl Polym Sci in press.

19. Barry, A.O., Peng, W., and Riedl, B. 1993. The effect of lignin content on the cure properties of phenol-formaldehyde resin as determined by differential scanning calorimetry. Holzforschung 47:247-252.

20. Simitzis, J., Karagiannis, K., and Zoumpoulakis, L. 1995. Curing of novolac-lignocellulosic composites. Polym Int 38:183-189.

21. Myers, G. E., Christiansen, A. W., Geimer, R. L., Follensbee, R. A., and Koutsky, J. A. 1991. Phenol-formaldehyde resin curing and bonding in steam-injection pressing. I. Resin synthesis, characterization, and cure behavior. J. App. Polym. Sci. 43: 237-250.

22. Holopainen, T., Alivila, L., Rainio, J., and Pakkanen, T.T. 1998. IR spectroscopy as a quantitative and predictive analysis method of phenol-formaldehyde resol resins. J. App. Polym. Sci. 69:2175-2185.

23. Crews, P., Rodriguez, J., and Jaspars, M. 1998. Organic structure analysis. Oxford university press, New York, Oxford. 326p.

24. Kristkova, M., Filip, P., Weiss, Z., and Peter, R. 2004. Influence of metals on the phenol-formaldehyde resin degradation in friction composites. Polym. Degrad. Stab. 84:49-60.

25. Costa, L., Montelera, L. R., Camino, G., Weil, E. D., and Pearce, E. M. 1997. Structure-charring relationship in phenol-formaldehyde type resins. Polym. Degrad. Stab. 56:23-35.

26. Pecsok, R. L. and Shields, L. D. 1968. Modern methods of chemical analysis. John wiley & sons. Inc, New York, 205p.

27. Poljansek, I. and Krajnc, M. 2005. Characterization of phenol-formaldehyde prepolymer resins by in line FT-IR spectroscopy. Acta Chim. Slov. 52:238-244.

28. Hasllam, J. and Willis, H. A.1965. Identification and analysis of plastics. D. Van Nosrand company, Inc. New Jersey. 231p.

29. Kissinger, H. E. 1957. Reaction kinetics in differential thermal analysis. Anal Chem 29:1702-1706.

30. Kamal, M. R. 1974. Thermoset characterization for mobility analysis. Polym Eng Sci 14:231-239.

31. Opalicki, M., Kenny, J. M., and Nicolais, L. 1996. Cure kinetics of neat and carbon fiber reinforced TGDDM/DDS epoxy systems. J Appl Polym Sci 61:1025-1037.

32. Park, S. J., Seo, M. K., and Lee, J. R. 2000. Isothermal cure kinetics of epoxy/phenol-novolac resin blend system initiated by cationic laten thermal catalyst. J Polym Sci: Part A: Polym Chem 38:2945-2956.

33. Hseih, H. K., Su, C. C., and Woo, E. M. 1998. Cure kinetics and inter-domain etherification in an amine-cured phenoxy/epoxy system. Polym 39(11):2175-2183.

CHAPTER 4

MECHANICAL AND PHYSICAL PROPERTIES OF BIO-COMPOSITES USING NOVOLAC TYPE LIQUEFIED WOOD RESIN

4.1 Introduction

The rapidly changing economic and environmental needs of society are placing increasing pressure on the forest products industry to increase the conversion and efficient use of wood resources. Competition in high volume markets has focused attention on low priced materials that offer a more favorable strength to weight ratio. Wood fiber composites have the lowest material cost compared to other polymeric industries.[1] Liquefied wood can be developed to novolac type phenolic resin as discussed in previous chapters. Several studies have made molded composites using liquefied wood resin as the matrix resin. The effects of combined phenol and phenol to formaldehyde ratio on the flexural properties of the composites have been investigated.[2, 3] It was reported that the mechanical properties of the molding composites using novolac type liquefied wood resin were much higher than those using the phenolated wood and also somewhat superior to those using the conventional novolac resin.[2]

Oxalic acid was used as the catalyst in the liquefaction step of this study, which resulted in a greater amount of wood residues in the liquefied wood mixture than if a strong acid catalyst had been used. In addition, the liquefied residue contains more cellulose than the original wood since the lignin has been partially removed during the liquefaction reaction. Therefore, the liquefied wood residue was used as part of the filler of the bio-composite in this study. Based on a preliminary study on composites from liquefied wood resin,[4] a phenol to wood ratio of 2/1 was selected for the liquefaction

stage to obtain composites with acceptable mechanical properties and favorable cost factor. Thus, the objectives of this chapter were to 1) investigate the effects of selected liquefaction variables (i.e., liquefaction temperature and reactor type) on the mechanical and physical properties of the composites, and 2) investigate the effects of hot press temperature and time on the mechanical and physical properties of the composites.

4.2 Experimental

4.2.1 Materials

The materials used in wood liquefaction and resin synthesis were the same as in Chapters 2 and 3. Additional wood flour was used as the filler of the composites and was the same as used for the wood liquefaction.

4.2.2 Preparation of liquefied wood and novolac type liquefied wood resin

The processes of wood liquefaction and resin synthesis were the same as described in Chapter 2 and 3.

4.2.3 Preparation of bio-composite

The compositions of the bio-composites are listed in Table 1. The novolac type liquefied wood resin was first mixed with hexamine, calcium hydroxide, and zinc stearate. Sufficient acetone was then added to the mixture and stirred to thoroughly dissolve the resin. Wood filler was then added to the acetone mixture to make a homogeneous mixture. After thoroughly mixing, the acetone was removed from the mixture under reduced-pressure at 50 ºC. The mixture was then freeze-dried overnight to

remove water and any remaining acetone. The dried material was sieved again to pass through a 20 mesh sieve and aggregated materials remaining on the 20 mesh sieve were ground into powder. The resulting material was subjected to compression molding to fabricate 5×5×1/8 in. panels using a 6× 6 in. single-opening laboratory hot-press. The panels were first compressed under a selected temperature and time and then cooled under the same pressure for 10 min. Three hot pressing temperatures (155, 175, and 195 ˚C) and two hot pressing times (2 and 4 min.) were used for the molding process. Two panels were produced for each hot pressing temperature and time combination.

Table 4.1. Compositions of the composite.

Liquefied wood resin	Hexamine	Calcium hydroxide	Zinc stearate	Wood filler
30.0%	8.0%	1.0%	1.0%	60.0%

4.2.4 Test of mechanical properties

Flexural and tensile test were performed on an Instron-4465 test machine in accordance with ASTM D-1037-96 (6).[5] Each panel was cut to yield two static-bending specimens (1/2×5 in.) and two dimensional stability test specimens (1/2×5 in.). The span for flexural test was 4 in. and the crosshead speed was 0.107 in/min. according to the standard.[5] Data for modulus of rupture (MOR) and modulus of elasticity (MOE) were automatically collected and computed by the Instron Series IX Automated Materials Tester program.

4.2.5 Test of dimensional stabilities

Two specimens from each composite were chosen for the 24 to 96 h soaking and 2 to 8 h boiling test. The thickness of the specimens before and after the tests was measured. The percent of thickness swelling was calculated by equation 1:

$$TS(\%) = \frac{T_1 - T_0}{T_0} \times 100 \quad (1)$$

TS is the percent of thickness swelling and T_0 and T_1 are the thickness of the specimen before and after the test, respectively.

4.2.6 Statistic analysis

Analysis of variance (ANOVA) was used to analyze the effects of the variables during the liquefaction stage and the compressing stage on the mechanical properties and dimensional stabilities of the molded composites.

4.3 Results and Discussion

4.3.1 Effects of liquefaction temperature and reactor type

As discussed in Chapter 2 and 3, liquefaction temperature and reactor type caused some variations between the liquefied wood and liquefied wood resins. Consequently, the physical and mechanical properties of the composites using the liquefied wood resin as a matrix resin also varied as shown in Table 4.2.

Table 4.2. Flexural and tensile strength of the composites using different liquefied wood resin.

	Three neck flask				Parr reactor			
	Flexural		Tensile		Flexural		Tensile	
	MOR	MOE	MOR	MOE	MOR	MOE	MOR	MOE
	(psi)		(psi)		(psi)		(psi)	
150 ˚C	8,008	934,279	6,308	530,711	9,090	1,193,544	6,357	613,410
180 ˚C	10,305	1,252,251	7,369	645,472	8,890	1,131,397	6,203	625,624

Table 4.3. ANOVA results of the effects of reactor type and temperature during the liquefaction process on the flexural properties of the panels.

Source	df	Type III SS	Mean Square	F Value	Pr > F
1. dependent variable: modulus of rupture (MOR)					
M[a]	1	110556	110556	1.12	0.3109
T[b]	1	4395312	4395312	44.50	<.0001
M*T	1	6237506	6237506	63.15	<.0001
2. dependent variable: modulus of elasticity (MOE)					
M[a]	1	19157466510	19157466510	25.68	0.0003
T[b]	1	65446174800	65446174800	87.71	<.0001
M*T	1	144490834280	144490834280	193.65	<.0001

[a]Reactor type.
[b]Liquefaction temperature.

Table 4.3 shows the effects of two liquefaction factors on the flexural properties of the composites. It can be seen that liquefaction temperature had a significant effect on the modulus of rupture (MOR) of the composites. Both reactor type and liquefaction temperature had significant effects on the modulus of elasticity (MOE) of the composites. Furthermore, these two factors had significant interactions for both MOR and MOE as shown in Figure 4.1. It is interesting to note that although the two types of reactors showed opposite trends to each other for MOR or MOE, each individual reactor displayed consistent trends for both MOR and MOE. In other words, the composites made with the liquefied wood resin from the atmospheric three neck flask showed higher

MOR and MOE at higher liquefaction temperatures. On the contrary, the composites showed a slightly lower MOR and MOE with the liquefied wood resin from the sealed Parr reactor at higher liquefaction temperatures.

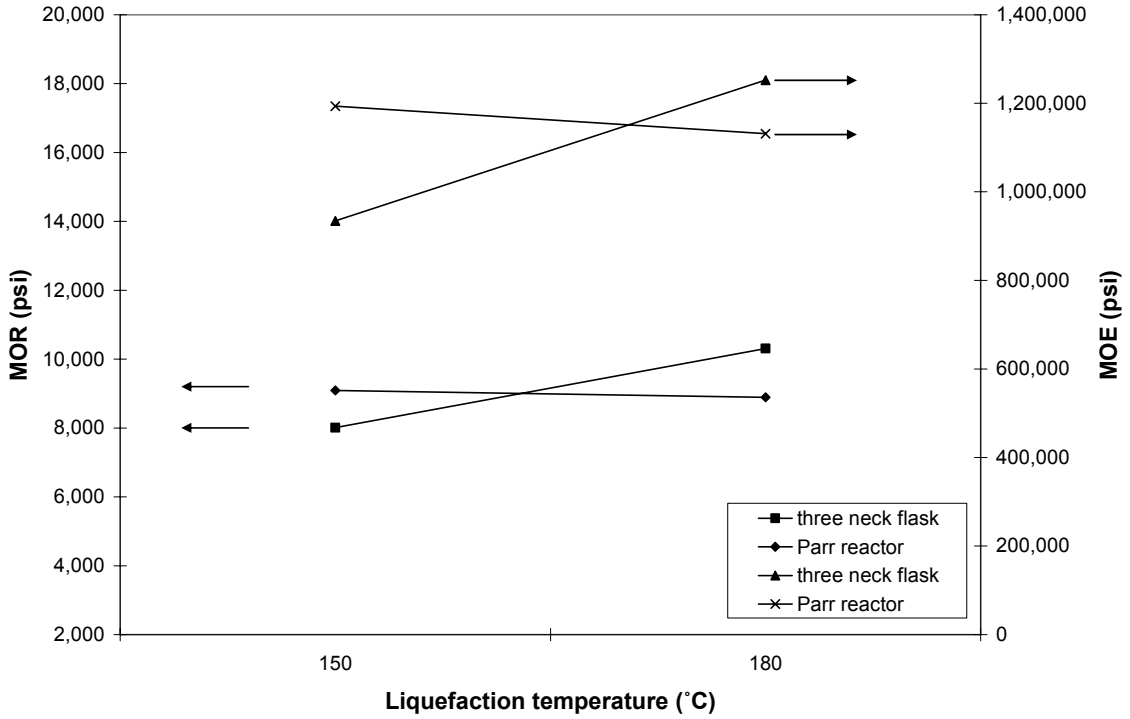

Figure 4.1. Interaction plot of reactor type and liquefaction temperature on flexural properties of the panels.

Table 4.4. ANOVA results of the effects of reactor type and temperature during the liquefaction process on the tensile properties of the panels.

Source	df	Type III SS	Mean Square	F Value	Pr > F
1. dependent variable: modulus of rupture (MOR)					
M[a]	1	1244675	1244675	4.50	0.0553
T[b]	1	821869	821869	2.97	0.1103
M*T	1	1476043	1476043	5.34	0.0394
2. dependent variable: modulus of elasticity (MOE)					
M[a]	1	3950091075	3950091075	8.83	0.0117
T[b]	1	16122968064	16122968064	36.03	<.0001
M*T	1	10516041030	10516041030	23.50	0.0004

[a]Reactor type
[b]Liquefaction temperature

The effects of liquefaction factors on the tensile strength of the composites were also analyzed by ANVOA and the results were summarized in Table 4.4. Reactor type had a significant effect on the MOR of the composites while both factors had significant effects on the MOE. Moreover, the interactions of these two factors were significant in both MOR and MOE. Similar to the trends shown for the flexural strength as shown in Figure 4.2, the composites with the liquefied wood resin from the atmospheric three neck flask had increased MOR and MOE when the liquefaction temperature increased from 150 to 180 ˚C. However, the composites with the liquefied wood resin from the sealed Parr reactor had slightly decreased MOR and slightly increased MOE with increasing liquefaction temperature.

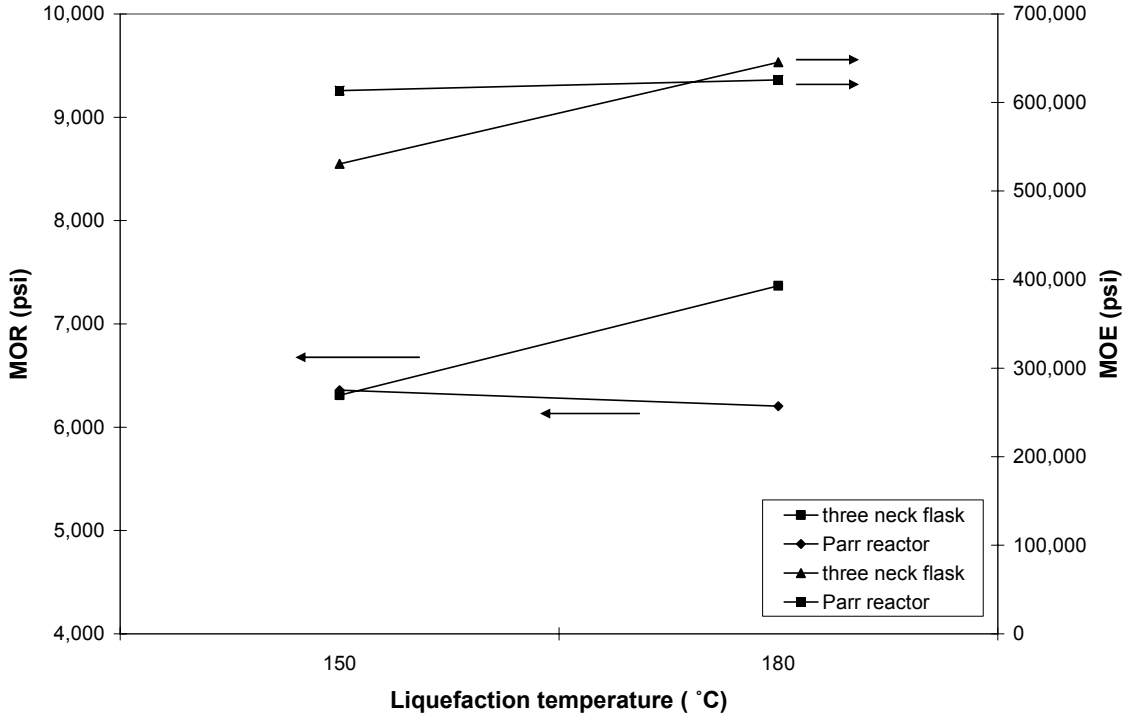

Figure 4.2. Interaction plot of reactor type and liquefaction temperature on tensile properties of the panels.

Figure 4.3 illustrates the dimensional stabilities of the composites in (a) soaking and (b) boiling tests. The composites with the liquefied wood resin from the sealed Parr reactor yielded higher thickness swelling than those with the liquefied wood from the three neck flask in both soaking and boiling test. On average, the composites with the liquefied wood resin under higher liquefaction temperature had higher thickness swelling. These results are understandable. Wood is a very hydrophilic material due to the large amount of hydroxyl groups in the major wood components. It could be assumed that liquefied wood resin would retain the hydrophilic characteristics of wood. Based on the liquefaction results of Chapter 2, the liquefaction reaction conducted in the sealed Parr reactor had a greater liquefaction level than that performed in the three neck flask. Therefore, the composites with the liquefied wood resin containing more wood components would be more easily accessible to water resulting in a higher thickness swelling. Similar results have also been reported in the literature.[6] In addition to the hydrophilic features of the matrix resin, the cross-link density within the matrix resin and between the matrix resin and wood filler is also a critical factor for the dimensional stability of the composites. As discussed in Chapter 3, the condensation reaction between free phenol and formaldehyde could be the dominant reaction during the resin synthesis process of the liquefied wood from the three neck flask. In the meantime, there would be a large amount of wood components incorporated into the liquefied wood resin during the resin synthesis process of the liquefied wood from the Parr reactor. Although the resulting liquefied wood resin from these two systems had similar average molecular weights at the same phenol to wood ratio, the liquefied wood resin with more wood components would yield fewer cross-links during the resin cure process due to fewer

reaction sites as compared with the liquefied wood resin with a lower wood component content.

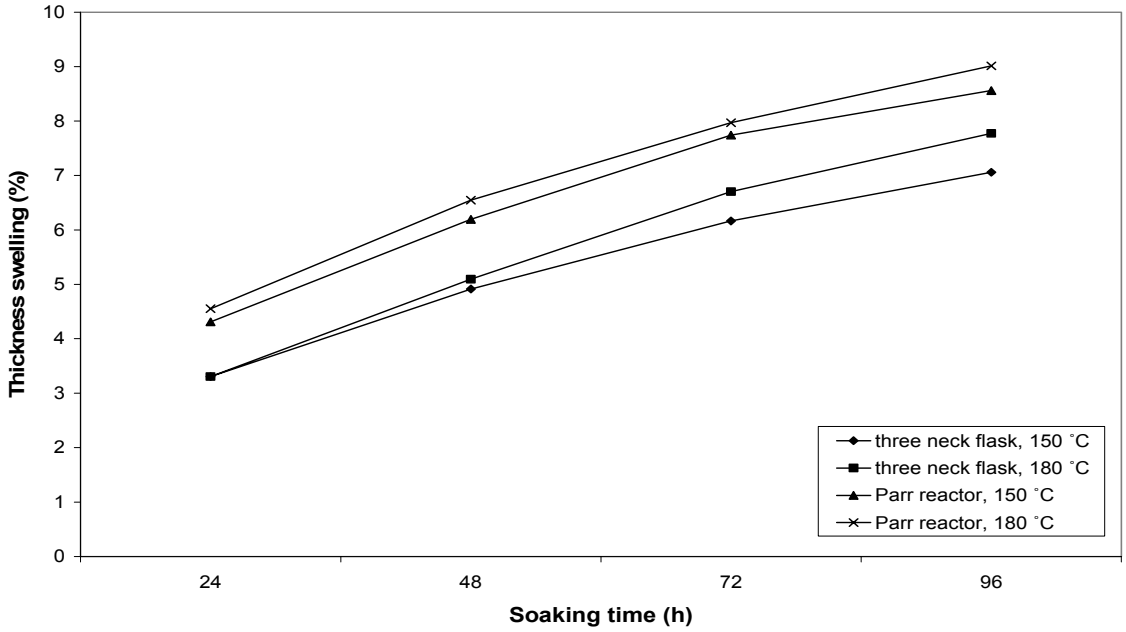

(a)

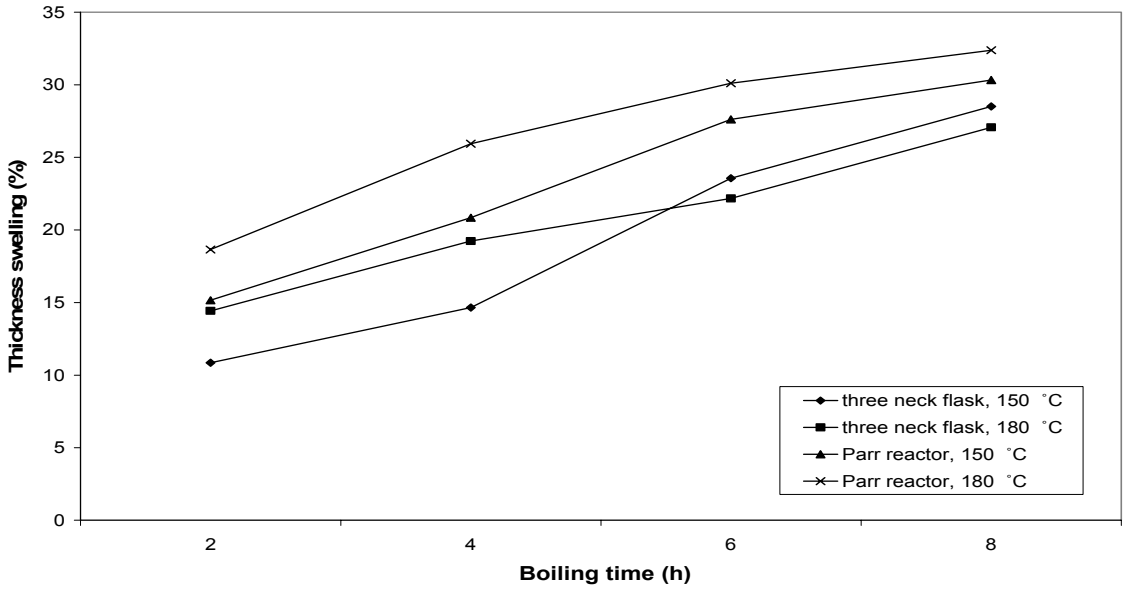

(b)

Figure 4.3. Thickness swelling of the composites as a function of (a) soaking and (b) boiling time.

4.3.2 Effects of hot press temperature and time.

Hot press temperature and time are two factors highly related to the economic cost of the panel products. Table 4.5 summarizes the flexural and tensile strength of the composites fabricated under different temperatures and time.

Table 4.5. Flexural and tensile strength of composites under different hot press temperature and time.

	2 min. Hot Press Time				4 min. Hot Press Time			
	Flexural		Tensile		Flexural		Tensile	
	MOR	MOE	MOR	MOE	MOR	MOE	MOR	MOE
	(psi)		(psi)		(psi)		(psi)	
155 ˚C	4596	676870	2769	326068	8488	1134845	4725	483873
175 ˚C	8430	1111775	5273	482262	8512	1096622	5927	467720
195 ˚C	8598	1091481	5707	484342	9356	1068845	5991	473841

Table 4.6. ANOVA results of the effects of hot press temperature and time on the flexural properties of the panels.

Source	df	Type III SS	Mean Square	F Value	Pr > F
1. dependent variable: modulus of rupture (MOR)					
Te[a]	2	26423444	13211722	44.72	<.0001
Ti[b]	1	14936540	14936540	39.55	<.0001
Te*Ti	2	16516622	8258311	24.72	<.0001
2. dependent variable: modulus of elasticity (MOE)					
Te[a]	2	187465325483	93732662742	55.77	<.0001
Ti[b]	1	117704743453	117704743453	44.41	<.0001
Te*Ti	2	303261494936	151630747468	71.84	<.0001

[a]Temperature of hot press process.
[b]Time of hot press process.

Table 4.7. ANOVA results of the effects of hot press temperature and time on the tensile properties of the panels.

Source	df	Type III SS	Mean Square	F Value	Pr > F
1. dependent variable: modulus of rupture (MOR)					
Te[a]	2	21100164	10550082	36.00	<.0001
Ti[b]	1	5582084	5582084	68.05	<.0001
Te*Ti	2	3083221	1541611	9.94	0.0012
2. dependent variable: modulus of elasticity (MOE)					
Te[a]	2	27769937362	13884968681	11.57	0.0032
Ti[b]	1	11750327657	11750327657	13.67	0.0002
Te*Ti	2	38698139756	19349069878	19.04	<.0001

[a]Temperature of hot press process.
[b]Time of hot press process.

The ANOVA results show that both hot press temperature and time had significant effects on the flexural and tensile strength of the composites (Table 4.6 and 4.7). Generally, the composites made under higher hot press temperatures and longer press time yielded higher flexural and tensile strength. However, these properties changed at different rates with different press times, as the hot press temperature changed from 155 to 195 ˚C. As shown in Figure 4.4 and 4.5, both the flexural and tensile strength of the composites with a press time of 2 min. increased dramatically when the hot press temperature was increased from 155 to 175 ˚C. The slope of the curves then decreased as the hot press temperature increased to 195 ˚C. When the press time increased to 4 min., only a slight increase is observed in the tensile MOR of the composites as the temperature changed for 155 to 175 ˚C. All other values did not change markedly upon changes in hot press temperature. This result infers that a certain amount energy is needed to cure the matrix resin. When the hot press temperature is not high enough to give the needed energy, a prolonged press time will be necessary.

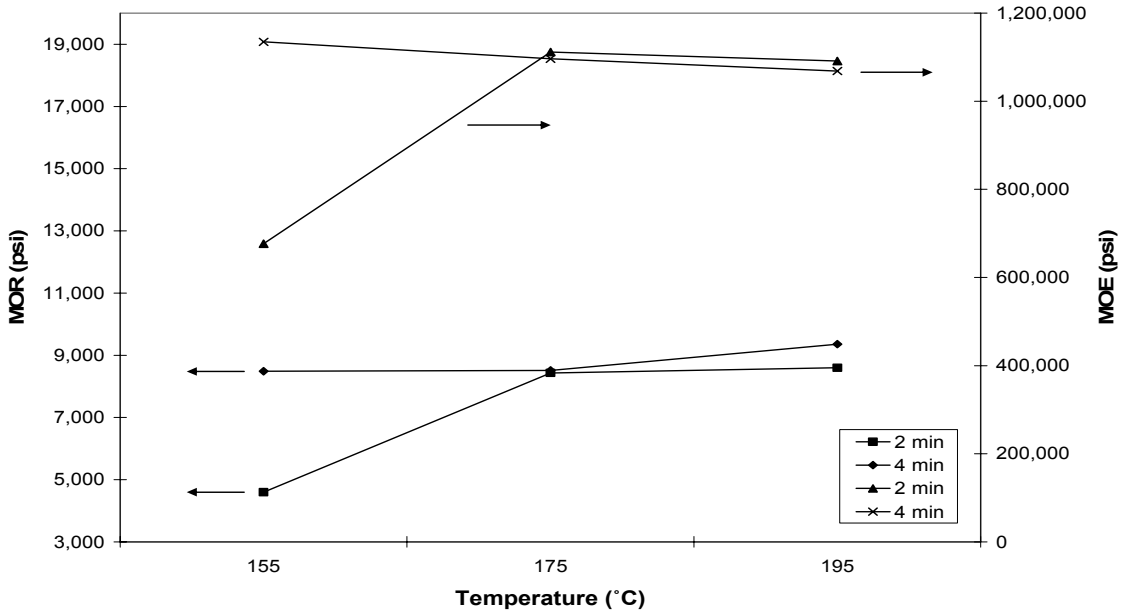

Figure 4.4. Interaction plot of hot press temperature and time on flexural properties of the panels.

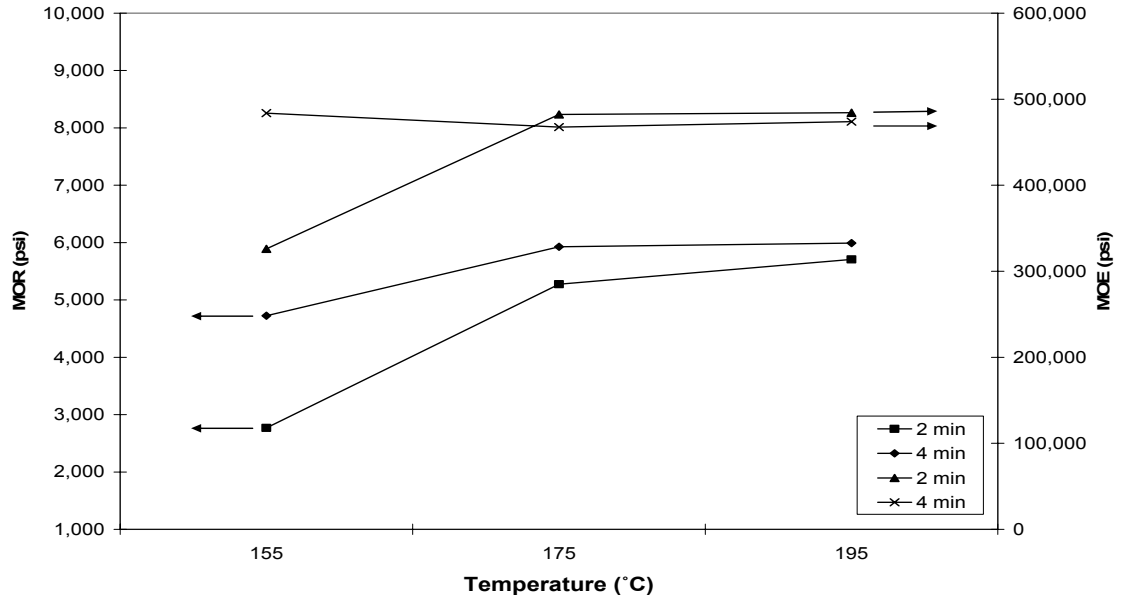

Figure 4.5. Interaction plot of hot press temperature and time on tensile properties of the panels.

The results of the soaking and boiling tests of the composites under different hot press temperaturse and time are shown in Figure 4.6 and 4.7. No test specimen from the composite made with 155 ˚C and 2 min. could withstand for the entire soaking and boiling tests. Moreover, the composites compressed for 4 min. at 155 ˚C had much higher thickness swelling than any other composites in both soaking and boiling tests. Therefore, it can be concluded that the matrix resin did not cure well at the hot press temperature of 155 ˚C even with prolonged press time. It is also worthwhile to note that the order of the thickness swelling decreased as 155 ˚C, 4 min. >175 ˚C, 2 min. >195 ˚C, 2 min. >175 ˚C, 4 min >195 ˚C, 4 min. in the boiling test, indicating that the temperature takes precedence over time during the molding process.

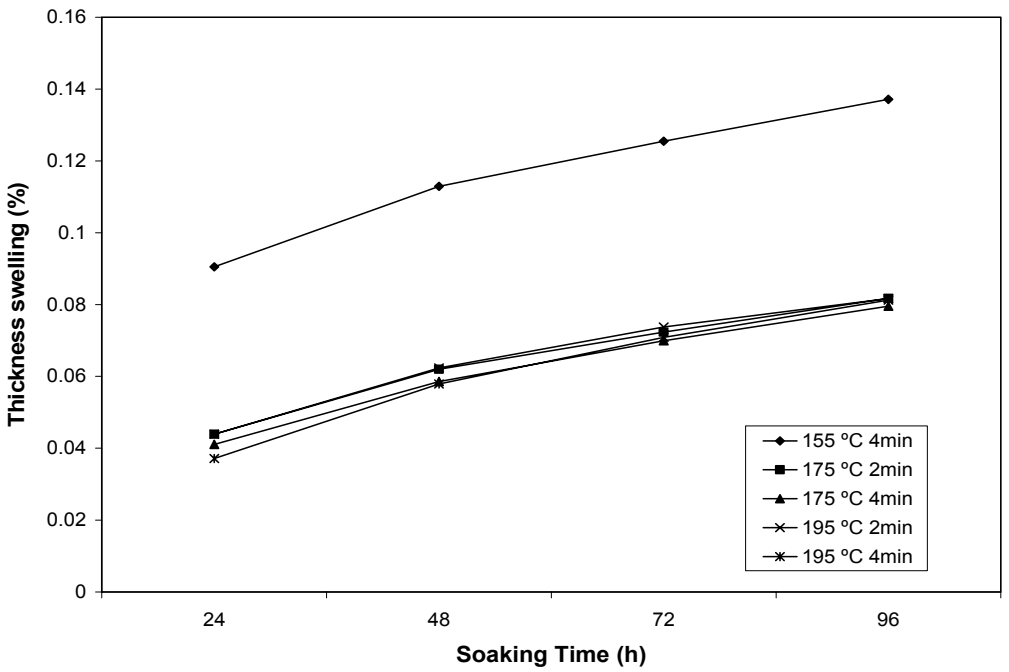

(a)

Figure 4.6. Thickness swelling of the composites as a function of (a) soaking and (b) boiling time. (figure continued)

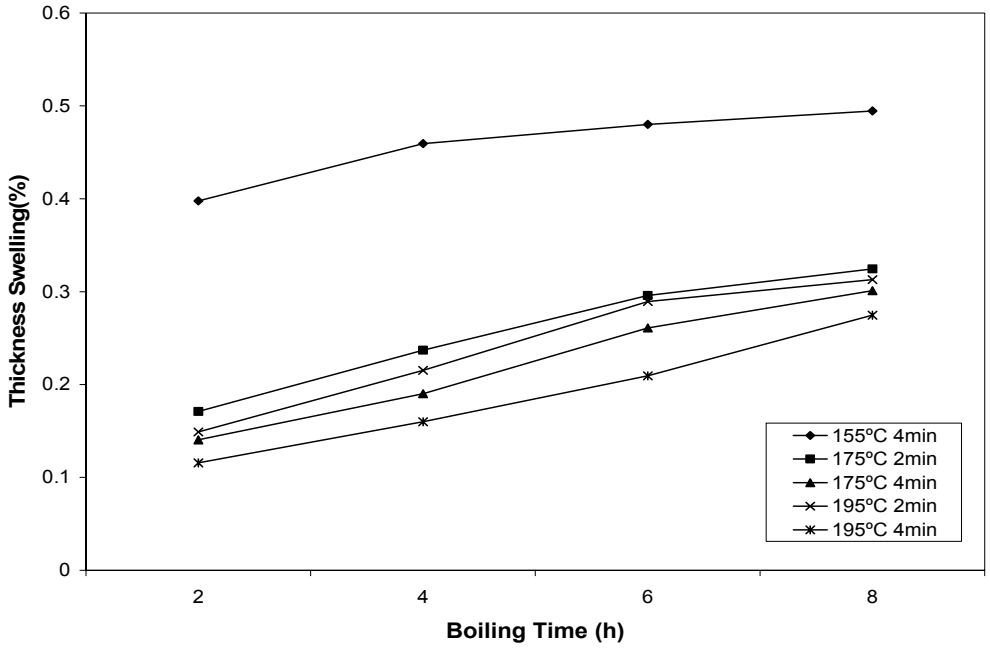

(b)

4.4 Conclusions

Bio-composites were fabricated from wood flour and novolac type liquefied wood resins. The effects of liquefaction temperature, reactor type, hot press temperature, and press time on the mechanical and physical properties of the composites were investigated. The composites with the liquefied wood resin from the atmospheric three neck flask showed increased flexural and tensile strength when liquefaction temperature increased from 150 to 180 ˚C. The composites with the liquefied wood resin from the sealed Parr reactor yielded higher thickness swelling than those with the liquefied wood resin from the three neck flask likely due to the hydrophilic wood components incorporated in it and the lower cross-link density than the liquefied wood resin from the three neck flask during the resin cure process.

Both hot press temperature and press time had significant effects on the mechanical and physical properties of the composites. The flexural and tensile strength of the composites with a press time of 2 min. increased dramatically when the hot press temperature increased from 155 to 175 ˚C. But the rate of increase decreased as the temperature changed from 175 to 195 ˚C and with the press time of 4 min. The results of dimensional stability tests implied that the matrix resin didn't cure well at the hot press temperature 155 ˚C. Hot press temperature takes precedence over time during the mat consolidation process.

4.5 References

1. Rowell, R.M., Cleary, B.A., Rowell, J.S., Clemons, C., and Young, R.A. 1993. Results of chemical modification of lignocellulosic fiber for use in composites. In: M.P. Wolcott (ed.) Wood Fiber/Polymer Composites: Fundamental Concepts, Processes, and Material Options. Forest Products Society, Madison, USA. 121-127 pp.

2. Lin, L., Yoshioka, M., Yao, Y., and Shiraishi, N. 1995. Preparation and properties of phenolated wood/phenol/formaldehyde cocondensed resin. J. App. Polymer Sci. 58: 1297-1304.

3. Alma, M. H., Yoshioka, M., Yao, Y., and Shiraishi, N. 1995. Preparation of oxalic acid catalyzed resinified phenolated wood and its characterization. Mokuzai Gakkaishi 41(12): 1122-1131.

4. Pan, H., Shupe, T. F, and Hse, C.Y. 2005. Preliminary investigation of bio-composites fabricated from liquefied wood/phenol/formaldehyde co-condensed resin. In: C.R. Frihart (ed.) Wood Adhesives 2005. Forest Products Society, Madison, USA. 257-262 pp.

5. American Society for Testing and Materials (ASTM). 1996. Standard test method for evaluating properties of wood-base fiber and particle panel materials. ASTM D 1037-96.

6. Lin, L., Yoshioka, M., Yao, Y., and Shiraishi, N. 1995. Physical properties of moldings from liquefied wood resins. J. App. Polymer Sci. 55: 1563-1571.

CONCLUSIONS

Wood liquefaction is a thermochemical conversion technique that partially or completely dissolves wood with a reagent solvent at a temperature of 120 to 250 ˚C with or without an acid catalyst. Most previous studies on wood liquefaction have focused on completely converting wood into a liquid via a strong acid catalyst or high reagent solvent to wood ratios, which has resulted in a liquefaction process that is not economically favorable because special production equipment are required due to the high corrosiveness of the strong acids. Therefore, in my research on wood liquefaction I have focused on a process with a weak acid catalyst system to develop a bio-composite product from liquefied wood resin and liquefied wood residue with improved economic feasibility.

One significant difference of a weak-acid-catalyzed system in comparison to a strong acid system is the high wood residue content due to the strong network of cellulose, hemicellulose, and lignin in wood. A comprehensive study on liquefied wood residue was conducted in this work. It was found that most lignin can be removed from wood at a phenol to wood ratio of 3/1. At this ratio most of the carbohydrates in the wood were resistant to phenol liquefaction and remained in the liquefied wood residue, which resulted in a higher crystallinity index of the liquefied wood residue than the original wood. The Fourier transform infrared spectroscopy (FT-IR) absorbance of the carbonyl groups in hemicellulose disappeared in the spectra of the liquefied wood residue from the metal Parr reactor. A series of comparative studies were conducted to differentiate the effects of the pressure during the liquefaction and the metal elements

from the Parr reactor. The FT-IR results indicated a possible catalytic effect of Fe^{3+} and/or Fe^{2+} on the liquefaction of carbohydrates in wood.

Liquefied wood resins (LWR) were synthesized from liquefied wood and formaldehyde. It was found that the liquefied wood from a greater liquefaction extent system yielded a lower average molecular weight likely due to less reaction sites on the liquefied wood and the steric hindrance during the polymerization reaction. The FT-IR spectra of the LWR revealed the incorporation of wood components into the novolac type resins. Moreover, the FT-IR results of the LWR also confirmed the broken carbonyl groups in hemicellulose from the sealed Parr reactor system. The cure kinetic study of two typical LWR showed that the activation energies of LWR were higher than conventional phenolic resins and close to that of a lignin-phenol-formaldehyde resin reported in another study. It was found that LWR followed an autocatalytic cure mechanism. Two kinetic models were proposed for LWR based on the isothermal DSC methods.

Bio-composites were fabricated from wood flour and novolac type LWR. The flexural strengths of the composites were comparable to that of similar products reported in other studies, indicating that the liquefied wood resin and liquefied wood residue from a weak acid catalyzed liquefaction could be successfully applied to molded composite products as a substitute for conventional novolac resin. However, future research is needed to improve the dimensional stabilities of the composite products with the LWR which have a higher wood components percentage.

VITA

Hui Pan was born in May, 1971 in Huangzhou, Hu Bei, P.R. China. After graduation from Huanggang High School in 1989, she attended Northeast Forestry University in Harbin, P.R. China where she received a Bachelor of Science degree in wood processing in 1993. Afterwards, she worked for a local wood products company for almost 5 years. She then went back to school for further study. One year later, she went back to Northeast Forestry University and received a Master of Science degree in wood science and technology in summer, 2002. During her master study, her desire for learning never stopped. Thus, she started preparations to apply to a university in the United States. In January, 2003, she enrolled in the graduate program at Louisiana State University. She will receive the degree of Doctor of Philosophy in forestry in fall, 2007. Her major area of research emphasis was wood liquefaction.